Active

Project #: E-18-665   Cost share #:   Rev #: 14
Center # : R6693-0A0   Center shr #:   OCA file #:
                                                         Work type : RES
Contract#: N00014-89-J-1708   Mod #: ADM. REVISION   Document : GRANT
Prime   #:   Contract entity: GTRC

Subprojects ? : Y   CFDA: 12.AAA
Main project #:   .   PE #: N/A

Project unit: MSE   Unit code: 02.010.112
Project director(s):
    STOCK S R   MSE   (404)894-6882

Sponsor/division names: NAVY   / OFC OF NAVAL RESEARCH
Sponsor/division codes: 103   / 025

Award period: 890301   to   930930 (performance)   930930 (reports)

Sponsor amount   New this change   Total to date
    Contract value   0.00   446,146.00
    Funded   0.00   446,146.00
Cost sharing amount   0.00

Does subcontracting plan apply ?: N

Title: A STUDY OF THE RELATIONSHIP BETWEEN MACROSCOPIC MEASURE & PHYSICAL...

                    PROJECT ADMINISTRATION DATA

OCA contact: E. Faith Gleason   894-4820

 Sponsor technical contact   Sponsor issuing office

 GEORGE R. YODER, CODE 1131   BETTI SUE MOYA, CODE 1512:BSM
 (202)696-4401   (202)696-2584

 MATERIALS DIV., OFFICE OF THE CHIEF   OFFICE OF NAVAL RESEARCH
 OF NAVAL RESEARCH   800 NORTH QUINCY STREET
 ARLINGTON, VA 22217-5000   ARLINGTON, VA 22217-5000

                                        FAX: (703) 696-0993

Security class (U,C,S,TS) : U   ONR resident rep. is ACO (Y/N): Y
Defense priority rating   :   N/A   ONR supplemental sheet
Equipment title vests with: Sponsor   GIT X

Administrative comments -
    ISSUED TO CORRECT PREVIOUS REVISION #13. FUNDS IN THE AMOUNT OF $13,040
    SHOULD HAVE BEEN BUDGETED IN SUBPROJECT E-18-666. FUNDS WILL BE MOVED TO SUB.

GEORGIA INSTITUTE OF TECHNOLOGY
OFFICE OF CONTRACT ADMINISTRATION

NOTICE OF PROJECT CLOSEOUT

Closeout Notice Date 09/08/94

Project No. E-18-665_____   Center No. R6693-0A0_____

Project Director STOCK S R_____   School/Lab MSE_____

Sponsor NAVY/OFC OF NAVAL RESEARCH_____

Contract/Grant No. N00014-89-J-1708_____ Contract Entity GTRC

Prime Contract No. _____

Title A STUDY OF THE RELATIONSHIP BETWEEN MACROSCOPIC MEASURE & PHYSICAL..._____

Effective Completion Date 930930 (Performance) 930930 (Reports)

		Date
Closeout Actions Required:	Y/N	Submitted
Final Invoice or Copy of Final Invoice	Y	_____
Final Repo. ` of Inventions and/or Subcontracts	Y	_____
Government Property Inventory & Related Certificate	N	_____
Classified Material Certificate	N	_____
Release and Assignment	Y	_____
Other _____	N	_____

Comments_____

Subproject Under Main Project No. _____

Continues Project No. _____

Distribution Required:

Project Director	Y
Administrative Network Representative	Y
GTRI Accounting/Grants and Contracts	Y
Procurement/Supply Services	Y
Research Property Managment	Y
Research Security Services	N
Reports Coordinator (OCA)	Y
GTRC	Y
Project File	Y
Other _____	N
_____	N

NOTE: Final Patent Questionnaire sent to PDPI.

GEORGIA INSTITUTE OF TECHNOLOGY
OFFICE OF CONTRACT ADMINISTRATION

NOTICE OF PROJECT CLOSEOUT (SUBPROJECTS)

Closeout Notice Date 09/08/94

Project No. E-18-665   Center No. R6693-0A0_____

Project Director STOCK S R_____   School/Lab MSE_____

Sponsor NAVY/OFC OF NAVAL RESEARCH_____

Project # E-18-666   PD STOCK S R   Unit 02.010.112   T
GRANT #   N00014-89-J-1708   MOD#   ADM. REVISION   MSE *
Ctr # R6693-0A1   Main proj # E-18-665   OCA CO EFG
Sponsor-NAVY   /OFC OF NAVAL RESEARC   103/025
A STUDY OF THE RELAT
Start 890301 End 930531 Funded   65,040.00 Contract   65,040.00

LEGEND
1. * indicates the project is a subproject.
2. I indicates the project is active and being updated.
3. A indicates the project is currently active.
4. T indicates the project has been terminated.
5. R indicates a terminated project that is being modified.
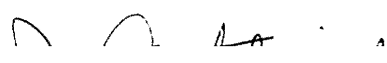
Georgia Tech

E13.

NIA

December 10, 1991

Dr. R.C. Pohanka
Code 1131
Office of Naval Research
800 N. Quincy Street
Arlington, VA   22217-5000

Dear Dr. Pohanka:

Enclosed is a copy of the fiscal year report on the ONR-sponsored project entitled "Study of the Relationship Between Macroscopic Measures and Physical Processes Occurring During Crack Closure." The contract # is 89-J-1708 and the R & T # is 4311931. The ONR scientific officer is Dr. George Yoder.

Should you have any questions, please do not hesitate to contact me or Dr. Stuart R. Stock.

Sincerely,

Stephen D. Antolovich
Director and Professor
School of Materials Engineering

Enclosures

cc: Dr. Stuart R. Stock
      Dr. George Yoder

<u>FY90 End of Fiscal Year Letter</u>
(01 Oct 1990 - 30 Sep 1991)

ONR CONTRACT INFORMATION

Contract Title: "Study of the Relationship Between Macroscopic Measures
and Physical Processes Occurring during Crack Closure"

Performing Organization: Georgia Tech

Principal Investigator: S. D. Antolovich

Contract Number: 89-J-1708

R & T Project Number: 4311931

ONR Scientific Officer: Dr. G. Yoder

A.   Description of the scientific research goals

The approach involves simultaneous measurement of crack closure by macroscopic techniques and XTM (x-ray tomographic microscopy). Real fracture surfaces will be characterized numerically for use in finite element models of closure. The data obtained will allow the effects of crack surface geometry and the material's mechanical properties to be correlated with closure. The specific objectives are:

1.   Measure crack closure accurately in advanced aerospace materials using a novel three-dimensional, nondestructive approach (XTM).

2.   Develop a numerical approach for computing crack closure taking into the geometry of the fracture surface and the properties of the material.

3.   Use the results of these studies to define an appropriate driving force for fatigue crack growth under conditions where closure is important.

B.   Significant results in the past year

1.   Generated additional fatigue crack growth data on small compact tension samples. Excellent agreement was found between NRL and Georgia Tech data, despite the much smaller sample dimensions of the Georgia Tech samples.

2.   Measured physical crack opening at specific positions as a function of applied load. Ten load levels were examined for the notched tensile sample studied 9/91 at Cornell. This approach not totally satisfactory as it is difficult to assure that the same position on the crack face is investigated at each load level. A new approach has been implemented (see B4. below).

3.   Reliably quantified crack openings with XTM occupying one-tenth of a voxel or less (e.g. 0.6 μm crack openings for the data described in B2.).

4.   Measured crack opening over entire crack face for loads of 45.5 (max. load during crack propagation), 36.4 and 27.3 Kg for the sample described in B2. This eliminates potential errors from incorrect registration of sample for different load levels.

5.   Technical transfer to two computed tomography groups through discussions (BP Research, Cleveland, OH) and through preprint of the 1990 ASTM

Fracture Mechanics Symposium paper (Swiss Federal Laboratories for Materials Testing and Research). Load frames modeled after the Georgia Tech design have been constructed at these locations. The design is also to be used with the Topography-Tomography Imaging Collaborating Access Team for the Advanced Photon Source (S.R. Stock is Deputy Director of this team).

6.   Second synchrotron XTM in situ loading experiment attempted with 4mm diameter notched tensile samples and compact tension samples. During sample alignment, a major storage ring failure ended the experimental run.

7.   Have developed a closure model for multiple asperities.

8.   Have characterized the roughness profiles for experimental FCP specimens.

9.   Have identified microstructural features associated with crack closure in modes I, II and III.

C.   Plans for next year's research

1.   Perform XTM on cracked compact tension samples at different applied loads. The most likely approach will to be to develop region of interest sampling, where data is collected at high resolution only from a small subset of the actual cross-section of the sample.

2.   Continue analysis of crack opening in notched tensile samples as a function of applied load across the entire crack face. This data will be related to the actual crack face using optical and scanning electron microscopy.

3.   Devise new three-dimensional rendering approach to show crack geometry simultaneously with measured crack face opening.

4.   Plan to complete FEM work on real fracture surfaces.

5.   Plan to link the analytical results with the XTM results.

3

D. List of Publications/Reports/Presentations

3. Presentations

      a. Invited

"Nondestructive Imaging of Materials Microstructures Using X-ray Tomographic Microscopy," (presented by J.H. Kinney) Fall 1990 Materials Research Society Symposium on Advanced Tomographic Imaging Methods for the Analysis of Materials, November 1990, Boston.

"A Portable Load Frame for in situ Computed Tomography of Monolithic and Composite Materials," (presented by T.M. Breunig), April/May 1991 ASTM E9.04 Meeting, Indianapolis.

"X-ray Tomographic Microscopy and its Applications - Fatigue Crack Closure in Al-Li 2090, Damage Accumulation in SiC/Al and Chemical Vapor Infiltration Processing of Nicalon/SiC," (presented by S.R. Stock) Air Force Wright Laboratories (WL/MLLM), October 1991, Dayton.

"X-ray Tomographic Microscopy and its Applications: Fatigue Crack Closure in Al-Li 2090, Damage Accumulation in SiC/Al and Chemical Vapor Infiltration Processing of Nicalon/SiC," (presented by S.R. Stock) Quality Technology Division, General Electric Aircraft Engines, October 1991, Cincinnati.

"X-ray Tomographic Microscopy and its Applications in Fatigue Crack Closure and in Damage Accumulation in Composites," (presented by S.R. Stock) BP Research, October 1991, Cleveland.

      b. Contributed

"X-ray Tomographic Microscopy of Materials," (presented by S. R. Stock) TMS-AIME Fall Meeting, October 1990, Detroit.

"Impact of X-ray Tomographic Microscopy on Deformation Studies," (presented by T.M. Breunig) Fall 1990 Materials Research Society Symposium on Advanced Tomographic Imaging Methods for the Analysis of Materials, November 1990, Boston.

"Damage in Metal Matrix Composites and Crack Face Interactions During in situ Loading

of Al-Li Alloy 2090 Studied by X-ray Tomographic Microscopy," 1991 Industrial Computed Tomography II Topical Conference, American Society for Nondestructive Testing, May 1991, San Diego.

"X-ray Tomographic Microscopy of Sample Response During in situ and Interrupted Mechanical Testing," (poster presented by S.R. Stock), Pacific International Congress on X-ray Analytical Methods, August 1991, Honolulu.

"Crack Face Separation in the Interior of Al-Li 2090 Samples Quantified as a Function of Applied Load by in situ X-ray Tomographic Microscopy," (presented by A. Guvenilir) TMS-AIME Fall Meeting, October 1991, Cincinnati.

4.   Books (and sections thereof)

"Damage in Metal Matrix Composites and Crack Face Interactions During In situ Loading of Al-Li Alloy 2090 Studied by X-ray Tomographic Microscopy," S.R. Stock, T.M. Breunig, A. Guvenilir, J.H. Kinney and M.C. Nichols, in 1991 Industrial Computed Tomography II Topical Conference Paper Summaries, ASNT, pp. 158-162, 1991.

(refereed) "Impact of X-ray Tomographic Microscopy on Deformation Studies of a SiC/Al MMC," T.M. Breunig, S.R. Stock, J.H. Kinney, A. Guvenilir and M.C. Nichols, in Advanced Tomographic Imaging Methods for the Analysis of Materials, MRS vol. 217, pp. 135-141, 1991.

(refereed) "Nondestructive Imaging of Materials Microstructures Using X-ray Tomographic Microscopy," J.H. Kinney, M.C. Nichols, U. Bonse, S.R. Stock, T.M. Breunig, A. Guvenilir and R.A. Saroyan, in Advanced Tomographic Imaging Methods for Analysis of Materials, MRS vol. 217, pp. 81-95, 1991.

E. List of Honors/Awards

Name of Person Receiving Award	Recipient's Institution	Name, Sponsor and Purpose of Award
T. M. Breunig	Georgia Tech	Outstanding Graduate Student Award, Materials Research Society, to recognize outstanding achievement in research.
T. M. Breunig and S. R. Stock	Georgia Tech	R & D 100, R & D Magazine, Recognize the 100 most technologically significant product innovations of 1990.

F. Participants and their status

1. Senior staff

a.   Stephen D. Antolovich, Professor and Director, School of Materials Engineering, and Director of the Mechanical Properties Research Laboratory.

b.   Stuart R. Stock, Associate Professor of Materials Engineering.

2. Graduate Students

a.   T. M. Breunig, Ph.D. student
b.   A. Guvenilir, Ph.D. student
c.   H.-Y. Jung, Ph.D. student

G. Other sponsored research

1.   STUART R. STOCK (7/1/90-6/30/91)

Source of Support	Project Title	Annual Amount	Period of Award	% of Effort
NSF	1	$ 5,013	11/88-4/92	0
Univ. Dayton Res. Inst.	2	$ 6,000	1/89-9/91	0

Project Titles
1.   "Novel X-ray Methods for Characterization of the Spatial Distribution of Inhomegenities in Materials"
2.   "Double Crystals Rocking Curve Analysis of MBE Superlattices"

2.   **STEPHEN D. ANTOLOVICH**

Source of Support	Project Title	Annual Amount	Period of Award	% of Effort
AFOSR	1	$127,465	5/90-4/93	20
NASA	2	$74,249	1/89-12/91	5

Project Titles

1.   "Deformation, Constitutive Behavior and Damage of Advanced Structural Materials Under Multiaxial Loading"

2.   "Microstructure Mechanical Properties of Rapidly Solidified NbAl and NiAl"

H. SUMMARY OF FY91
PUBLICATIONS/PATENTS/PRESENTATIONS/HONORS/PARTICIPANTS
(Number Only)

		ONR	non ONR
a.	Number of papers Submitted to Refereed Journal but not yet published:	0	
b.	Number of Papers Published in Refereed Journals:	0	
c.	Number of Books or Chapters Submitted but not yet published:	0	
d.	Number of Books or Chapters Published:	3	
e.	Number of Printed Technical Reports & Non-Refereed Papers:	0	
f.	Number of Patents Filed:	0	
g.	Number of Patents Granted:	0	
h.	Number of Invited Presentations at Workshops or Professional Society Meetings:	2	
i.	Number of Contributed Presentations at Workshops or Professional Society Meetings:	5	
j.	Honors/Awards/Prizes for contract/Grant Employees:	2	
k.	Number of Graduate Students and Post-Docs Supported at least 25% this year on contract grant:	3*	
	Grad Students: TOTAL	3	
	Female	0	
	Minority	0	
	Post Doc: TOTAL	0	
	Female	0	
	Minority	0	
l.	Number of Female or Minority PIs or CO-PIs		
	New Female	0	
	Continuing Female	0	
	New Minority	0	
	Continuing Minority	0	

*including Georgia Tech cost sharing

Annual Report for

A Study of the Relationship Between Macroscopic
Measures and Physical Processes Occuring during
Crack Closure

N0014-89-J-1708

submitted to:

Office of Naval Research
Attn. Dr. George Yoder
ONR Code 1131
800 N. Quincy
Arlington, Virginia 22217-5000

by

Stephen D. Antolovich
Mechanical Properties Research Lab
School of Materials Engineering
Georgia Institute of Technology
Atlanta, GA 30332-0245

Stuart R. Stock
Mechanical Properties Research Lab
School of Materials Engineering
Georgia Institute of Technology
Atlanta, GA 30332-0245

I. Introduction

Crack closure in fatigue has been used to explain FCP behavior in certain alloys in which relatively low FCP rates have been observed. The basic notion is that the effective stress intensity range is reduced as a result of premature crack face contact which means that the driving force for FCP is also reduced. This is expressed as:

$$\Delta K_{eff} = K_{max} - K_{op} \qquad \qquad \cdots \quad (1)$$

In addition to the way in which K_{op} is measured, another very important fundamental question is the way in which ΔK_{eff} is correctly calculated. The stress intensity parameter for the compact tension and other specimen geometries, the effective stress intensity parameter range, is usually expressed as:

$$\Delta K_{eff} = (P_{max} - P_{cl})/BW^{1/2} \cdot g(a/W) \qquad \cdots (2)$$

The most fundamental question that arises relates to the correctness of Eq.2. For example, even if the closure load can be measured correctly, why should Eq. 2 apply. One obvious area of concern is the fact that no length parameter appears in the expression for the effective stress intensity parameter even though closure that is developed through surface roughness would seem in some way to require *explicit* incorporation of some measure of the roughness into the formula.

The theoretical and experimental portions of this report are split into two sections, Analytical and Numerical Studies and Experimental Studies, (II and III, respectively) for the readers' convenience. Results, discussion, summary and plans for next year are grouped together, therefore, for each activity.

II. Analytical and Numerical Studies of Crack Closure

As part of this research program, analytical and numerical studies are being carried out to assess the fundamental correctness of conventional means for accounting for closure. These results will be used, if necessary and where appropriate, to develop fundamentally correct ways of taking closure into account in the computation of ΔK_{eff}. In that spirit a series of problems of increasing complexity are being addressed.

A. Analytical Computations of the Effective Stress Intensity Parameter

1. Rigid Circular Cylinder in Infinite Body with Remote Stress σ

The situation is shown schematically in Fig. 1. Using a displacement-based approach, K_{op} is given by:

$$K_{op} = G/2(1-\nu)\nu\sqrt{2\pi/c} \cdot L \qquad \qquad \cdots \quad (3)$$

The effective stress intensity parameter, using the above result, is

given by:

$$\Delta K_{eff}^{op} = \frac{\sqrt{2\Pi}}{2(1-\nu^2)} \sqrt{2a-e} \ \Delta \qquad \ldots \text{(4)}$$

2. Rigid Circular Cylinder in Infinite Body with Point Load P at the Crack Surface

If the model is modified somewhat to have point loadings applied at the crack surface, Fig. 2, the stress intensity parameter is:

$$K_{el} = P \cdot \sqrt{\frac{2}{\pi e}} \qquad \ldots \text{(5)}$$

Using this result, ΔK_{eff} is given by:

$$\Delta K_{eff}^{cl} = \sqrt{\frac{2}{\pi e}} \Delta p \qquad \ldots \text{(6)}$$

The closure load is given by:

$$P_{el} = \frac{\pi G}{2(1-\nu)} \cdot L \qquad \ldots \text{(7)}$$

3. Point Load P at the Crack Surface of Symmetrical Crack in Infinite Body

The situation is shown schematically in Fig. 3. The closure load is given by:

$$K_{cl} = P / \sqrt{\nu \pi a \nu} \sqrt{2}/c/a-1 \qquad \ldots \text{(8)}$$

The expressions developed above have a sound analytical foundation and can be used as a basis for verifying the finite element results.

B. Finite Element Approach to Computation of Stress Intensity Parameters

The problem of describing crack closure eventually reduces to finding K for any given crack/load geometry. This can be done numerically using the finite element (FE) approach. In this approach, K may be obtained by several means after the stresses and strains in the cracked body have been determined. The simplest and most obvious approach is to relate the analytical solutions for the near-crack-tip stress and displacement fields to the values obtained from FE analysis. K is then determined as a fitting parameter that brings the analytical solution into close agreement with the FE results. Of course extrapolation procedures are

3

required to force the fit in the near-crack-tip region. For linear elastic problems, the strain energy release rate, G, can be associated with infinitesimal crack advance to obtain K. Two different FE analyses are required to obtain the strain energy differences for two very close but different crack lengths. In a somewhat similar way, the J-integral can be used for elastic/plastic problems. The following sections report FE results using a variety of approaches. These include:

1. Extrapolation at $\theta = 180°$ from the crack tip,
2. Singular element techniques using so-called quarter point elements,
3. Virtual crack extension,
4. J-integral and
5. Strain energy release rate using the nodal release technique.

1. Results of FE Calculations

A center-cracked thick plate with 2 symmetric point loads applied on the crack face, Fig. 4, was adopted for the initial study of closure by the FE technique. Because of symmetry, only half of the specimen was modelled, Fig. 5. Two different FE meshes, composed of 450 and 677 quadratic, iso-parametric elements, were used. The first mesh, shown in Fig. 6, was used for the extrapolation and quarter point element techniques. The second mesh was used for the virtual crack extension, J-integral and strain energy release rate methods. The results are compared to each other and to the theoretical values in Tables 1 and 2 and Figs. 7-9.

2. Assessment of Results

a. Extrapolation Singular Element Technique

The results are shown in Table 2 and Fig. 8. It was found that the calculated K's depend very much upon modelling a singularity dominated zone from the eigenvalue analysis and a trial-and-error mesh discretization. Furthermore, if a point load is applied extremely close to the crack tip, the resulting localized deformation at that position gives difficulty in extrapolating the stress intensity factors as a function of distance from the crack tip. This is shown quite clearly in Fig. 9. This problem cannot be eliminated if the displacements on the crack surface at $\theta = 180°$ are used in the evaluation.

b. Virtual Crack Extension and J-integral Techniques

The size of the perturbed area and the J-integral path affect the results. If such a path or area includes an applied point load, the errors in K are increased. This is shown in Fig. 7.

4

There is no way to exclude a point load from the perturbed area or J-integral, however, if a point load close to the crack tip is considered.

    c.   Strain Energy Release Rate Technique

    This method produces fairly good results and requires only whole calculation for any given geometry loading. The degree of agreement is shown in Fig. 7.

C.   Principal Results of Analytical/Numerical Studies

    To date the analytical studies have shown that not only closure loads need to be considered in evaluating the effective stress intensity range but also the details of where the interference or closure load occurs. Of course the calculations have been made only for idealized cases but the results tend to support one of the basic premises of this study viz. more care needs to be taken in incorporating closure measurements into expressions for K. We have also demonstrated that computations can be made for K using a number of different FE approaches and that at least one approach (i.e. the strain energy release rate) gives excellent agreement between the analytical expressions and the numerical results.

D.   Analytical/Numerical Activities for Next Year

    During the next year, cases of increased complexity will be considered. For example, the next increase in difficulty will be to consider an elastically deformable interference. After that we will consider an interference that is elastic/plastic but which retains a simple cylindrical geometry. After completing those tasks, we will then do a finite element computation of K for our exact specimen geometry. When we demonstrate that this can be successfully done, we will then begin to model roughness induced closure that arises from an actual crack surface. This will be done by first measuring the appropriate statistical parameters from the fracture surface (e.g. roughness, mean asperity height, asperity spacing etc.) and then making a two dimensional idealization of the surface. With this we will do finite element calculations to compute stresses and strains for various simple cases (e.g. constant asperity height and spacing, non-deformable asperities etc.). Finally we will compare those results to currently used expressions for K_{eff} to see what degree of agreement

5

exists.   In the final phase of the project, "real" fracture
surfaces with elastic/plastic asperities will be considered.

III. Experimental Studies of Crack Closure

There has been considerable activity both in the macroscopic
testing of samples and in development of in situ x-ray computed
tomography (CT) and x-ray tomograpic microscopy (XTM) for study of
crack closure.   The following two sections detail these results,
and the third section describes plans for the next years' research.

A.   Selection of Material and Sample Geometry

The Al-Li alloy 2090 was chosen because of the magnitude of
the crack closure effects and because of the large available data-
base developed by NRL and ONR researchers.   Studying this system,
therefore, allows maximum effort to be devoted to studying closure.
All samples will be taken from the center portion of the sheet of
2090 which was used in the earlier NRL/ONR study.

Two sample designs have been chosen (Fig. 10).   Correlation
of macroscopic measures of closure with XTM data on physical
processes will utilize the side grooved compact tension sample.
Dimensions were selected to allow maximum x-ray transmissivity
while still remaining within ASTM specifications.   The early XTM
work will concentrate on the notched tensile samples; the goal of
this is to demonstrate that physical changes in the crack can be
seen and to perfect our capabilities for in situ loading.

B.   Testing of Specimens on Conventional Servohydraulic Machines

The principal effort in this portion of the project centered
on preparing partially-cracked notched tensile samples for proof-
of-principle XTM characterization of crack closure effects.   This
sample geometry is ideal for XTM in situ loading studies, will
reveal any unanticipated difficulties before experiments with the
more difficult compact tension specimens are underway and will
allow XTM's ability to quantify crack face displacements to be
assessed.   In addition to the six notched tensile specimens, two
notched compact tensions samples were tested.

1.   Notched Tensile Specimens:

The first sample (NT-1) failed prematurely during an attempt
to monotonically load it to failure.   Initially, the sample was
loaded to stress of 714.3MPA at the base of the notch, which was
the maximum load of the low pressure hydraulics.   Failure occurred
during specimen installation in high pressure hydraulic mode.

The second sample (NT-2) was yielded monotonically prior to
growth of a fatigue crack.   The stress-displacement curve deviated

6

from linearity at 75.4MPa, and a maximum stress of 675.5MPa was reached. The test was performed at constant load until the crack growth became unstable. The effective diameter (i.e. crack "length") was calculated assuming that all changes in compliance were due to cracking in the notched area. No cracks were observed visually except at the base of the notch.

The remaining few samples were not overloaded prior to fatigue crack growth. The load required to initiate crack growth was approximately 186MPa to 193MPa. The loads were decreased during testing to keep crack growth rates below 10^{-4}mm^2/cycle. Below this growth rate, crack growth was stable. The effective diameters of the samples range from 1.680mm to 1.848mm after crack propagation was ended. The change in effective diameter ranges from 110μm to 358μm. The tests were stopped at various crack lengths so that the effects of crack length on closure could be investigated. Figure 11 shows all of this "crack growth" data, and interpretation of this data is presently underway.

2.   Compact Tension Specimens

The side grooved compact tension specimens have been designed to constrain the crack tip to a plane. The side grooves are 0.005 in. deep on both sides of the samples, and the remaining specimen thickness is 0.069 in (Fig. 10). The experience of NRL researchers on fatigue testing of this alloy was fully used to minimize duplication of effort. A considerable amount of white powder, apparently aluminum oxide, was extruded from the crack while the test was running. This environmental interaction was unexpected and may explain the variation of crack growth rates reported below from those reported by NRL investigators.

The first sample was tested (CT-1) at $\Delta K=11$MPam$^{1/2}$ for crack initiation. The crack began to grow within the first 20,000 cycles. The load was decreased periodically in an attempt to obtain maintain stable crack growth for a/W approaching 0.75. The rate of load shedding might have been too great, since the plots of ΔK vs da/dN (Fig. 12) indicate load interaction effects. Some of the apparent load interaction effects may also have been caused by the crack path. The crack tip was observed to grow up onto the side grooves, the crack growth rates decreased. As the crack tip returned towards the base of the side grooves, the crack growth rates increased rapidly.

The first sample failed at a/W=0.7274 with $\Delta K=25.54$MPam$^{1/2}$. The sample deflection at large a/W was very significant as were the effects of closure. The observed crack growth rate at failure was decreasing due to the crack tip wandering up the side groove.

The second sample, (CT-2), used $\Delta K=15$MPa$^{1/2}$m for crack initiation. The load was decreased after crack initiation in an attempt to reduce ΔK below 8MPam$^{1/2}$ for the start of a constant

load test. The lowest ΔK reached was $9.2 \text{MPam}^{1/2}$ at a/W=0.32, and the load was then increased so that $\Delta K=11.8 \text{MPam}^{1/2}$. The load was decreased when ΔK reached $17.2 \text{MPam}^{1/2}$, and a constant load was used to grow the crack to a/W =0.576 and $\Delta K=21.0 \text{MPam}^{1/2}$. After decreasing the load, the test was stopped at a/W=0.5987 for radiographic and industrial CT examination with and without load at General Electric Corporation (described in the section on future work).

A summary of crack growth data for these two samples is shown in Fig. 13 and interpretation of the data is presently underway.

C.   X-ray Tomographic Microscopy

The notched tensile samples have only recently been available for XTM characterization of cracks, and no synchrotron time has been available since then. One preliminary characterization run was recently completed using x-rays from conventional generators.

The first used the Lawrence Livermore National Laboratory (LLNL) apparatus whose CCD-based design allows multiple hundred slices to be recorded simultaneously. A broad focus silver tube was used so that penumbral blurring limits resolution to no better than $12\mu m$. The crack in a notched tensile specimen was not detected due to an apparent shift in the x-ray spot: the unusual distribution of absorption in background pixels indicates this kind of blurring occurred. A second laboratory scan has not yet been run.

Proposals for beam time at SSRL (Stanford Synchrotron Radiation Laboratory), CHESS (Cornell High Energy Synchrotron Source) and NSLS (National Synchrotron Light Source) were prepared during the first year of the proposal. The ratings for the CHESS and NSLS proposals were 9.0 (scale of 1-10, with 10 being the highest priority) and 2.0 (scale of 1-5, with 1 being the highest priority), respectively; the SSRL proposal has been refereed but not yet rated. Time at NSLS was scheduled in March, but it had to be abandoned due to mid-fiscal year cuts to our collaborators budget.

A number of adjacent, industrial CT slices have been obtained from a large compact tension sample (2" width), of Cu-1% Sb which was deformed in creep (this work would have been done on a similar sized Al-Li sample but none were available); the purpose of this was to gain experience in data analysis similar to that which will be required in interpreting the XTM data of the closure process. The creep process in this sample resulted in a non-planar crack, and this part of the project has focussed on finding economical means of representing the two surfaces and on acquiring ability to transport the CT/XTM data between computer systems and between graphical software packages, a non-trivial operation. By dealing

with this early in the program, we hope to eliminate potential bottleneck after the XTM data is obtained.

D.   Micro-Tensile Load Frame:

The in situ tensile stage has been designed to load a sample and maintain that load during XTM data collection (Fig. 15). The loading will be accomplished by using a pneumatic cylinder and a polycarbonate standoff tube. The standoff tube is nearly transparent to the x-ray energies to be used. Sample rotation and translation will be performed by the XTM apparatus. The stage has been designed to fit onto the LLNL XTM apparatus or to fit onto the new LHMC XTM apparatus (currently being constructed in collaboration with LHMC). An alternative design has been developed in the event the current configuration causes too much x-ray signal attenuation. Nearly all of the components have been assembled and all parts have been constructed; we anticipate having tested the stage by the end of April.

E.   Experimental Activities for Next Year

A very full experimental program is planned for next year. Emphasis in the conventional servohadraulic testing will be on the compact tension samples. Thus far crack growth rates in these samples have been somewhat different from those reported earlier; this will be addressed early in the year for addition to this mechanical testing, other samples will have cracks grown to predetermined lengths before the cycling is ended. These will be used for in situ XTM loading studies. Experiments are scheduled at SSRL at the end of April; this should be the first in situ XTM loading experiments. There will also probably be XTM experiments at CHESS later this year.

We also anticipate other experimental time becoming available (through Georgia Tech proposals) after December 1990 when the SSRL dedicated injector comes on line. It is hoped that the XTM characterization of closure in the notched tensile samples will be complete by the end of the program's second year; analysis of these results will almost certainly extend well into the third program year.

The synchrotron XTM characterization will also be supplemented by laboratory XTM at LLNL and LHMC when needed. The resolution is poorer with the instruments, but the additional slices which can be obtained will allow a more complete picture to emerge. The first in-situ characterization of physical closure in compact tension samples is planned using the G.E. industrial CT apparatus. There is no difficulty in penetrating the sample with their x-ray source, and the as-tested sample will be examined in the in situ loading apparatus. Resolution will be quite poor compared to XTM

but it should be sufficient for much to be learned. This will be, we believe, the first tomography study of in situ loadings, and, as such, will be of intrinsic importance.

IV. Personnel

The following personnel have worked on the project

A. Principal Investigators

1.	Stephen D. Antolovich	Fracture Mechanics, analytical studies, mechanical testing issues
2.	Stuart R. Stock	Tomography, radiography, specimen design, primary contacts with synchrotron sources, design of rig, mechanical testing issues

B. Students

1.	Thomas Breunig	Design of tensile rig, mechanical testing, tomography data acquisition
2.	Abbas Guvenilir	Assistance with design of experiments, analysis of data, tomography data acquisition
3.	Y. Jung	Finite element calculations

V. Interactions

Interaction with other groups is important to the success of the project. The following interactions have been (or are being) established:

	Organization	Person	Comments
1.	Lawrence Livermore National Lab	John Kinney	Active collaboration software, laboratory and synchrotron x-ray tomographic microscopy
2.	Southwest Research Institute	David Davidson	Continuing discussion on closure

3.	CNAM (France	C. Bathias	Discussions of closure in AL-Li alloys, discussions on possible use of his laboratory CT system
4.	General Electric	R. Issacs	Began laboratory CT at GE, Evendale, OH
5.	Stanford Synchrotron Radiation Laboratory	-	Proposal for beam time
6.	National Sychrotron Light Source		Proposal for beam time
7.	Cornell High Energy Synchrotron Source	-	Proposal for beam time

Table 1. Comparison of $K_1/P \mapsto \sqrt{\pi a}$

	$K_1/P \mapsto \sqrt{\pi a}$			
c/a	$\sqrt{\dfrac{2}{c/a} - 1}$	V.C.E.T.* out of zone	V.C.E.T.** within zone	S.E.R.R.***
0.1	4.36	2.32	0.44	4.3
0.2	3.0	2.21	0.55	2.94
0.3	2.38	2.03	0.93	-
0.4	2.0	1.99	1.99	2.02
0.5	1.73	1.77	1.77	-
0.6	1.53	-	-	1.5
0.7	1.36	1.39	1.39	-
0.8	1.22	-	-	1.22
1.0	1.0	0.98	0.98	1.0
1.6	0.5	-	-	0.6
2.0	0.0	-	-	-

* S.I.F.s are evaluated by Virtual Crack Extension
   Technique using data out of the perturbed zone.
** S.I.F.s are evaluated by Virtual Crack Extension
   Technique using data within the perturbed zone.
*** Strain Energy Release Rate Method.

Table 2. Comparison of $K_1/P \mapsto \sqrt{\pi a}$

	$K_1/P \mapsto \sqrt{\pi a}$		
c/a	$\sqrt{\dfrac{2}{c/a} - 1}$	Extrapol. Technique	Q.P.E.*
0.17	3.28	-	3.66
0.29	2.43	1.95	2.68
0.45	1.86	1.75	2.06
0.67	1.41	1.35	1.55
1.0	1.0	0.98	1.11

* Quarter Point Element has a length of
   0.4 a.
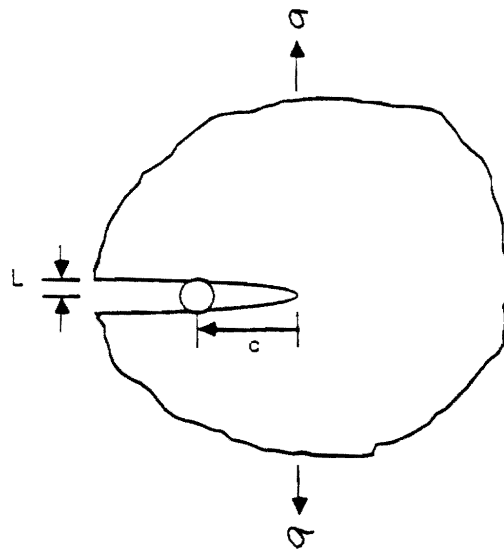
Fig. 1 Asperity in infinite body.
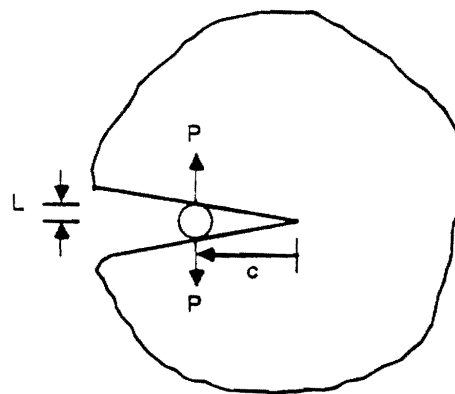
Fig. 2 Asperity in infinite body.
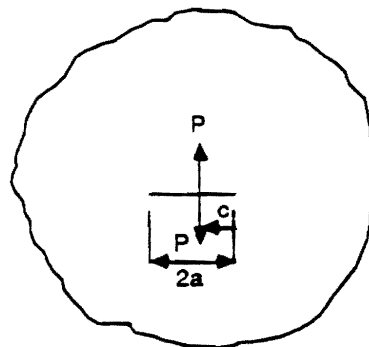
Fig. 3 Point load in infinite body.
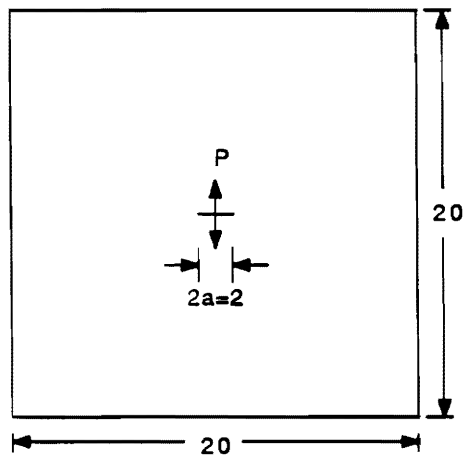
Fig. 4 Specimen Geometry
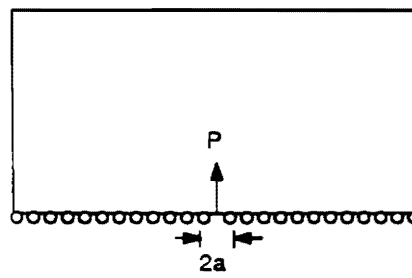
Fig. 5 Half Model
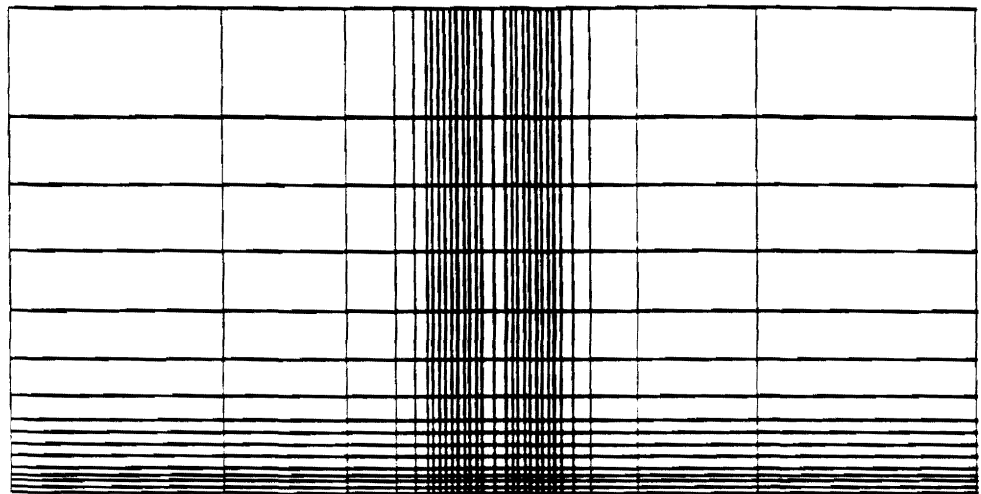
Fig 6(a). Finite Element Mesh (Total 450 Elements)
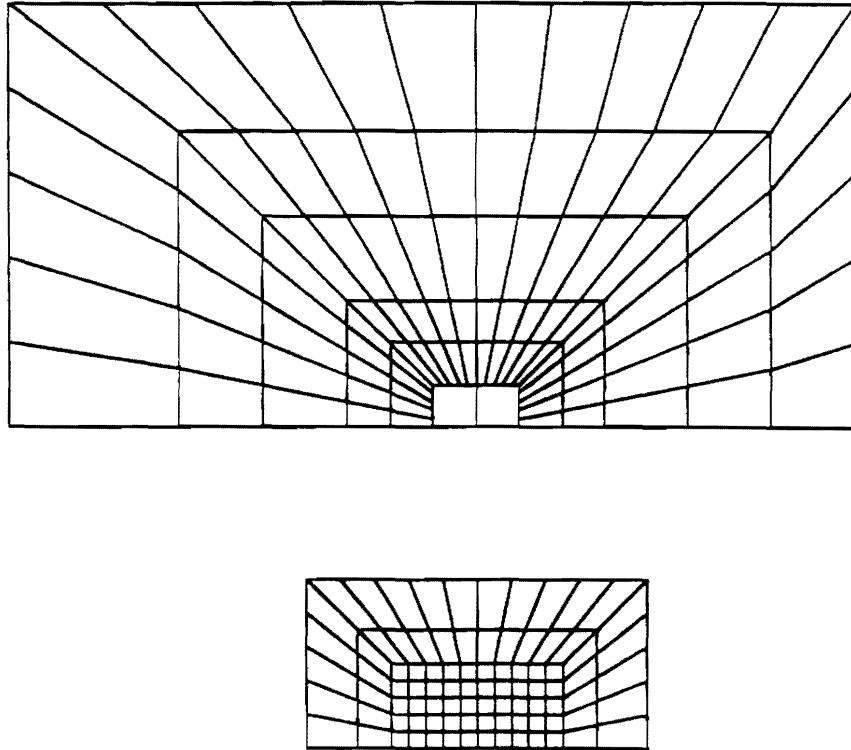
Fig. 6(b)   Finite Element Mesh (Total 677 Elements)
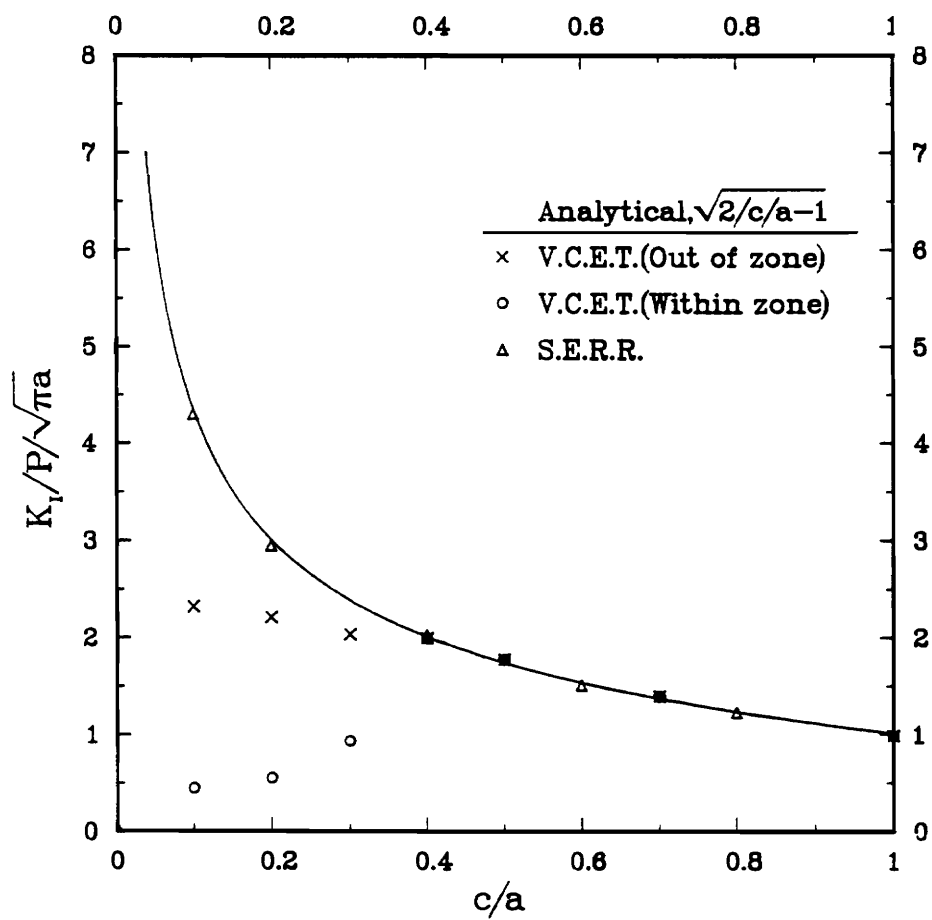
Fig. 7 Comparison of $K_I/P/\sqrt{\pi a}$
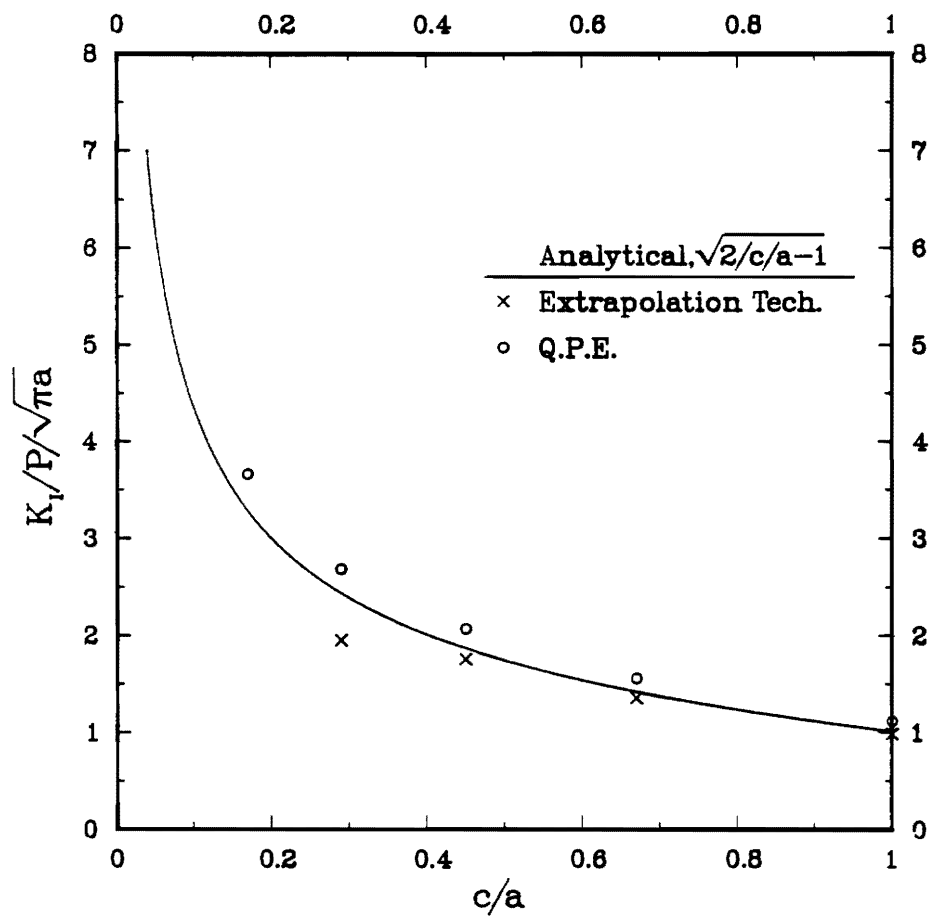
Fig. 8 Comparison of $K_I/P/\sqrt{\pi a}$
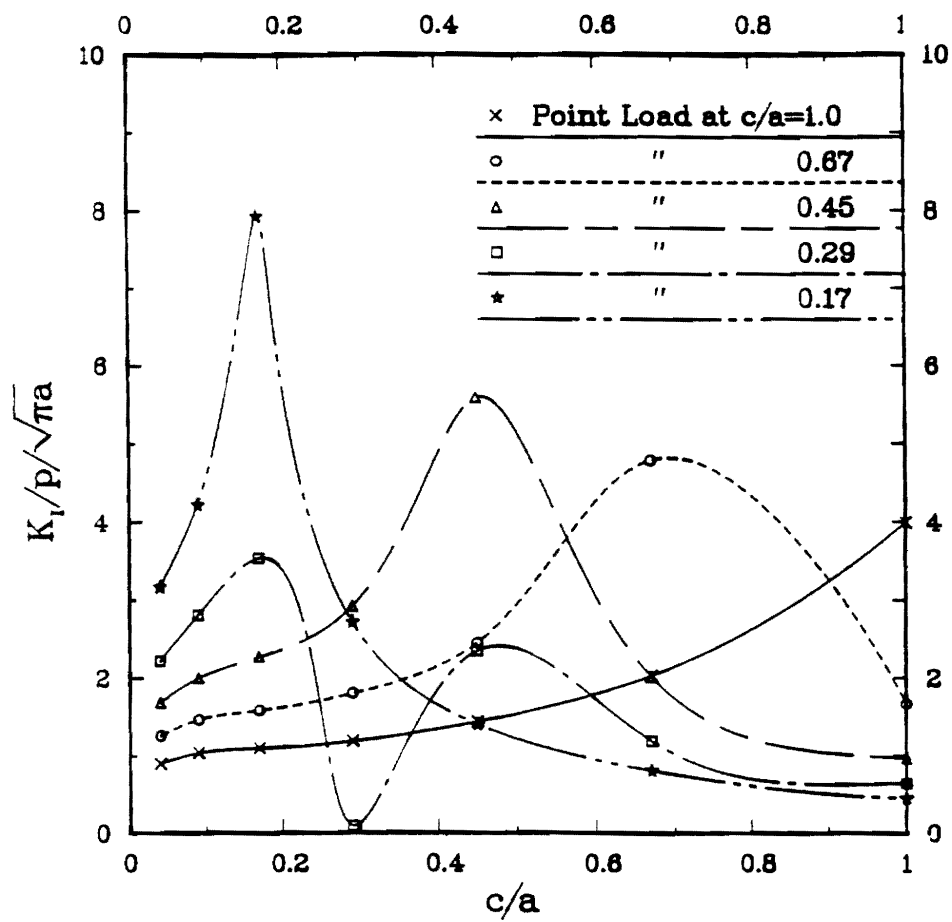
Fig. 9 $K_I/P/\sqrt{\pi a}$ in Extrapolation Tech.

TOOL MARKS IN THICKNESS DIRECTION. TOOL MARKS WILL BE CAUSE FOR RETURN FOR FURTHER TREATMENT.

OTE 2 – NOTCH ROOT CENTERLINE SHALL BE CONCENTRIC WITH THE CENTERLINE OF THE SLOT.

OTE 3 – CENTERLINE OF SIDE-GROOVES MUST BE COINCIDENT WITH NOTCH CENTER-LINE WITHIN ±0.001.

CENTER OF PLATE.

$45° ± 2°$

$0.005 ± 0.001$

◎ | .001 | B

SEE NOTE 3

DETAIL B
NOT TO SCALE

Figure 10a. Side-grooved Compact Tension Sample Geometry

⟋ | .002
—A—

∥ | .002 | A

$0.100 {}^{+0.005}_{-0.000}$

—B—

0.093

16   16

—C—

1.250

[1.000]

0.800

SEE DETAIL A

0.275

0.275

1.200

0.600

—D—

SEE DETAIL B

16

$0.250 {}^{+0.002}_{-0.000}$

⊕ | .001 | A | C | D

2 HOLES

DETAIL A
NOT TO SCALE

$40° ± 2°$ SEE NOTE 2

◎ | .005 | B

$0.010 ± 0.001$ R
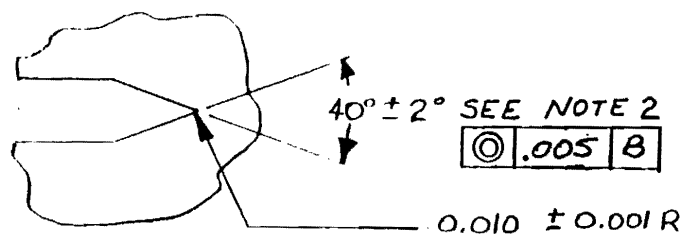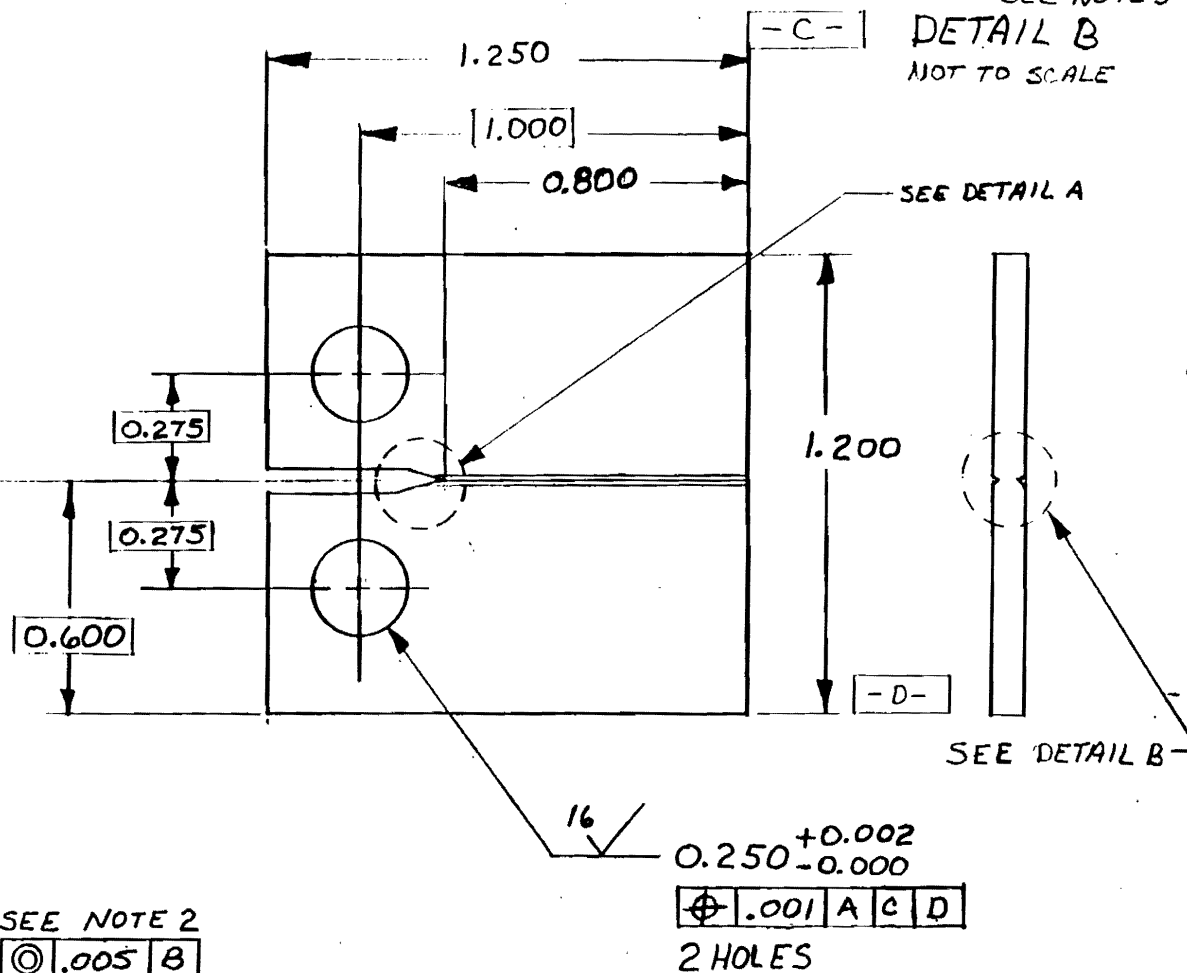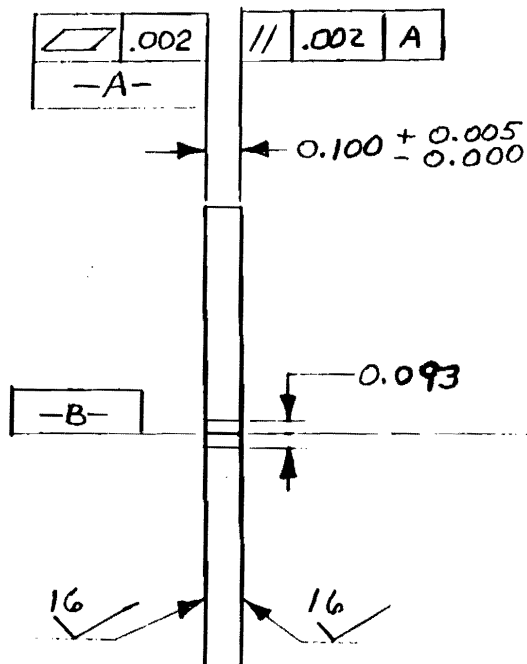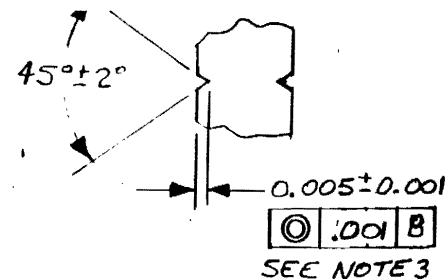
SCALE = 2:1   TOLERANCE = ±0.005   SURFACE FINISH = 32

Figure 10b.   Notched Tensile Sample

MATERIAL: ALUMINUM-LITHIUM
ALLOY 2090

(0.211)

0.289±0.005

0.093R
BOTH ENDS
SEE NOTE 2

0.079±0.001

⊙ | .001 | A

60°±5°

SEE NOTE 1

Ø 0.113±0.002

— A —

0.625±.005

0.313±0.005

1.203±0.010

(0.289)

(0.211)

0.250-28 UNF   ⊙ | .001 | A
BOTH ENDS
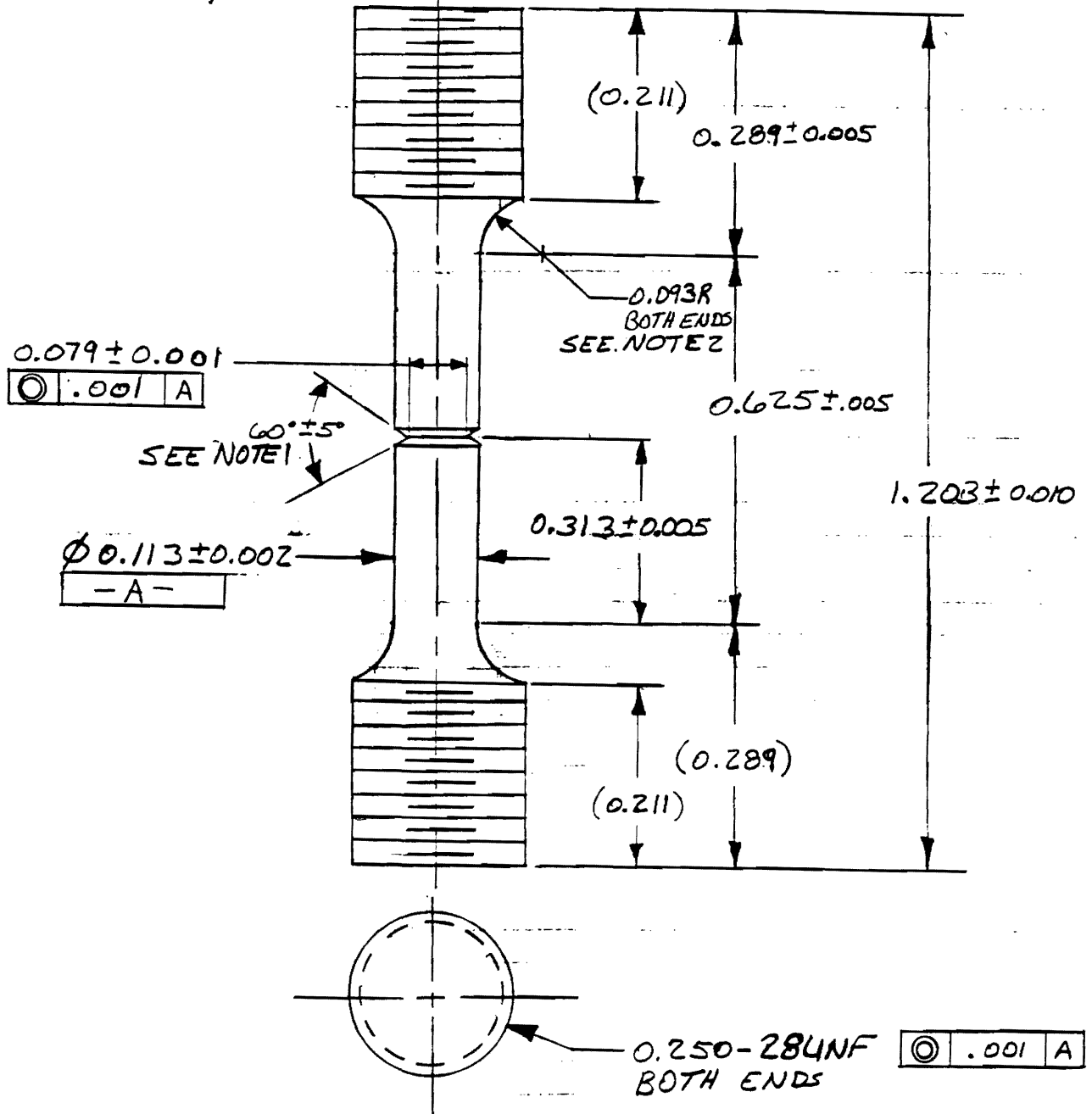
NOTE 1:   NOTCH ROOT RADIUS REQUIRED IS 0.0007. THE
FINAL CUTS SHALL BE LIGHT AND SLOW, TO AVOID THE INTRODUCTION
OF SIGNIFICANT RESIDUAL STRESS. THE NOTCH TIP RADIUS SHALL
BE MEASURED PRIOR TO TESTING AND ANY SPECIMEN THAT
DOES NOT MEET THE 0.0007 LIMIT SHALL BE RETURNED
FOR FURTHER TREATMENT.

NOTE 2: NO UNDERCUTS ARE ALLOWED.

NOTCH DETAILS ARE PER ASTM E-602

Al−Li NOTCHED TENSILE FATIGUE CRACK GROWTH
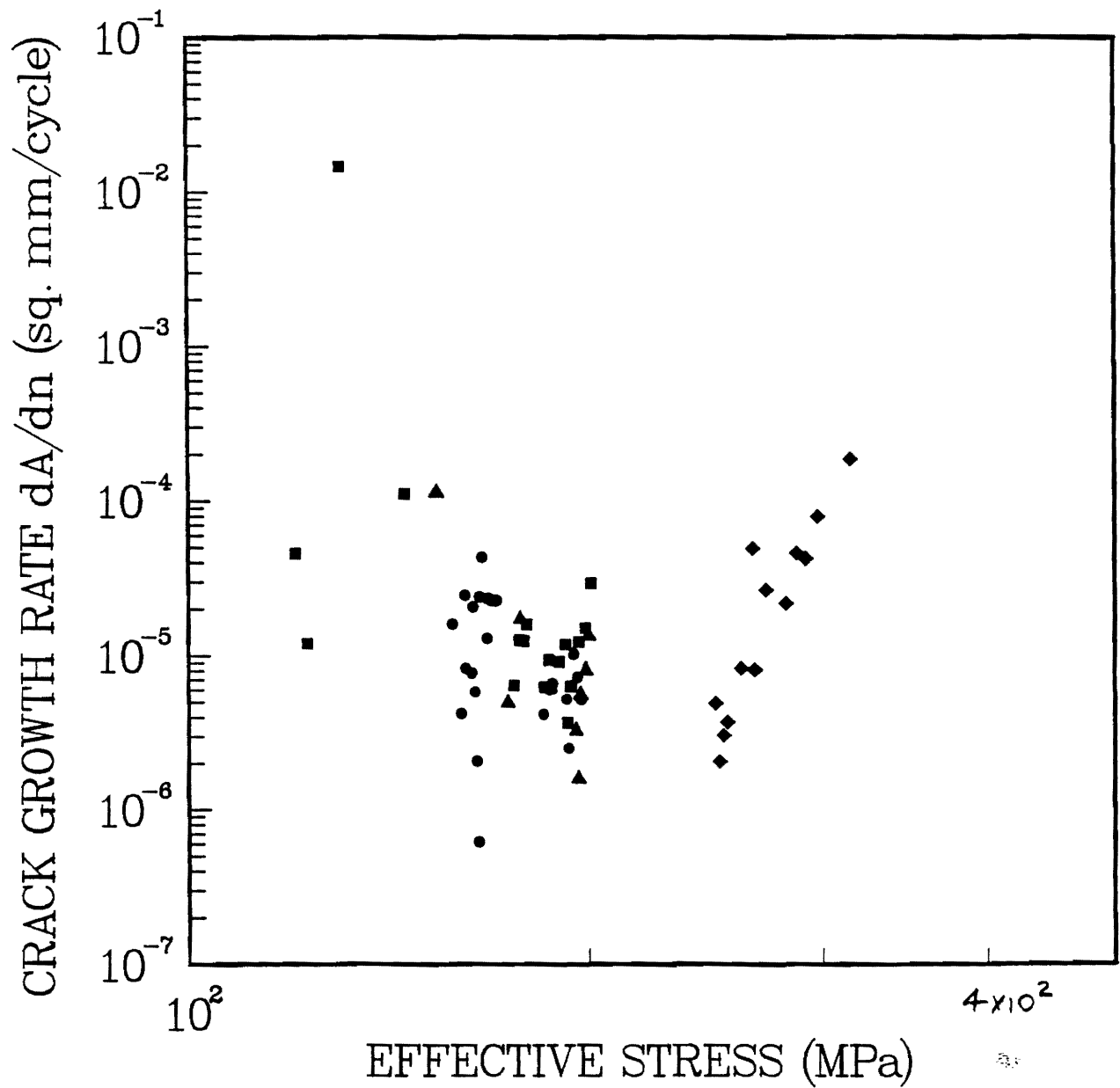
Figure 11. Crack Growth Rates for Notched Tensile Samples
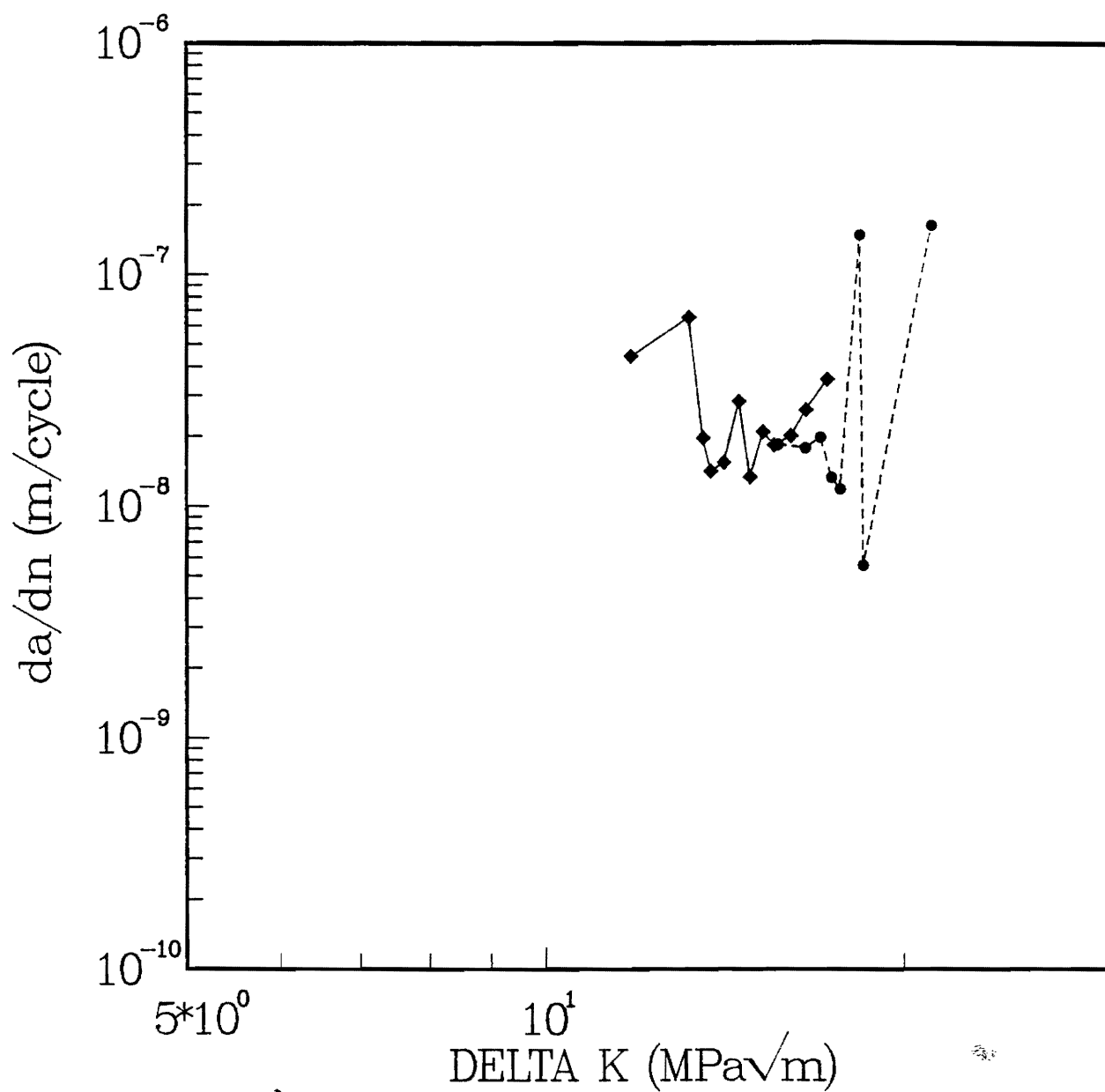
Figure 12. Data for CT-1.

Al–Li COMPACT TENSION FATIGUE CRACK GROWTH
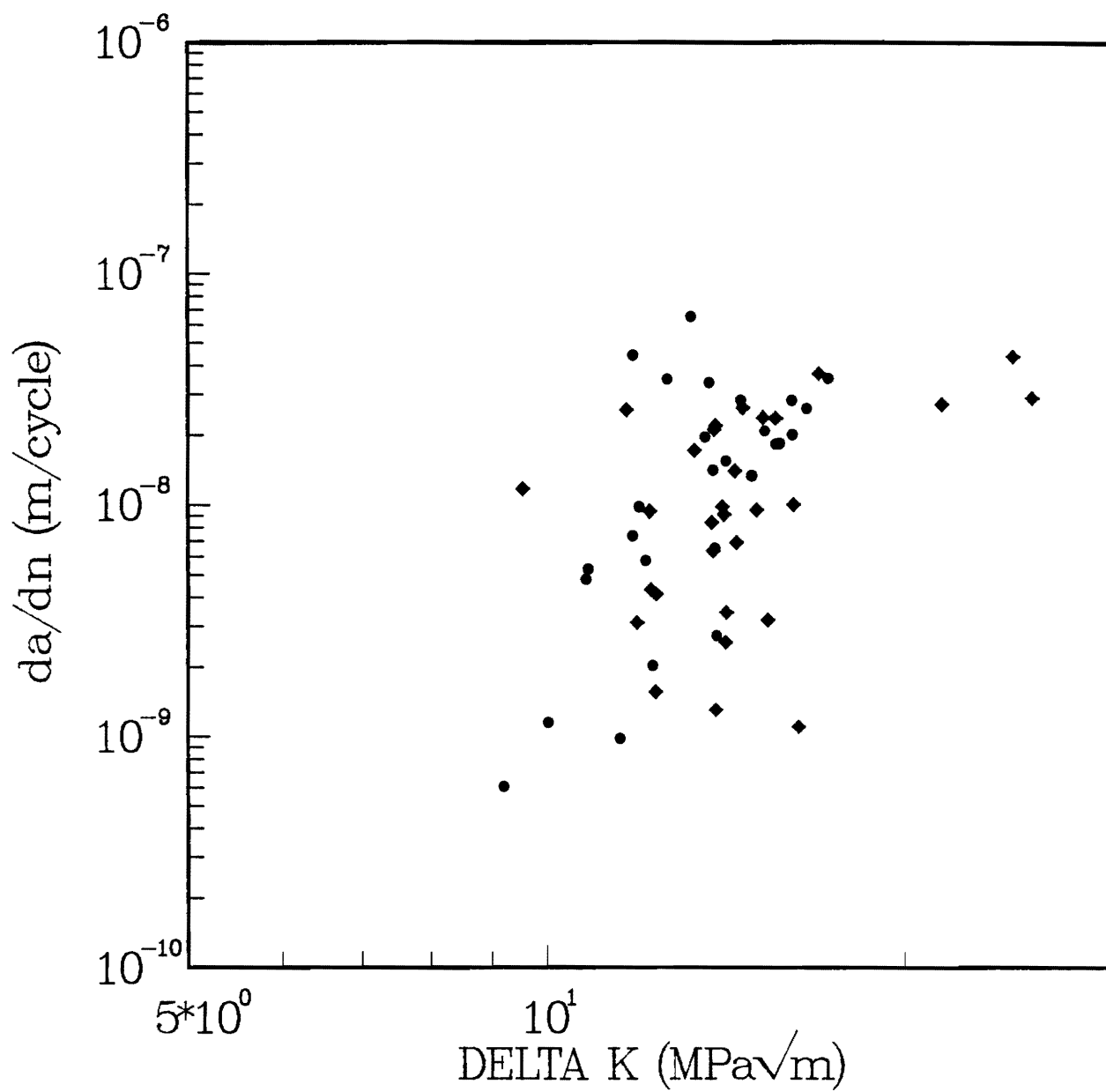
Figure 13.   Summary of Data for CT-1 and CT-2.
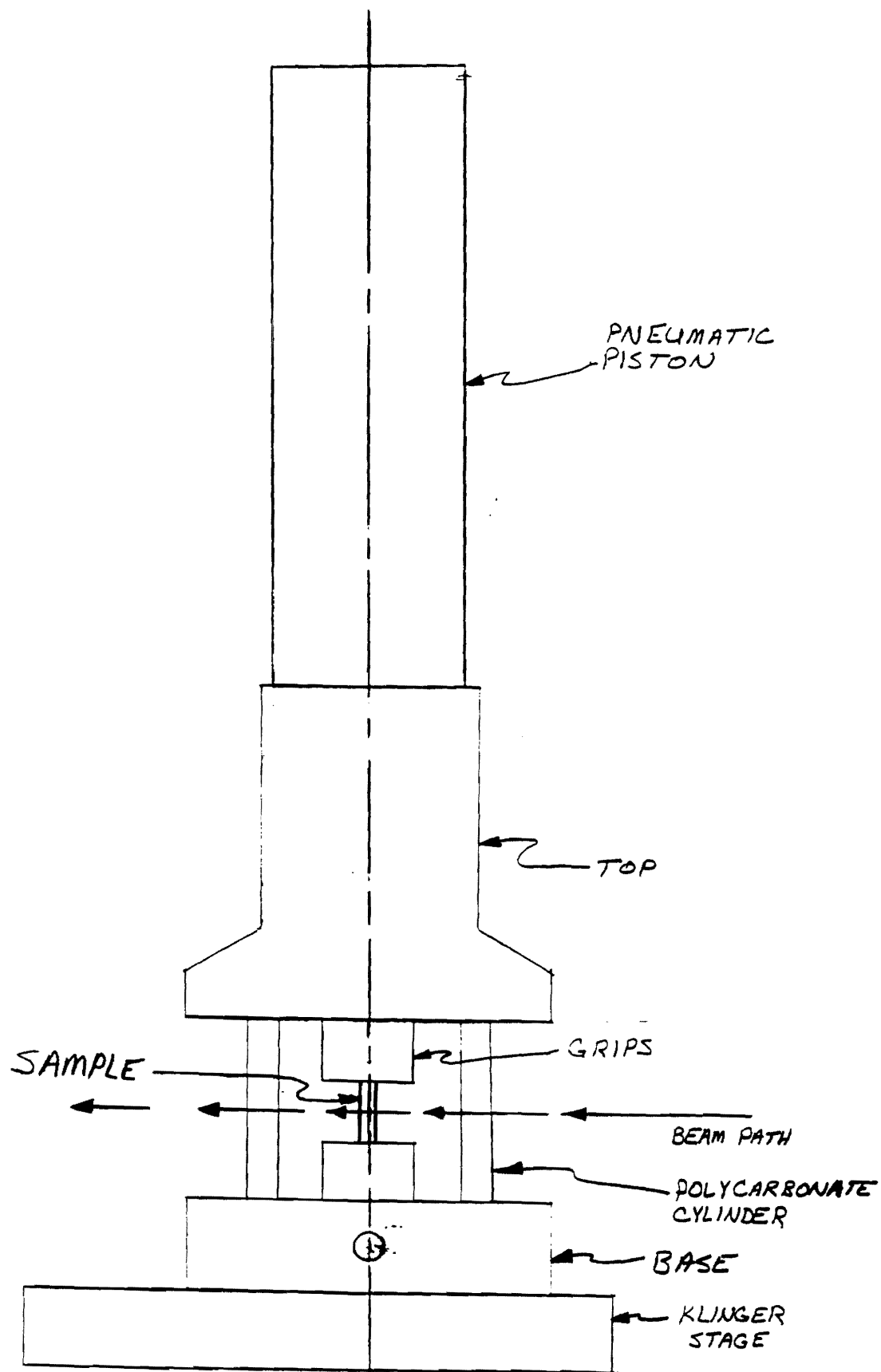
Figure 14. An in-situ load device designed such that a 180° scan of the specimen can be made with minimal x-ray attenuation and distortion in the support member.

Georgia Tech

June 14, 1991

Dr. R. C. Pohanka
Code 1131
Office of Naval Research
800 N. Quincy Street
Arlington, VA 22217-5000

Dear Dr. Pohanka:

Enclosed is a copy of the annual report on the ONR-sponsored project entitled "Study of the Relationship Between Macroscopic Measures and Physical Processes Occurring During Crack Closure". The contract # is 89-J-1708 and the R & T # is 4311931. The ONR Scientific Officer is Dr. George Yoder.

Should you have any questions, please do not hesitate to contact me or Dr. Stuart R. Stock.

Sincerely,

Stephen D. Antolovich
Director and Professor
School of Materials Engineering

Enclosures

cc: Dr. Stuart R. Stock
     Dr. George Yoder

Annual Report for
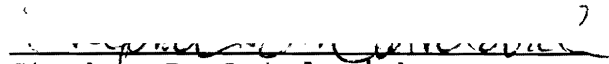
A Study of the Relationship Between Macroscopic
Measures and Physical Processes Occuring during

N0014-89-J-1708

submitted to:

by

Stephen D. Antolovich   Stuart R. Stock
Mechanical Properties Research Lab Mechanical Properties Research Lab
School of Materials Engineering   School of Materials Engineering
Georgia Institute of Technology   Georgia Institute of Technology
Atlanta, GA 30332-0245   Atlanta, GA 30332-0245

TABLE OF CONTENTS

TABLE OF CONTENTS - CONTINUED

I.   Physical Measurements of Crack Closure

A.   Accomplishments during the past year

The principal experimental accomplishments during the second year of the program were two sets of x-ray tomographic microscopy (XTM) measurements on notched tensile samples. Fatigue crack growth was in a conventional servo-hydraulic machine before the samples were mounted in the in situ load frame. The particulars for crack growth were: R=0.1 and 5 Hz haversine waveform. Some alteration of the maximum load was used; these details are outlined in the technical publications. Once the samples were gripped in place in the minature load frame (pictured with the CCD x-ray camera in Fig. 1), the sample was loaded to the maximum level (a load equal to or slightly less than that used to propagate the crack, depending on whether the crack was propagating stably at the end of crack growth in the servo-hydraulic apparatus) and was allowed to equilibrate mechanically. The first set of projections were then recorded. The load was decremented by a pre-determined fraction of the maximum load for that sample, and another set of projections was recorded. This progression was repeated until data for reconstructions was obtained for all desired loads. Reconstruction of slices of the sample followed the end of the experiments and was with the filtered back projection method.

The choice of the extremely small (by fracture mechanics standards) samples was dictated by the need to have good sample transparency at the synchrotron x-ray energies with the highest fluxes (typically up to about 25 keV before the flux starts to drop dramatically). A second consideration limiting the sample diameter is the number of detector elements and the maximum cross-sectional dimension of the sample: a 10 mm diameter sample sampled with 10^3 detector elements yield a minimum pixel dimension of 10 μm; closure measurement requires pixels smaller than this. An unanticipated advantage of the smaller sample size is that the load-displacement record shows features which are normally not present in traces of larger samples. Presumably this is due to more "averaging" in larger samples. The enhanced sensitivity will be very interesting to interpret. As is noted in the future work section, XTM should be able to obtain similar resolution images in both large (10 mm maximum diameter) and small (2 mm diameter) samples if region-of-interest (ROI) sampling techniques are used whereas the sensitivity of stiffness measurements cannot be preserved.

The first notched tensile sample examined with XTM (NT-3) had an initial diameter of 2.09 mm, and at the end of the test (after 61850 cycles) the crack had decreased the effective load-carrying cross-section of the sample to 1.85 mm (as measured by the change in compliance of the sample). The original plan was to collect data at Stanford Synchrotron Radiation Laboratory (SSRL) in April 1990 using beamtime assigned to our collaborators at Lawrence Livermore National Laboratory (LLNL); the Georgia Tech proposal for crack closure

1

measurements, however, was not yet eligible for beamtime. Some very curious choices were made by those responsible at LLNL for assigning their portion of beamtime on beamline X; no time was given to our collaborators at LLNL despite their strong record of scientific accomplishment and the fact that they were the only LLNL group (using synchrotron radiation) to obtain external funding for their research. Instead of running at SSRL, the XTM experiments were performed at Dr. J.H. Kinney's laboratory at LLNL using a standard sealed tube x-ray source.

The experiments at LLNL were very successful. The x-ray source was an Ag tube with effective spot size of 1 x 1 mm^2 (producing penumbral blurring of about 13 μm at the CCD detector-- compared to essentially no penumbral blurring for synchrotron radiation experiments) and was operated at 40 kV and 30 mA. One sample was characterized during the experiment; loads of 81.7, 50.0, 25.0, 4.5 and 0 kg (95, 58, 29, 5 and 0 %, respectively, of the maximum load under which the crack propagated) were studied. The 2.9 mm diameter slice, shown in Fig. 2, was reconstructed with 6.2 μm pixels using 1 deg angular increments between views. Note that the slice was from just above the center of the notch and that the data was obtained at an applied load of 81.7 kg. The nonplanar fatigue crack was also clearly visible in many of the other simultaneously recorded slices.

It was found that a better way to visualize the three-dimensional crack (short of volume rendering!) was to use "cuts" parallel to the load axis instead of slices perpendicular to the load axis. The cuts shown in Fig. 2b-2d were obtained for 81.7, 50.0 and 25.0 kg loads; the scales throughout Fig. 2 were chosen to be identical. The same volume of material was sampled in the 6.2 μm thick cuts. Changes in crack opening were quite pronounced, and parts of the crack disappeared at low applied loads. Comparison of the cuts with a digital radiograph were quite revealing: even at high load the crack was invisible in radiographs (i.e. individual views) but the computed tomography reconstruction process allowed the volume of material outside of the cut of interest to be stripped away.

The fatigue crack in a second notched tensile sample (NT-4) was characterized at Cornell High Energy Synchrotron Source (CHESS) during September 1990. The sample's initial diameter was 1.89 mm, and the effective decrease in sample cross-section was 110 μm after 34,760 cycles. The testing parameters were the same as given above. The object in stopping the crack growth at a relatively short length was to test the sensitivity of XTM to the smallest range of crack openings one would be likely to encounter and to allow the crack to be grown further for additional XTM characterization. Looking at the same crack before and after it extends should allow ellucidation of the role of near-crack-tip closure and of contact "far" from the crack tip: the crack face positions near the crack tip in the first measurement could be compared, as a function of load, with the same faces, now far removed from crack tip, in the second measurement.

2

The XTM experiments at CHESS were also extremely successful and showed the ability of the GT/LLNL/Sandia team to perform the in situ XTM loading experiments in a routine fashion (at least of notched tensile samples!). The x-ray energy used to record the data was 22 keV, 1 deg angular increments were used between views and the sample volume containing the crack was reconstructed with 5.6 μm x 5.6 μm x 5.6 μm voxels. Ten load levels were studied: 45.5, 36.4, 27.0, 18.2 and 9.1 kg (100, 80, 60, 40 and 20 %, respectively, of the maximum load during the fatigue cycles preceeding the interuption of the test) on an unloading cycle and 40.9, 31.8, 22.7, 13.6 and 4.6 kg (90, 70, 50, 30 and 10 %, respectively, of the maximum load) on the next unloading cycle. Figure 3 shows a typical 1.9 mm slice under 45.5 kg load and three 5.6 μm thick cuts parallel to the load axis and through the same volume of material at 45.5 kg, 27.0 kg and 9.1 kg loads. In these cuts the crack is much less pronounced than in those of sample NT-3 which is expected because the crack in NT-4 is much shorter. It also is clear that the images are much sharper in the synchrotron data; this difference should persist, albeit much less prominently, even when a microfocus source (down to a 10 μm diameter spot size) is used to eliminate penumbural blurring in laboratory measurements.

Detailed analysis of the CHESS data is currently in progress. Crack opening in a given slice of the sample was the initial method used to quantify closure as a function of applied load. This simple approach appeared to be inadequate; large scatter in the opening measured in this fashion was superimposed on the overall decreasing crack width (for the corresponding pixel in different slices) as the load decreased. As the crack is at a significant angle to the slices (i.e. the crack's intersection with the slice was never planar), measuring changes in crack width in the plane of the slices would be particularly insensitive. A much more sensitive means of quantifying crack closure is to measure the crack opening in cuts parallel to the load axis; one can also easily focus on the tips of asperities and on the "peaks" and "valleys" of the zig-zag crack by using cuts. This work has begun, and the approach to be taken is described in the following section. One should note that one could also use the change in separation normal to the local crack faces as the measure of closure; plans for this type of analysis are described in the following section.

B.   Difficulties Encountered

Some difficulties which could not have been anticipated have been encountered during the past year. One was the difficulty obtaining beam time during SSRL's Spring 1990 run; this was described above. A benefit was that the laboratory XTM experiments on sample NT-3, the first for the in situ load frame (the first ever in situ loading during XTM), were conducted without the pressure of using every minute of beam time. Relatively minor problems (e.g. rubbing of the CCD detector faceplate and the stage's stand-off tube) were

ironed out without significant impact on the amount of data collected. The usefulness of laboratory XTM with the LLNL apparatus was clearly demonstrated; these results, even with the large penumbral blurring (which can be eliminated if a commonly available microfocus source is used), demonstrate that **XTM is a powerful technique for studying in situ materials processes--** a technique **which can be included in any laboratory.** The capital cost of the LLNL apparatus and a suitable x-ray generator are below those of a good SEM; the workstations required for apparatus control and data acquisition are relatively inexpensive, with prices rapidly decreasing. It should be possible to license the LLNL software if organizations wish to obtain first-rate XTM capabilities rapidly.

The second, more serious difficulty encountered was the need for considerably greater computing power <u>and</u> hard drive memory. The capabilities of the Micro VAX-II on which reconstructions have been performed and data analysis is done have been exceeded. Reconstruction of each slice requires about 45 minutes if this program is the only one being executed; current medium performance workstations require about 10 min per slice and a 40-processor SPRINT unit requires less than 0.5 min per slice. Also, the Micro VAX-II is required to operate in a multi-user mode, and some of the other users run fairly elaborate finite element programs. The competition tends to slow data analysis. A third area of concern is the availability of only 600 MBytes of storage for XTM data on the Micro VAX-II. This small size can be put in perspective by the following. The September run at CHESS brought back about **8 GBytes** of data on 8 mm tape, and a typical sample (e.g. a single load level in the present instance) occupies about 60 MBytes. If all ten loads recorded for NT-4 were on the hard drive at one time, no other work could proceed. One should note using supercomputers would require writing a considerable amount of code and would not address our data storage difficulties.

Contingency for upgrading computing capabilities was budgeted, and expenditure of these funds should improve the rate at which the closure data can be analyzed. Considerable leverage has been obtained with other funded programs. First, the School of Materials Engineering has designated two SUN workstations for use in XTM. These will be used for the most intensive numerical calculations (e.g. back projection) which will free the other computers for data analysis. A 1.2 GByte hard drive will be added to the SUNs. A second 1.2 GByte drive will be added to a DEC 3100 workstation (in the Georgia Tech Research Institute) which will also be available for XTM. Once these additions have been implemented, the bottleneck in processing the data should be reduced considerably.

II. Analytical Computations of the Effective Stress Intensity Factors

A. Rigid and Elastic Asperities in an Elastic Medium

In the previous report, some basic expressions for calculating the effective stress intensity factor for simple cases using a rigid cylinder were developed. In the present report, more realistic models for crack closure are analyzed by considering an asperity of an arbitrary shape which relates to different grain sizes and orientations. The width and the location of the asperity are parameterized. The same procedure as in the previous work is followed to obtain the effective stress intensity factor for rigid and elastic asperities between two crack surfaces. The appropriate models are shown in Figs. 4 and 5. The loading scheme and important quantities for crack closure are shown in Fig 6.

Considering the crack opening displacements due to the remote stress, σ, and the contact internal pressure, p', and the deformation of the asperity, the closure stress intensity factor in terms of asperity parameters and crack opening load, σ_{op} is as follows:

Case 1 $\sigma_{op} \geq \sigma_{cl} \geq - [\dfrac{C_i}{1 - C_i}] \sigma_{op}$

$$\frac{Ki}{\sigma_{op}\sqrt{\pi a}} = Ci + (1 - Ci)\frac{\sigma_{cl}}{\sigma_{op}} \qquad \dots (1)$$

(i=0, 1 for rigid and elastic cases respectively). C_0 and C_1 depend only on asperity properties. They are given by:

$$C_o = \frac{G'}{H} \qquad \dots (2)$$

and

$$C_1 = \frac{G'}{H + \dfrac{1}{4}(\dfrac{w}{a})\dfrac{1}{F}\alpha\pi} \qquad \dots (3)$$

Here, G', H and F are given as influence functions in the calculation of the stress intensity factor considering crack opening displacement for external and internal loads. The second term in the denominator of C_1 involving the asperity shape factor, α, accounts for elastic deformation of an asperity.

5

Case 2

(b) $\qquad \sigma_{cl} \leq - [\dfrac{C_i}{1-C_i}] \sigma_{op}$

$$K_i = 0 \qquad (i=0,1) \qquad \qquad \ldots(4)$$

Equations (1) and (4) are shown schematically in Fig. 7. The contact pressure between the crack surface and the asperity, Fig. 8, is calculated from:

$$\ldots(5)$$

$$P'_i = \dfrac{\pi C_i}{G'} (\sigma_{op} - \sigma_{cl}) \qquad (i=0,1)$$

Using the above results, the effective stress intensity factor is:

$$\Delta K = K_{max} - K_{cl} \qquad \qquad (6)$$
$$= [1 - C_i \dfrac{\sigma_{op}}{\sigma_{max}} - (1-Ci) \dfrac{\sigma_{cl}}{\sigma_{max}}] \sigma_{max}\sqrt{\pi a} \qquad (i=0,1)$$

When $\sigma_{cl} = \sigma_{op}$, there is no closure effect and ΔK is given by simply $(\sigma_{max} - \sigma_{op})\sqrt{\pi a}$. However, when $\sigma_{cl} = 0$, there is a factor of C_i in the opening stress, σ_{op}, i.e.

$$\Delta K = (\sigma_{max} - C_i \sigma_{op})\sqrt{\pi a} \qquad (i=0,1) \qquad \ldots(7)$$

B. Correction of the Stress Intensity Parameter Due to the Crack Tip Plastic Zone

Irwin's plastic zone correction model may be used for the correction of the stress intensity parameter if the strength of the singularity at the crack tip is considered to be primarily affected by plastic deformation. Then, in all previous expressions, a and c must be replaced by a' = a + r_p* and c' = c + r_p*, respectively. Here, γ_p* is $\dfrac{a}{6} (\dfrac{\sigma}{\sigma_{yp}})^2$

6

III. Finite Element Analysis for Computation of Stress Intensity Parameters

A center-cracked thick plate with remote stresses (Fig. 9) was used as a model for calculating stress intensity parameters. Due to symmetry, only the upper half of the specimen (Fig. 10) was discretized by using a total of 457 and 490 quadratic, isoparametric elements as shown in Figs. 11 and 12. A two step loading scheme composed of increasing and decreasing loads (Fig. 6) was adopted to study crack closure behavior. Crack closure for the rigid asperity was modelled by simply holding any points at which the asperity was located when the applied stress reached the opening stress, σ_{op}, and by decreasing the load until it reached any closure loads, σ_{cl}. In this study σ_{cl} was considered zero, so that the stress in the specimen body was fully relaxed. Crack closure for the elastic asperity was modelled by adding one or a few more elements at the position of the asperity on the crack surface and by holding the bottom side of additional elements in place when the element reached the specimen symmetric line during the decreasing loading process. This involved significant complexity in monitoring the displacement of the nodes of additional elements and determining the load which gave the predicted displacements. An incremental finite element approach was taken to adapt the two step loading scheme to numerical analysis. Node holding processes were performed by changing boundary conditions, i.e., from free to fixed boundary condition. (A secondary way of holding the node by assigning very large stiffness to the nodes was abandoned because of convergence problems.) The strain energy release rate method and J-integral method were used as solution techniques to find the stress intensity parameter. As seen in the previous report, the strain energy release rate method proved to be superior in solving the problem involving contact near the crack tip.

IV. Results and Discussion of Analytical Studies

Figs. 13 and 14 show variations of the closure stress intensity factors obtained from analytical computations for both rigid and elastic asperities. In Fig. 13, it is shown as a function of position for a given asperity width. In Fig. 14, it is shown in terms of width for a given asperity location. From Fig. 13, it is seen that there is not much difference in the stress intensity factor for rigid or elastic asperities. However, there are significant differences as the width changes, Fig. 14. In both cases, the closure stress intensity factors increase as the asperity approaches the crack tip, which is physically reasonable, since it is near the crack tip that the stress distribution would be most perturbed.

The same comparisons for contact pressure obtained from analytical work are made in Figs. 15 and 16. In these figures, the values of pressure are normalized by the difference between the opening and closure load. At a given asperity location, the pressure is higher for rigid material, as expected. In Figure 16, it is

7

important to note that the contact pressure drops rapidly for small increases in asperity width.

In Figs. 17, 18 and 19, finite element results confirm the correctness of the analytical work. As seen as in the previous report, the J-integral technique gives erroneous results near the crack tip, as evidenced by divergence from the analytical solutions. This can be understood in terms of a shrinking k-dominated zone when asperity contact is near the crack tip. Consequently, it is very difficult to model the crack tip behavior when J-integral approaches are used.

V. Plans for the Third Year of the Program

A. Closure Measurements

Activity during the coming year will cover many areas.

1. FCP Experiemnts

Fatigue crack propagation will be performed with the small compact tension samples. These experiments will determine whether or not testing procedures and sample size produce appreciable differences in crack propagation rates from those observed in earlier work. Initial indications are that we have excellent correspondence with the earlier work. If close agreement is found, interpretation of the XTM results and stiffness measurements on the much smaller samples will be considerably simplified. Conversely, if the crack growth rates differ due to an unanticipated size effect, this will indicate a more cautious extrapolation of XTM results to full-sized compact tension samples.

2. Closure in Notched Tensile Samples

Analysis of the physical closure process will continue for the notched tensile samples NT-3 and NT-4. Work will continue on crack face separations measured in cuts parallel to the load axis. Work will also begin on volume rendering of the three-dimensional data; this coupled with direct subtraction of volumes should provide superior visualization of the locations where significant crack face contact is occurring. The imaging language used by our group (IDL) should allow this to be done relatively efficiently.

3. Synchrotron XTM of NT-4 after Crack Extension

Synchrotron XTM will be carried out on sample NT-4 after crack extention. As discussed above, this would allow assessment of the relative contributions of near-tip and far-from-the-tip crack face interactions to the macroscopically observed closure. Whether or not this can be accomplished depends on whether the

8

crack can be extended without fracturing the sample.

4. Region of Interest XTM of CT Specimens

Synchrotron XTM will be performed on a compact tension sample using Region-of-Interest sampling. The first sample to be characterized will have the some of the back surface removed so that data collection will be relatively straight-forward. The crack will be grown prior to removing material, and the crack length will be kept short relative to the remaining ligament. Methods are being investigated for assuring that the crack-tip in the reduced section sample is brought to the same state during in situ XTM load experiments as in the full width sample. It should be emphasized that the reduced ligament compact tension samples are primarily intended as an evolutionary step before examining a completely intact compact tension sample-- a sample which can be remounted in a servohydraulic apparatus for further crack extension and for which interpretation of results will be straight-forward.

5. Load Frame Modifications

While the first generation load frame has worked exceptionally well, the stand-off tube does have a slight effect on the images obtained: the path length of the x-rays through the tube varies somewhat from the edge of a view to its center. A preliminary design for a second generation load frame has been completed. The new design eliminates the stand-off tube. Further refinement will continue, but it is unlikely that the load frame will be built unless further funds are available from another source; this is being actively pursued.

6. Publications

A considerable number of publications and presentations at national meetings are planned.

B. Analytical Studies

1. Multiple Asperity Studies

To date we have had success in modelling single asperities. In the next phase of the study, we will model multiple asperities to more closely approach what occurs in reality.

2. Modelling of Idealized Fracture Surface

In this phase of the study, we will use stereological techniques to characterize the the fracture surface. The surface will then be represented in 2-dimensional, idealized form with the widths and heights of the asperities corresponding to the most salient measured features on the actual fracture surface. FCP specimens

that were mentioned in the preceeding section will be used for the surface characterization studies.

3. Use of XTM Results in Analytical/Numerical Models

The experimental XTM results that are obtained (i.e. geometry and loads at closure) will be fed into the analytical/numerical models for computation of forcing functions and for "normalization" of the FCP rates. The advantage to this approach is that the forcing functions will have an analytical basis and the details of the loads and fracture surfaces will correspond to what is measured in the bulk of the material.

4. Forcing Functions for Real Fracture Surfaces

The next level of complexity will be to computer model the actual fracture surface to obtain appropriate forcing functions for the material of interest.

5. Publication

We now have significant results and intend to present them at numerous mechanics/materials related conferences during the next year.

VI. Personnel

The following personnel have worked on the project

A. Principal Investigators

1.	Stephen D. Antolovich	Fracture Mechanics analytical studies, mechanical testing issues
2.	Stuart R. Stock	Tomography, radiography, specimen design, primary contacts with synchrotron sources, design of rig, mechanical testing issues

B. Students

1.	Thomas Breunig	Design of tensile rig, mechanical testing, tomography data acquisition
2.	Abbas Guvenilir	Assistance with design of experiments, analysis of data, tomography data acquisition

3.   Y. Jung   Finite element calculations

VII. Interactions

        Interaction with other groups is important to the success of the
project.   The following interactions have been (or are being)
established:

           Organization   Person   Comments

   1.   Lawrence Livermore   John Kinney   A c t i v e
                                                       collaboration
                                                       s o f t w a r e ,
                                                       laboratory   and
                                                       synchrotron x-ray
                                                       t o m o g r a p h i c
                                                       microscopy

   2.   Southwest Research   David Davidson   Continuing
        Institute   discussion on
                                                       closure discussion

   3.   CNAM   (France)   C.Bathias   Discussions   of
                                                       closure in Al-Li
                                                       alloys

   4.   Stanford Synchrotron   -   Proposal for beam
        Radiation Laboratory   time

   5.   National Synchrotron   Proposal for beam
        Light Source   time

   6.   Cornell High Energy   -   E x p e r i m e n t
        Synchrotron Source   performed

VIII.   Presentations and Publications

        1.   (Invited) "X-Ray Tomographic Microscopy of Materials,"
             American Crystallographic Association, 40th Annual Meeting,
             April, 1990, New Orleans.

        2.   "A Framework Relating Macroscopic Measures and Physical
             Processes of Crack Closure of Al-Li Alloy 2090" (presented
             by T.M. Breunig), 22nd National Symposium on Fracture
             Mechanics, June 1990, Atlanta.

        3.   "X-Ray Tomographic Microscopy of Materials", TMS-AIME Fall
             Meeting, 1990, Detroit, MI, October 1990.

        4.   "Nondestructive X-ray Tomographic Microscopy of Damage in

Metal Matrix Composites", ASTM International Symposium on Damage Defection and Quality Assurance in Composite Materials, November 1990, San Antonio.

5.   "Impact of a SiC/Al MMC of X-ray Tomographic Microscopy on Deformation Studies," (presented by T.M. Breunig) Fall 1990 Materials Research Society Symposium on Advanced Tomographic Imaging Methods for the Analysis of Materials, November 1990, Boston.

<u>Publication</u>

"A Framework Relating Macroscopic Measures and Physical Processes of Crack Closure of Al-Li Alloy 2090," T.M. Breunig, S.R. Stock, S.D. Antolovich, J.H. Kinney, W.N. Massey and M.C. Nichols, to appear in <u>22nd National Symposium on Fracture Mechanics</u>, 1990.

IX.   **Trade journals articles (written by the journal's staff) mentioning the in situ load frame and the XTM results.**

Aerospace America, Feb. 1991, Designer's Notebook, pp.44-45.
Ceramic Bulletin, Feb. 1991, **70**, p. 203.
Metalworking News, June 18, 1990, pp. 6,20.

PNEUMATIC CYLINDER

ALUMINUM TOP

SPECIMEN

POLYCARBONATE STAND-OFF

GRIPS

ALUMINUM BASE
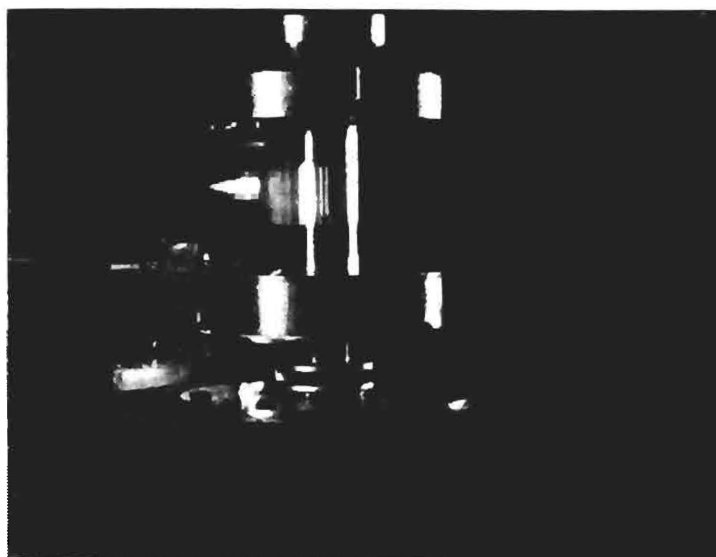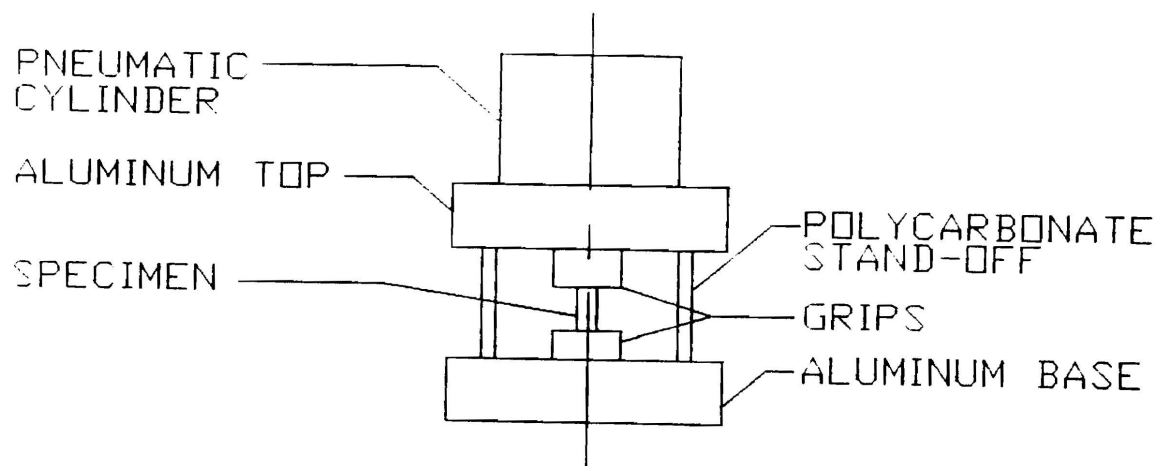
Figure 1. Schematic and photograph of the compact load frame for in situ XTM. The unique feature of this load frame is the polycarbonate stand-off supporting the applied load while allowing the sample to be viewed from all directions around the load axis.
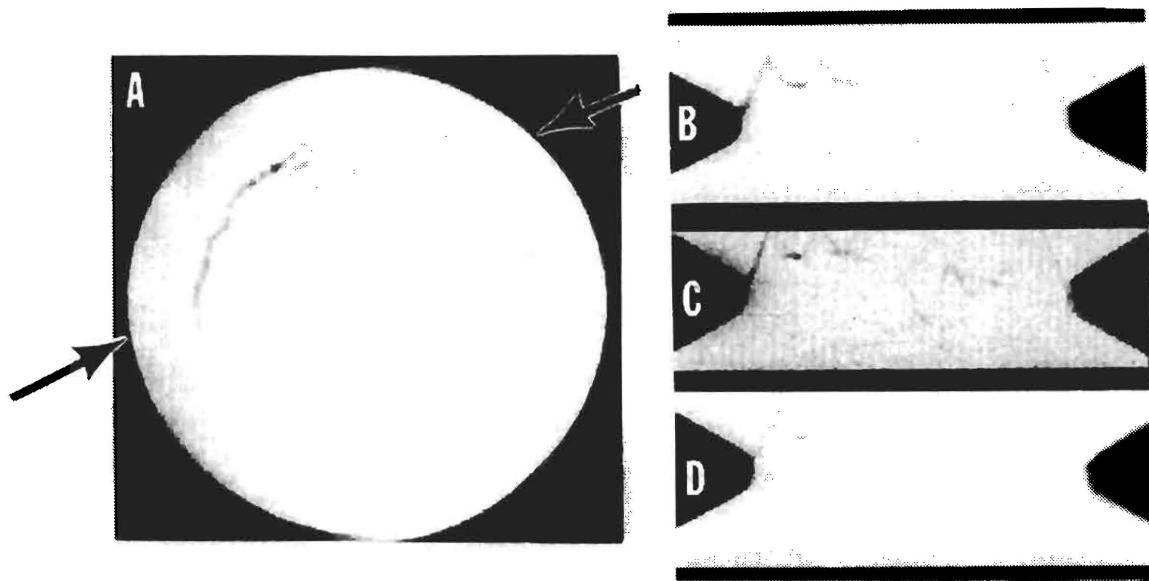
Figure 2. Laboratory XTM. a. Slice perpendicular to the load axis showing the fatigue crack darker than the matrix. The slice diameter is 2.9 mm, the applied load is 81.7 kg and the arrows show the location of the cuts. b.,c.,d. Cuts parallel to the load axis at loads of 81.7, 50.0 and 25.0 kg, respectively.
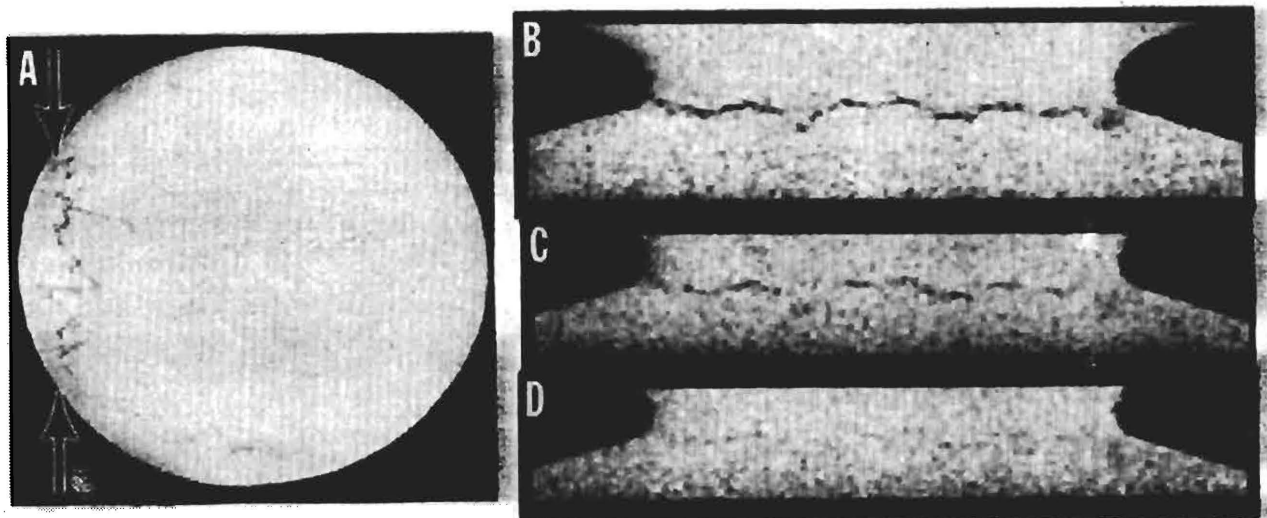
Figure 3. Synchrotron XTM. a. Slice perpendicular to the load axis showing the fatigue crack darker than the matrix. The sample diameter is 1.9 mm, the applied load is 45.5 kg and the arrows show the location of the cuts shown in b.- d. b.,c.,d. Cuts parallel to the load axis at loads of 45.5, 27.0 and 9.1 kg, respectively.
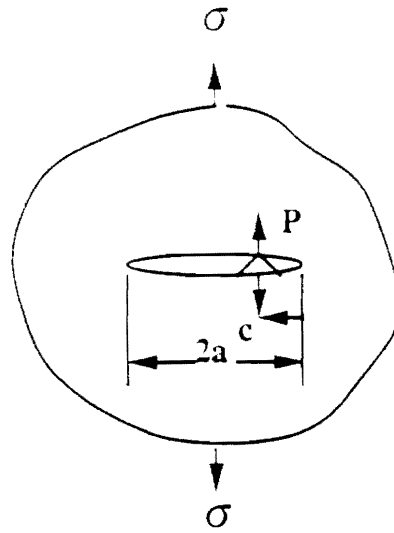
Fig. 4.   Asperity in an infinite body
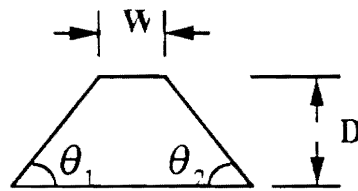
Fig. 5 Asperity Dimension
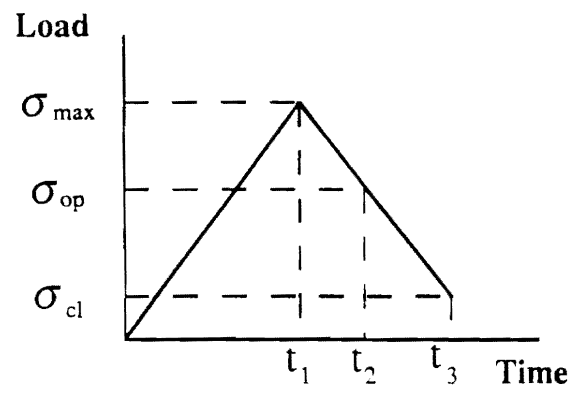
Fig. 6.   Loading Scheme
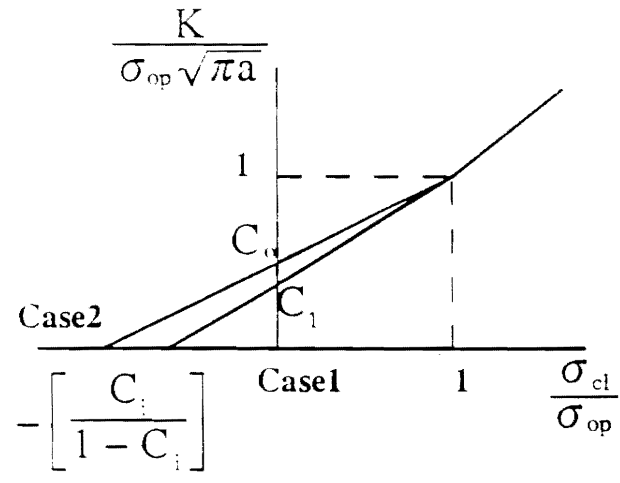
Fig 7. Graphical representation of K
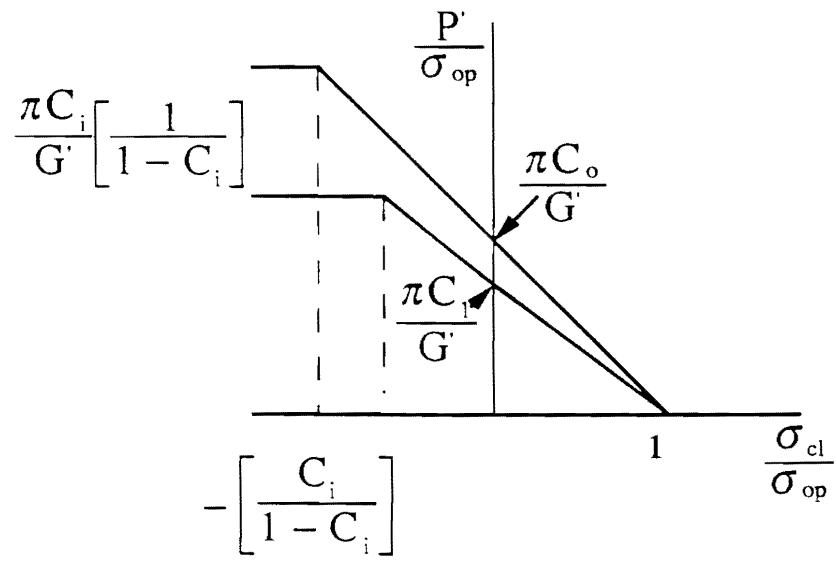
Fig. 8. P as a function of σ_{cl}/σ_{op}
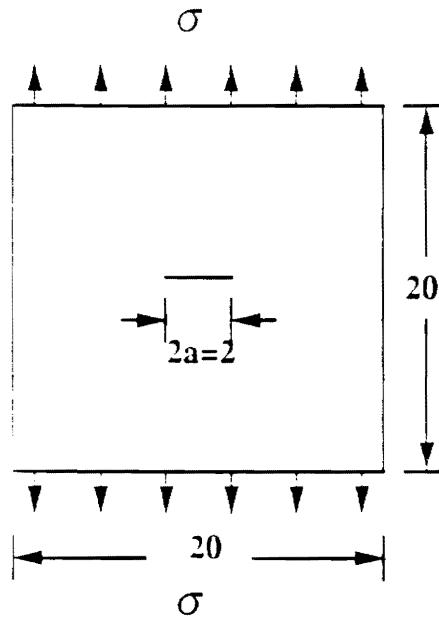
Fig. 9. Specimen Geometry
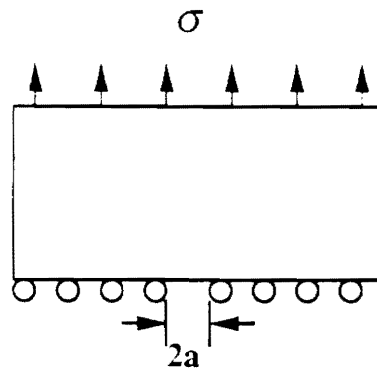
Fig. 10. Half Model
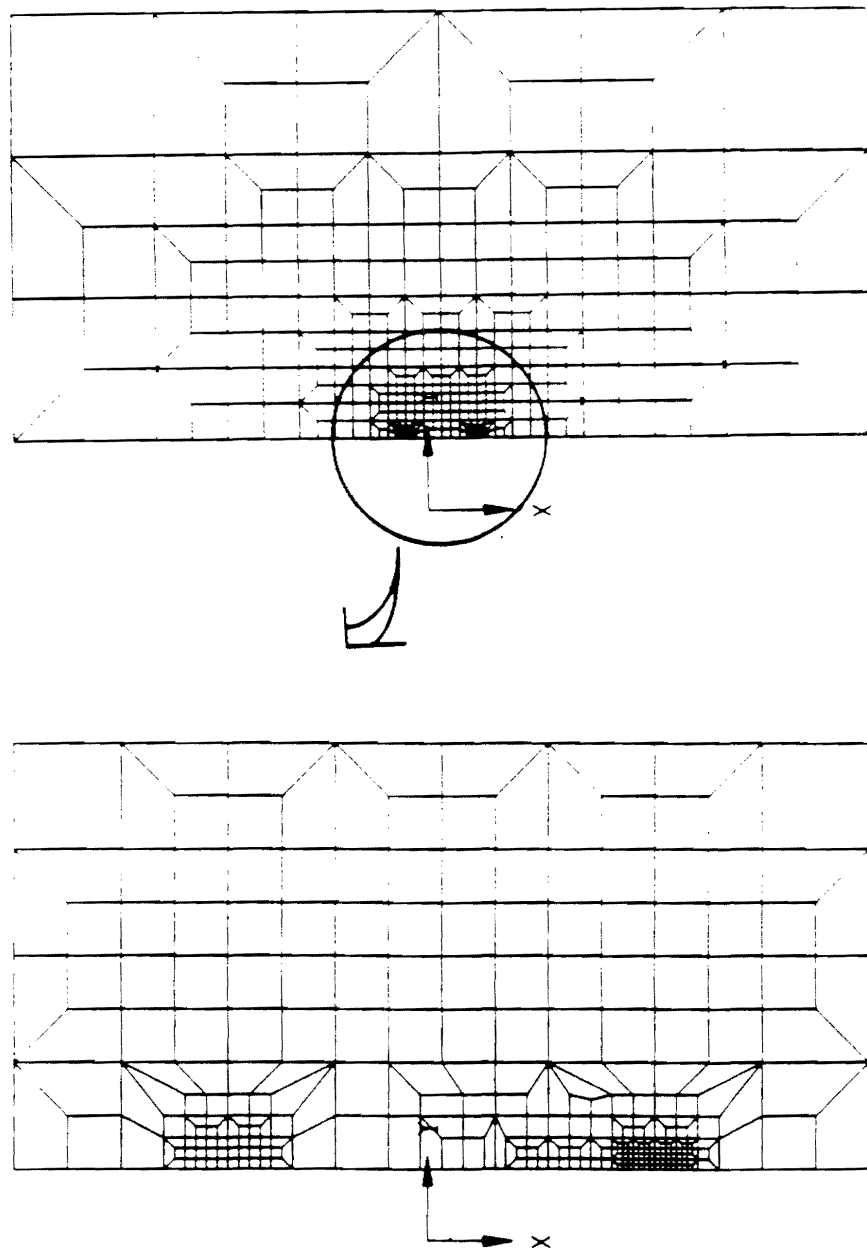
Fig. 11. Finite Element Mesh for a Rigid Asperity
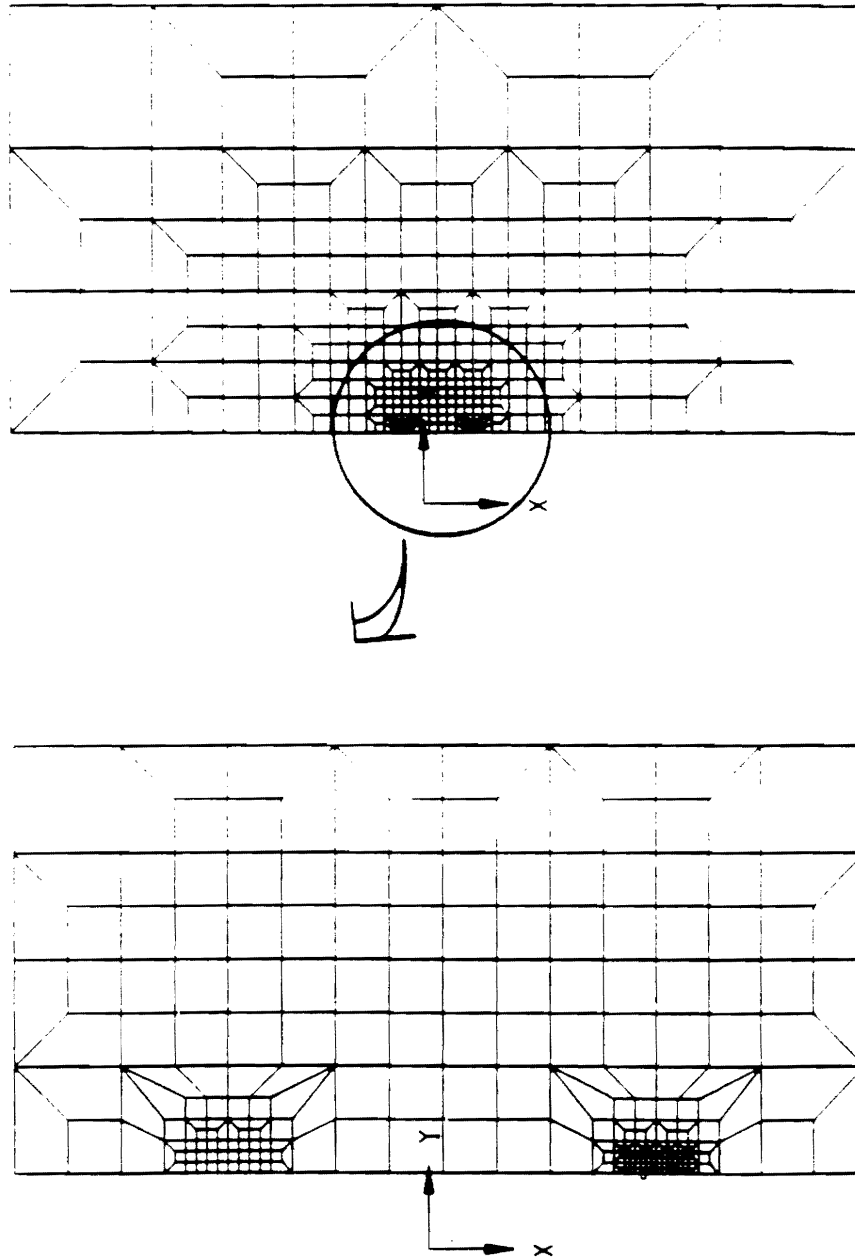
Fig. 12. Finite Element Mesh for an Elastic Asperity

Analytic Solution for K (w/a=0.0125)
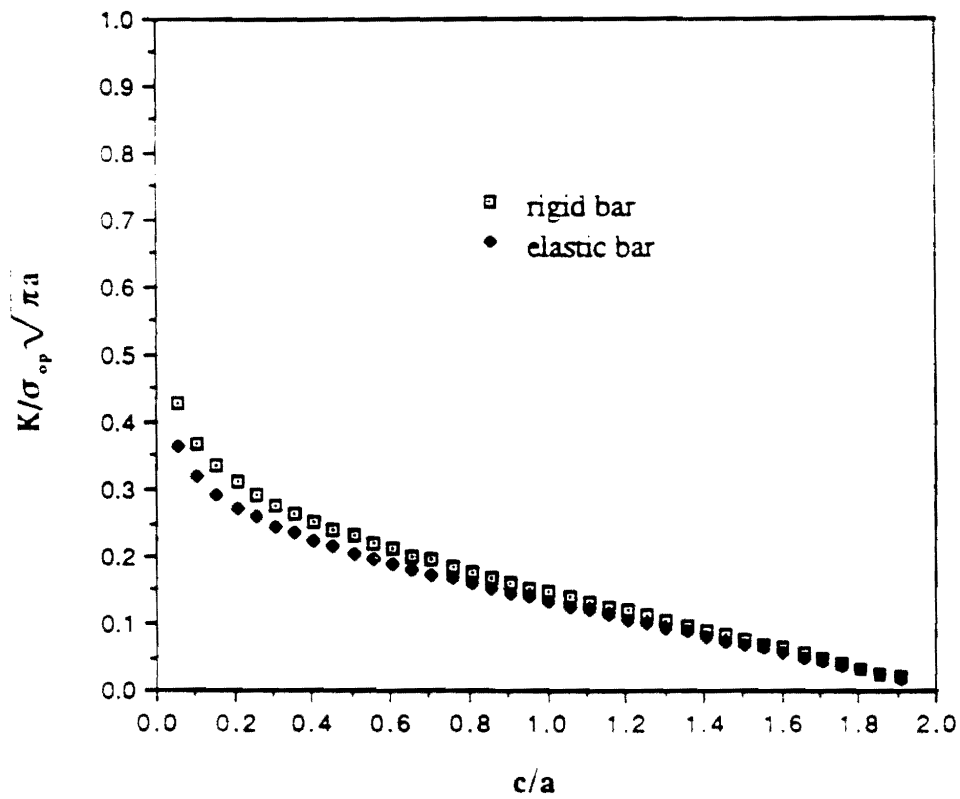
Fig. 13. Variations of K for different asperity locations. The asperity width (w) is fixed and the position (c) varies. Both w and c are normalized with respect to crack length.

Variation of K for w/a (c/a=0.40625)
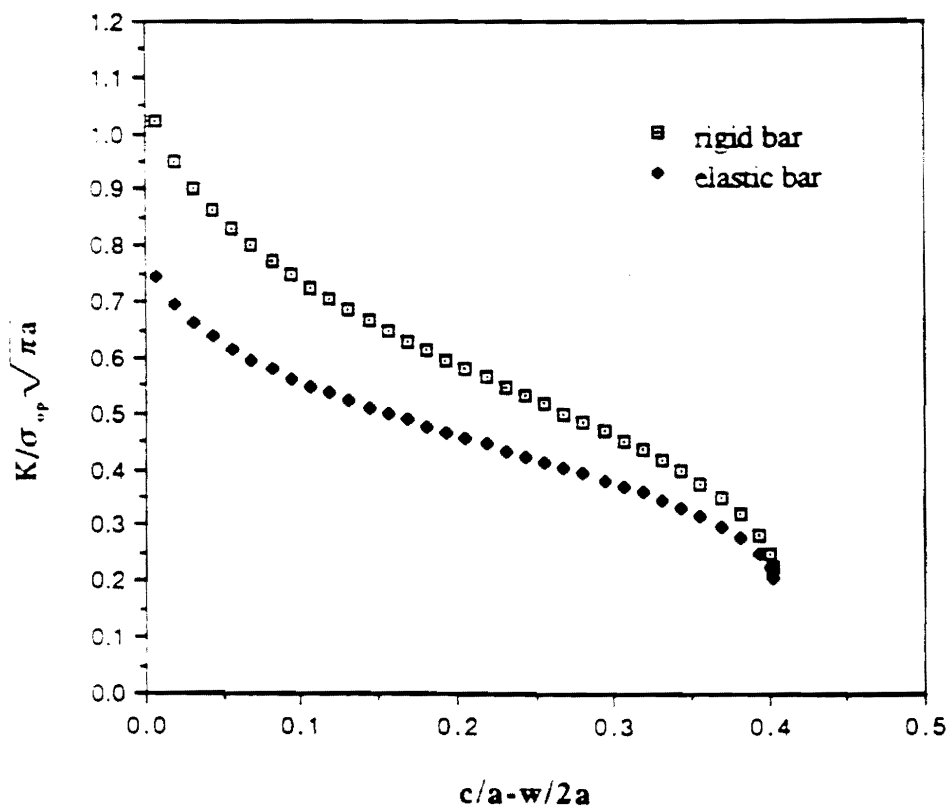
Fig. 14.   Variations of K with the asperity width. The position is fixed.

Contact Pressure vs. c/a (w/a=0.0125)
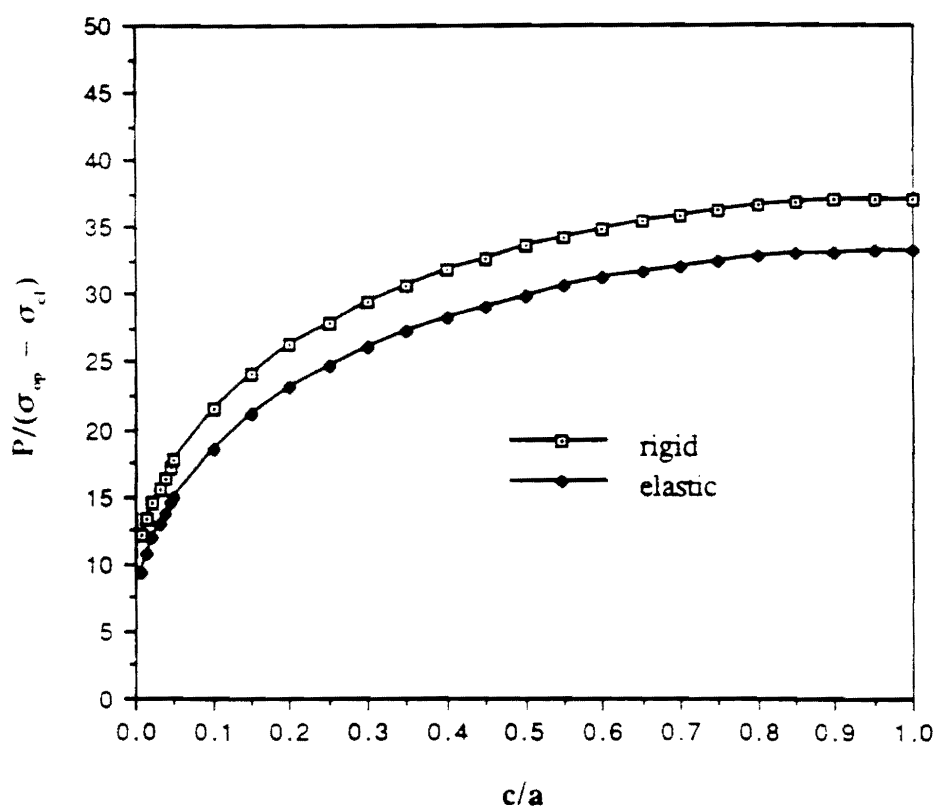
Fig. 15.   Variation of P along the asperity location

Contact Pressure vs. c/a-w/2a (c/a=0.40625)
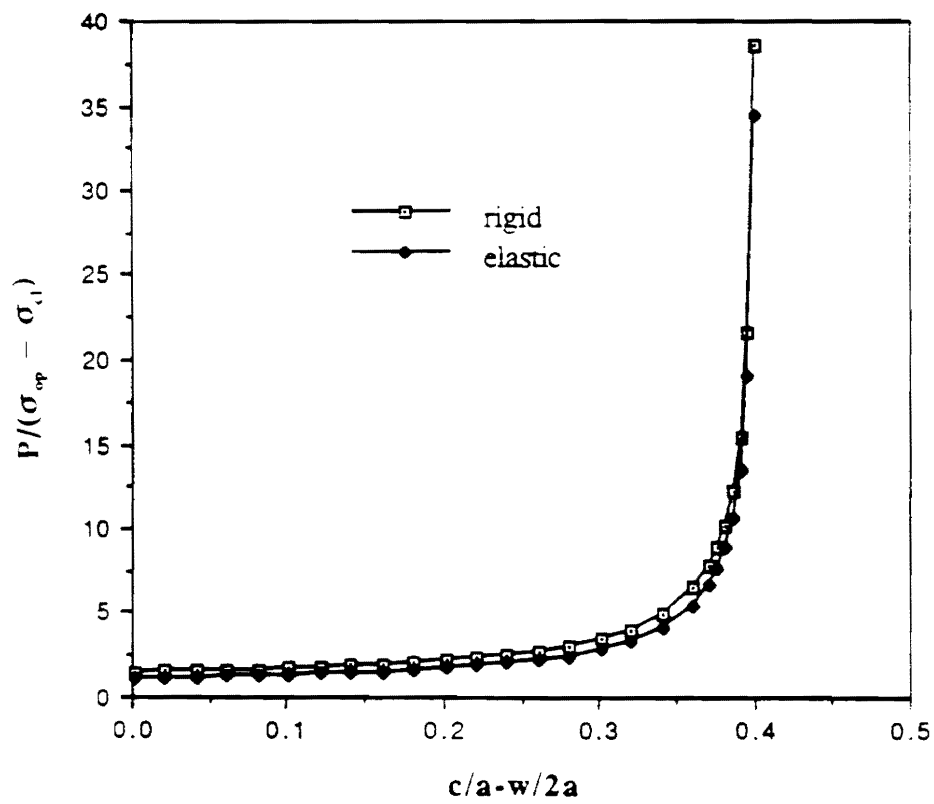
Fig. 16   Variation of P with the asperity width

Comparison Analytic K with FE Results
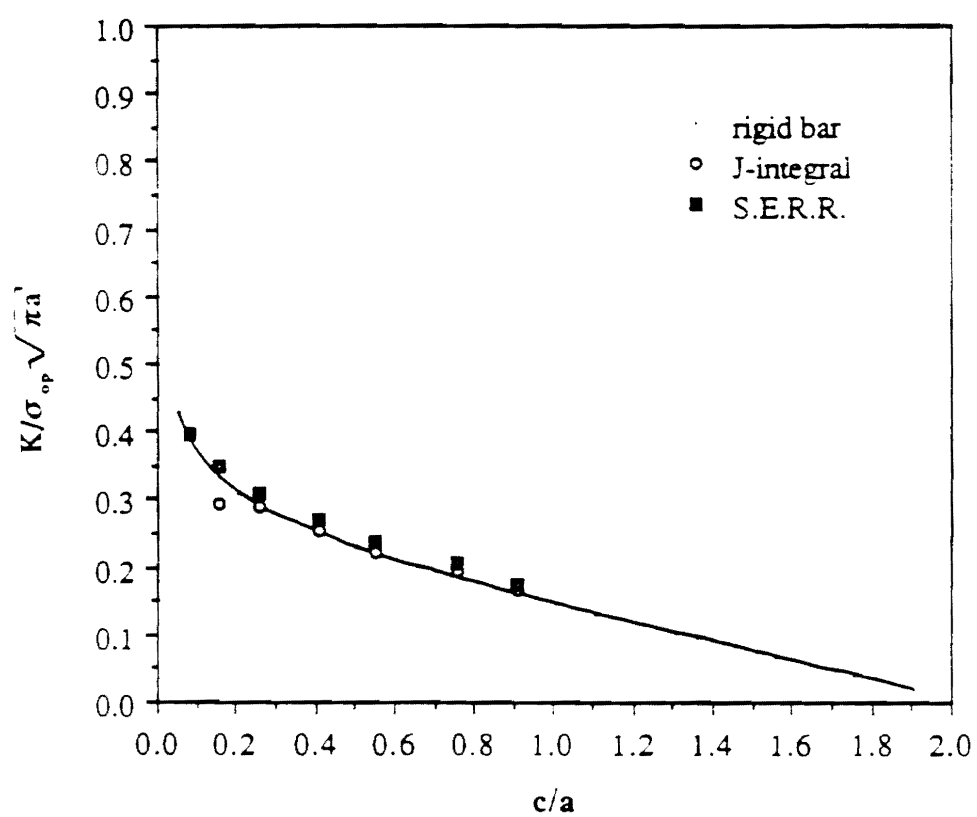
Fig. 17. Comparison of K for a rigid asperity

Comparison Analytic K with FE Results
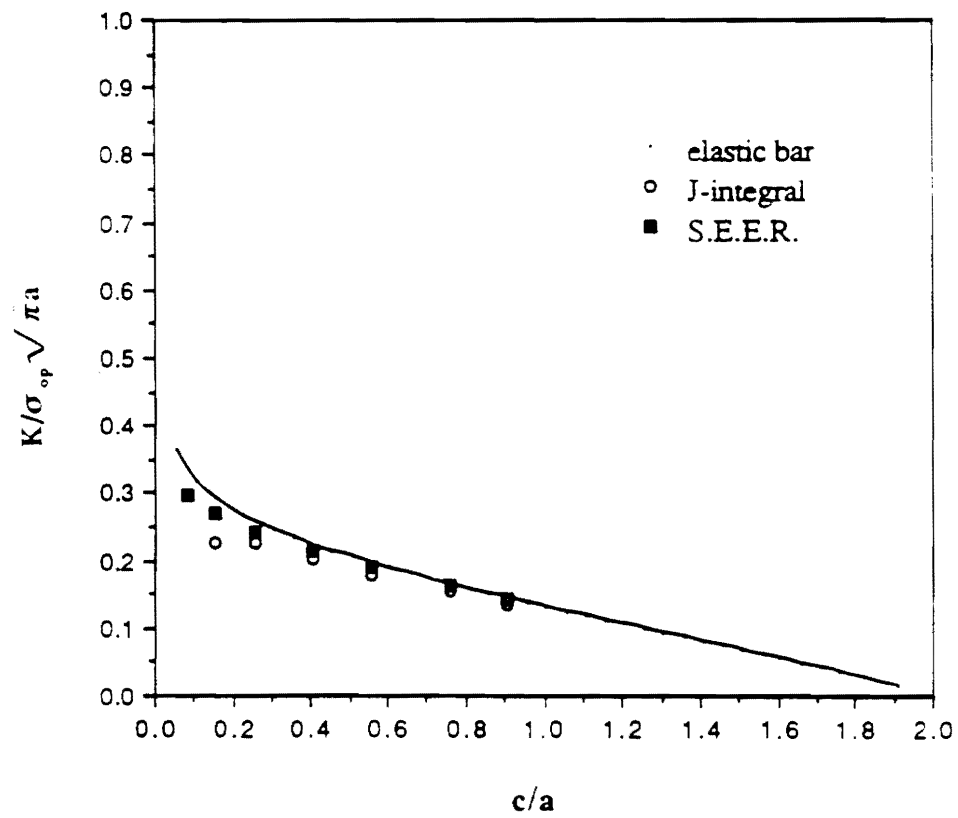
Fig. 18.   Comparison of K for an elastic asperity

Comparison of Analytic K with FEM Results
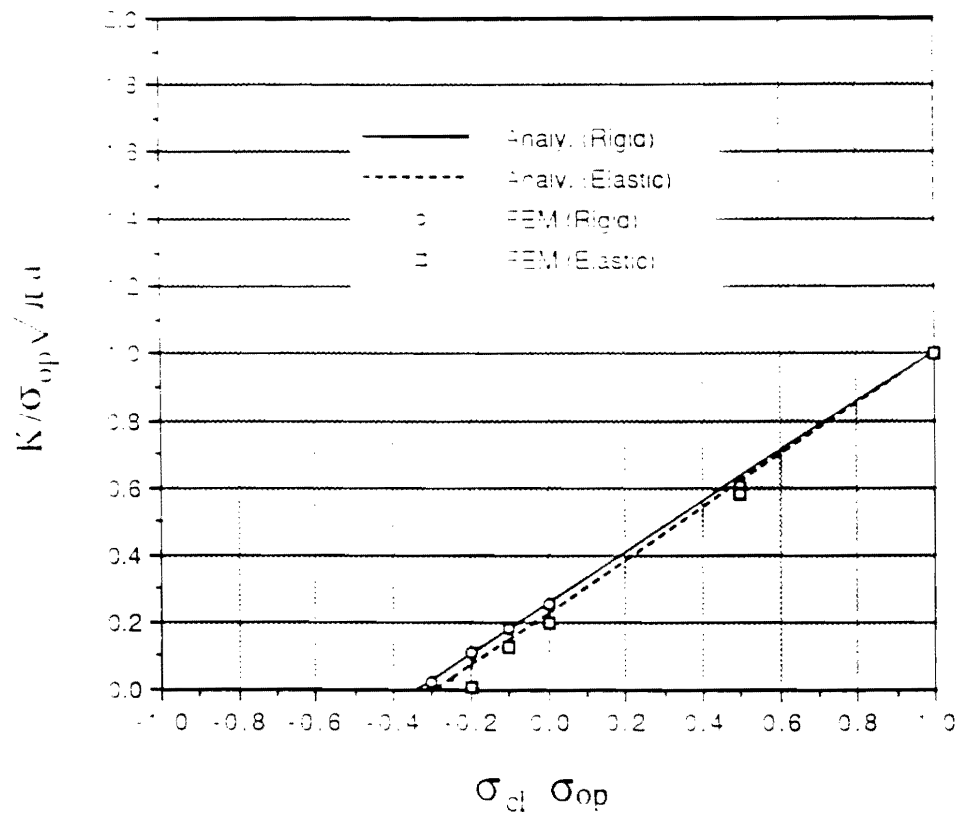
Fig. 19. Comparisons of K for various σ_{cl}/σ_{op}

Georgia Tech

School of Materials Science and Engineering

Georgia Institute of Technology
Atlanta, Georgia 30332-0245
USA
FAX: 404•853•9140

October 8, 1992

Dr. George Yoder
Office of Naval Research
Code 1131
800 N. Quincy
Arlington VA 22217-5000

Dear Dr. Yoder:

  Enclosed please find a copy of the Annual Report for Grant #N0014-89-J-1708 "A Study of the Relationship Between Macroscopic Measures and Physical Processes Occurring During Crack Closure".

  Should you have any questions or need further information, please do not hesitate to contact either myself or Dr. Stock.

Sincerely,

Stephen D. Antolovich
Professor of Materials Science and Engineering
Director, Mechanical Properties Research Lab.

Annual Report for

A Study of the Relationship Between Macroscopic Measures
and Physical Processes Occuring during Crack Closure

N0014-89-J-1708

submitted to:

Office of Naval Research
Attn. Dr. George Yoder
ONR Code 1131
800 N. Quincy
Arlington, Virginia 22217-5000

by

Stephen D. Antolovich
Mechanical Properties Res. Lab.
School of Materials Engineering
Georgia Institute of Technology
Atlanta, GA 30332-0245

·Stuart R. Stock
Mechanical Properties Res. Lab.
School of Materials Engineering
Georgia Institute of Technology
Atlanta, GA 30332-0245

TABLE OF CONTENTS

I. Physical Measurements of Crack Closure

Activity centered on the development and implementation of robust methods for measuring crack opening in the samples studied with X-ray Tomographic Microscopy (XTM). The existing XTM data of notched tensile (NT) samples consists of a three-dimensional stack of several hundred two-dimensional slices, each containing between 400x400 and 600x600 pixels. Analysis of the three-dimensional crack wandering through this volume is done in several steps. The first step is to determine the separation between crack faces using cuts perpendicular to the stack of slices (Figure 1). Separation will be measured as a function of position for the different applied loads. Cuts parallel to the load axis are expected to give a more precise measure of crack opening than measurements within planes parallel to the slices, especially when the openings are on the order of one or two pixels in size.

One way of easily following the variation of crack opening as a function of position in the sample is to project the amount of opening onto a single plane (Figure 2). This representation ignores the non-planarity of the crack, allows one to avoid the difficulties inherent in exactly registering images recorded at different load levels and produces higher precision in determining changes in crack openings for different loads. Many pixels along the crack plane are only partially occupied by the crack, and summing of partial volumes occuring along the load axis is necessary for accurate measurement of the total crack opening.

In calculating the partial volumes of pixels occupied by

1

cracks, it is crucial to define the precise attenuation of the matrix. Once this average is established, one needs to set a threshold value for the attenuation coefficient below which the voxel is considered to be occupied (partially) by a crack. On the one hand, this threshold must be close enough to the average so that crack opening is not significantly underestimated; and, on the other, it must be outside the noise in the reconstructed images so that automated crack measurement is robust. Typically, we have set the threshold by measuring the distribution of linear attenuation coefficients in a volume of the sample which did not contain the crack and by calculating the value of the absorption coefficient at a predetermined number of standard deviations below the average attenuation coefficient. Assuming that the attenuation of air is zero, the measured crack opening is the threshold value minus the value of pixel where crack is open.

Sample NT-4 was imaged with synchrotron XTM and had a 1.8 mm final diameter (initial diameter was 1.9 mm) after 34,760 cycles. This crack is quite short compared to that in NT-3 which was examined with laboratory XTM. Load levels up to the maximum load under which the crack propagated were examined. In the first series of data, the loads were 100, 80, 60, 40 and 20 lbs (45.4, 36.3, 27.2, 18.2 and 9.1 kg, respectively). A second series of XTM data was also collected at loads of 90, 70, 50, 30 and 10 lbs (40.9, 31.8, 22.7, 13.6 and 4.5 kg, respectively). The cuts intersecting the tip of the crack show an irregular crack front and a variable crack opening is calculated and mapped onto the nominal

crack plane (Figure 3). There are regions of closed or nearly closed cracks present far behind the crack tip, even at the maximum load level. Histograms of the measured crack openings show a significant decrease in crack opening from 45.4 kg (100 lbs) to 27.2 kg (60 lbs) and from 40.9 kg (90 lbs) to 22.7 kg (50 lbs) (Figure 4), but the shape of the histograms does not vary for the different loads. In this calculation, the threshold value is 90 to 92% of the average linear attenuation coefficient μ of Al-Li 2090, calculated from > 10^4 of pixels, and this corresponds to 0.6 standard deviations below the average attenuation coefficient.

Once "areas" of importance in the closure process are identified (i.e., positions where no changes in the opening are observed or where greatest changes are seen), we plan to examine the full three-dimensional data set quantitatively. This second step would focus on geometrical effects from the jagged crack, i.e., is the crack closing first at certain microstructural features such as the sides of ridges, etc. Three-dimensional renderings of the crack faces will be used to combine the complex crack geometry with the measured openings. The roughness of the crack, its nominal length and the presence of oxide particles can influence crack closure, and these aspects of microstructure will be examined carefully. These results will also be compared with SEM images of the crack face.

Discussions with Mr. R. Yancy of ARACOR, who operates the Air Force Materials Laboratory's medium resolution computed tomography apparatus, and with Air Force personnel have resulted in our group

being scheduled for time during summer 1992 in which to image the full compact tension samples under load. Also, continuing discussions with Dr. M. Barker of Lockheed Missles and Space Corporation are anticipated to allow imaging at still higher resolution of reduced cross-section compact tension samples; this will probably be done during Fall 1992.

II. Analytical Computations of the Effective Stress Intensity Factors

In the previous report, an analytical expression for calculating the effective stress intensity factor using multiple asperities on the fracture surface was developed. It was considered to be an appropriate model to study realistic closure mechanisms. While closure is expected to occur mostly near the crack front, the number of asperities interfering with each other will be determined by the roughness dimension and the extent of mismatch. If 15 asperities of different roughness dimension are assumed to be arbitrarily distributed near the crack tip and groups of three far from the tip are eliminated one group at a time, the closure stress intensity factors for all six cases are shown in Figure 5. Note that the closure stress intensity factor for six asperities converges to that for higher number of asperities for closure loads larger than zero.

So far, all previous analytical crack closure models were made for a crack in an infinite medium. However the closure stress intensity factors may be quite different from those for a specimen

of finite dimension. Some correction factors, α and α_1, were obtained for the influence functions in the calculation of stress intensity factor and COD under the internal pressure on the fracture surface. The correction factor, R_c, is defined as

$$R_c = \alpha\alpha_1 = K/K_{INF} = COD/COD_{INF} \quad , \quad (1)$$

where K_{INF} and COD_{INF} are the stress intensity factor and the crack opening displacement in an infinite medium, respectively. α and α_1 are the correction factors for semi-infinite and finite geometries, which are shown in Figure 6 and which are functions of a/b and c_i/a. Here, a, b, and c_i are the crack length, specimen width, and the distance from the center line of the pin hole to the applied load points. Their dimensions are shown in Figure 7. Table 1 shows comparisons of analytical α_1 values with finite element results. Three meshes with different crack lengths and contact points are shown in Figure 8. Figure 9 shows a plot of the correction factor, R_c, for different crack lengths (a/b) vs the contact point (c/a). Here, c/a=1 represents the crack tip location. From this, if contact occurs at c/a=0.8 for a/b=0.68 of the crack length, the stress intensity factor for the compact tension specimen will be 3.7 times larger than that for the infinite medium. In fact, some contacts at small c/a and large a/b were observed in Al-Li alloy crack propagation experiments. In this case the difference in the closure stress intensity factor will be quite large.

III. Fractography and Fatigue Crack Propagation (FCP) Rates

In the following sub-sections, experimental FCP data and fractographic observations are presented. This information provides a basis for correlating microscopic observations and macroscopic behavior with the analytical models.

FCP Testing of Al-Li Specimens

Three compact tension specimens mentioned in 1st annual report were tested for load ratios of R=0.1 and 0.7. The FCP data (obtained according to ASTM E-647 specifications) are shown in Figure 10; FCP data previously obtained in this program is shown in Fig. 11, and the solid line shows good agreement with the crack propagation rates obtained using conventional compact tension samples (Yoder et al, 1988). The data trends appeared to be the same as those in other publications (Rao and Ritchie, 1991). In order to investigate the closure effect of the alloy, the closure stress intensity factors were calculated using conventional approaches, in which the closure load is determined from the intersection of two tangential lines drawn at maximum and minimum load points on the load-displacement curve. Figure 12 shows the degree of closure vs ΔK. Note that the closure occured immediately upon crack initiation. When the parameter, ΔK_{eff}, accounting for the closure effect is used, the FCP rate is corrected as shown in Figure 13. The variation in data at early stages of crack growth is due to the thin specimen (≈ 0.08 inches), that yields less sensitivity in measuring potentials for the small amounts of crack

6

growth even if high currents (10 Amps) are applied.

B. Fractographic Analyses

The fracture surfaces of tested specimens were closely examined using SEM. When FCP rates are plotted against the crack length, the effect of closure is clear as shown in Figure 14. The FCP rate drops in the range of the crack length between 5.5 and 7.5mm, where large contact area were developed, instead of linearly increasing as the crack grows. The contact area is identified as the area in which an unusually large oxygen "peak" occurs in Auger spectroscopy. Micrographs (Figure 15 and 16) show the rough fracture surface, which is typical of this alloy; the fracture surface has the crystallographic features, and the change in fracture mode (illustrated by the dots in Figure 16) shows that the crack front was very irregular.

IV. Personnel

The following personnel have worked on the project

A. Principal Investigators

1. Stephen D. Antolovich   Fracture Mechanics analytical studies, mechanical testing issues

2. Stuart R. Stock   Tomography, radiography, specimen design, contacts with synchrotron sources, design of rig, mechanical testing issues

B. Students

1. Thomas Breunig   Design of tensile rig, mechanical testing,

		tomography data acquisition
2.	Abbas Guvenilir	Assistance with design of experiments, analysis of data, tomography data acquisition
3.	Y. Jung	Finite element calculations of crack closure

V.   Interactions

Interaction with other groups is important to the success of the project. The following interactions have been (or are being) established:

	Organization	Person	Comments
1.	Lawrence Livermore	John Kinney	Active collaboration software, laboratory and synchrotron x-ray tomographic microscopy
2.	Southwest Research Institute	David Davidson	Continuing discussion on closure
3.	CNAM (France)	C.Bathias	Discussions of closure in Al-Li alloys
4.	Stanford Synchrotron Radiation Laboratory	-	Proposal for beam time
5.	National Synchrotron		Proposal for beam time
6.	Cornell High Energy Synchrotron Source	-	Experiment performed

VI. **Presentations and Publications** (unless otherwise noted the presentation was given by S.R. Stock)

1. "A Portable Load Frame for in situ Computed Tomography of Monolithic and Composite Materials," (presented by T.M. Breunig), April/May 1991 ASTM E9.04 Meeting, Indianapolis.

2. "Damage in Metal Matrix Composites and Crack Face Interactions During in situ Loading of Al-Li Alloy 2090 Studied by X-ray Tomographic Microscopy," 1991 Industrial Computed Tomography II Topical Conference, American Society for Nondestructive Testing, May 1991, San Diego.

3. "X-ray Tomographic Microscopy of Sample Response During in situ and Interrupted Mechanical Testing," (poster), Pacific International Congress on X-ray Analytical Methods, August 1991, Honolulu.

4. "Crack Face Separation in the Interior of Al-Li 2090 Samples Quantified as a Function of Applied Load by in situ X-ray Tomographic Microscopy," (presented by A. Guvenilir) TMS-AIME Fall Meeting, October 1991, Cincinnati.

5. "X-ray Tomographic Microscopy and its Applications - Fatigue Crack Closure in Al-Li 2090, Damage Accumulation in SiC/Al and Chemical Vapor Infiltration Processing of Nicalon/SiC," Wright Laboratories (WL/MLLM), October 1991, Dayton.

6. "X-ray Tomographic Microscopy and its Applications: Fatigue Crack Closure in Al-Li 2090, Damage Accumulation in SiC/Al and Chemical Vapor Infiltration Processing of Nicalon/SiC," Quality Technology Division, General Electric Aircraft Engines, October 1991, Cincinnati.

7. "X-ray Tomographic Microscopy and its Applications in Fatigue Crack Closure and in Damage Accumulation in Composites," BP Research, October 1991, Cleveland.

8. T.M. Breunig, Y. Jung, S.R. Stock, J. Kinney and Stephen D. Antolovich: A Framework for Relating Macroscopic Measures and Physical Processes of Crack Closure Illustrated by a Study of Al-Li Alloy 2090. Presented at 22nd National Fracture Mechanics Symposium, June 28, 1990, Atlanta, Georgia. Fracture Mechanics: 22nd Symposium (Volume 1), ASTM STP 1131, H.A. Ernst, A. Saxena, and D.L. McDowell, Eds., American Society for Testing and Materials, 1992, pp. 749-761.

The final draft of one publication was being completed in February

1992 for publication in Materials Evaluation (the official journal

of the American Society for Nondestructive Testing). Its tentative title and authors are "A simple load frame forin situ computed tomography and x-ray tomographic microscopy," T. M. Breunig, S. R. Stock and R. C. Brown.

VII. Awards

T. M. Breunig and S.R. Stock, Georgia Institute of Technology, Co-recipients of an 1991 R&D 100 Award with Lawrence Livermore and Sandia-Livermore National Laboratories.

1. **ASME Nadai Award**, November, 1990. Award was granted by the American Society of Mechanical Engineers "for outstanding contributions toward understanding the relationships between microstructure, deformation mechanisms, fatigue and fracture in engineering alloys at high and low temperatures; for incorporating this understanding into the development of mechanical behavior and life prediction models, and for developing outstanding students in this and related areas".

2. Named as the first Honorary Professor (Professeur Invite') of the Conservatoire National des Arts et Metiers, Paris, France in 1989.

3. **Reaumur Medal of the French Metallurgical Society** in
    October 1988. This medal was awarded for "lifetime
    achievements in research having particular significance
    to industry". It is the top research award of the French
    Metallurgical Society.

4. Elected **Fellow of ASM International,** October 1987.

5. Named as charter member of the **Council of Fellows of ASM
    International** in January 1989.

Table 1. Comparison of Analytical α_1 Values with Finite Element Results.

a/b	0.36	0.44	0.52	0.60	0.68	0.76	0.84
α_1	1.085	1.088	1.049	1.008	0.982	0.975	0.980
FEM	—	—	1.040	0.996	0.964	—	—

μ_air μ_dense   fraction of pixel void

pixel position

0   1

crack

sum of partial volumes = crack opening

(a)   (b)
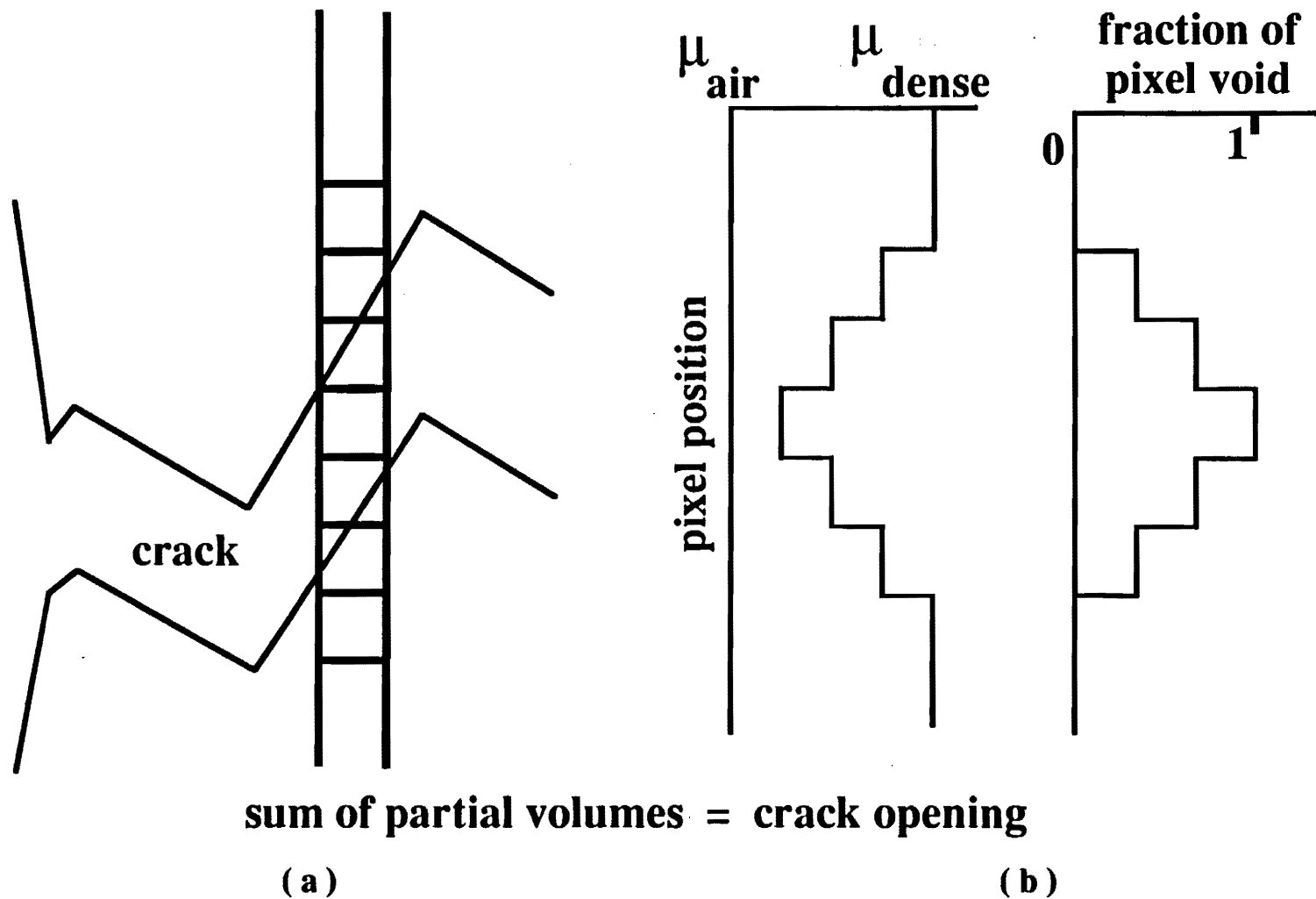
Figure 1 Measurement of crack opening as a function of position from XTM data. (a.) A column of voxels (parallel to the load axis) intersecting the crack. In the drawing, one voxel is completely within the crack, two voxels are predominantly within the crack and two voxels have only a small fraction of their volume within the crack. (b.) Schematic of the variation in linear attenuation of the pixels along the column shown in (a) and the corresponding fraction of voxels void.

13
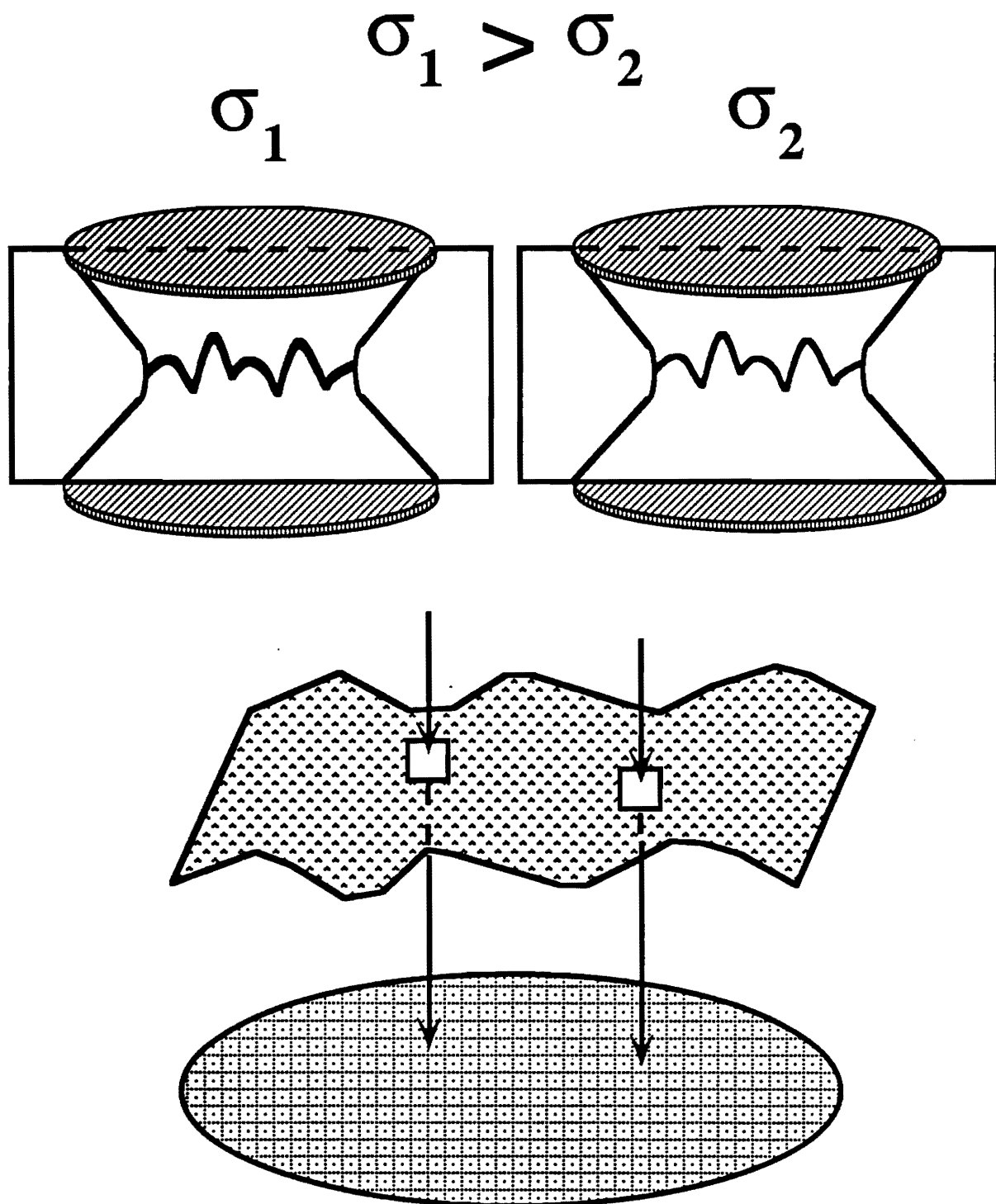
Figure 2 Illustration of projection of crack opening onto a single plain perpendicular to the load axis. The top figures show the crack's intersection with the surface of the sample. The drawing at the bottom of the page shows only the crack and the projection onto the plane perpendicular to the load axis.
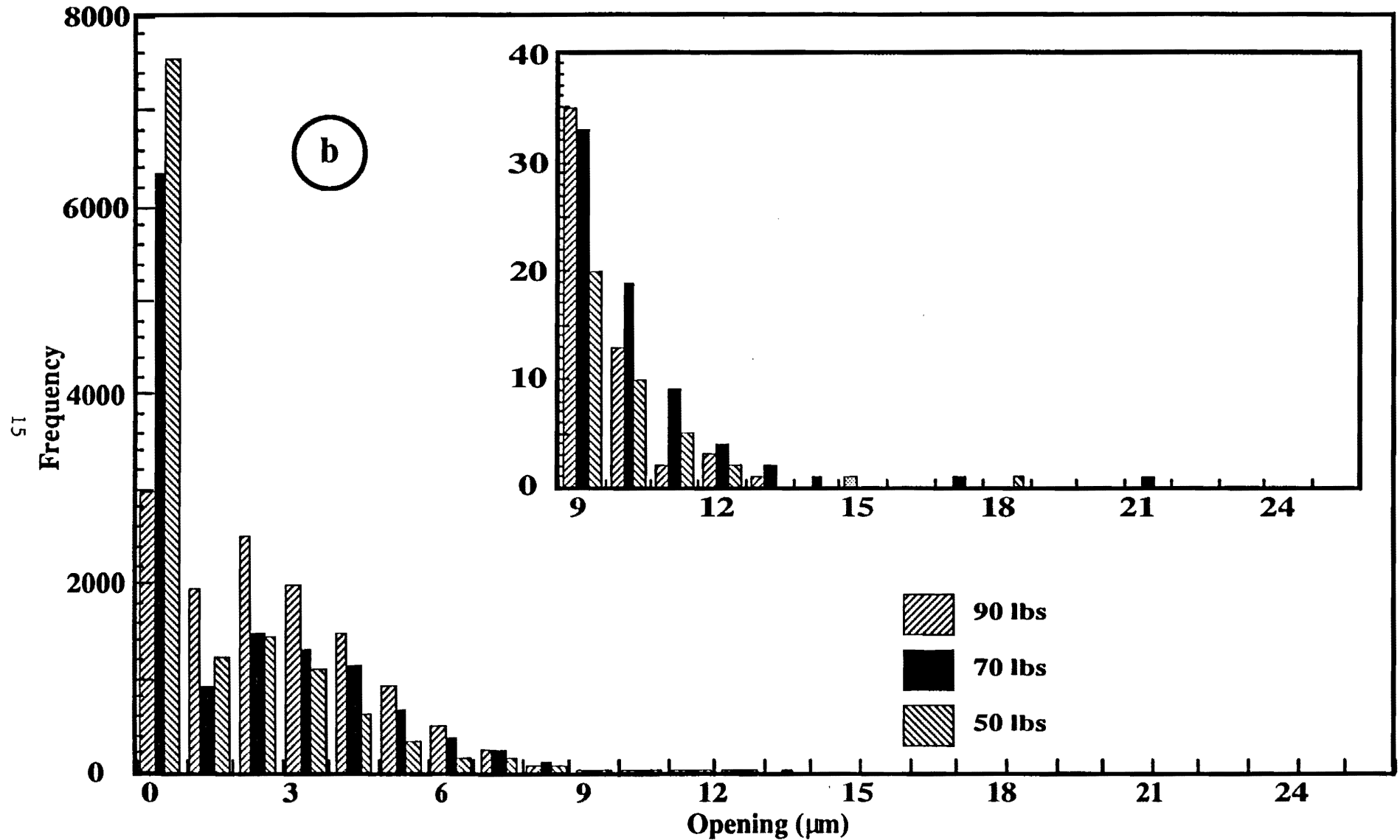
14

MEASURED CRACK OPENINGS

Figure 4   Histograms of crack opening measurements at : (a) 100, 80 and 60 lbs (45.4, 36.3 and 27.2 kg) and (b) 90, 70 and 50 lbs (40.9, 31.8 and 22.7 kg).
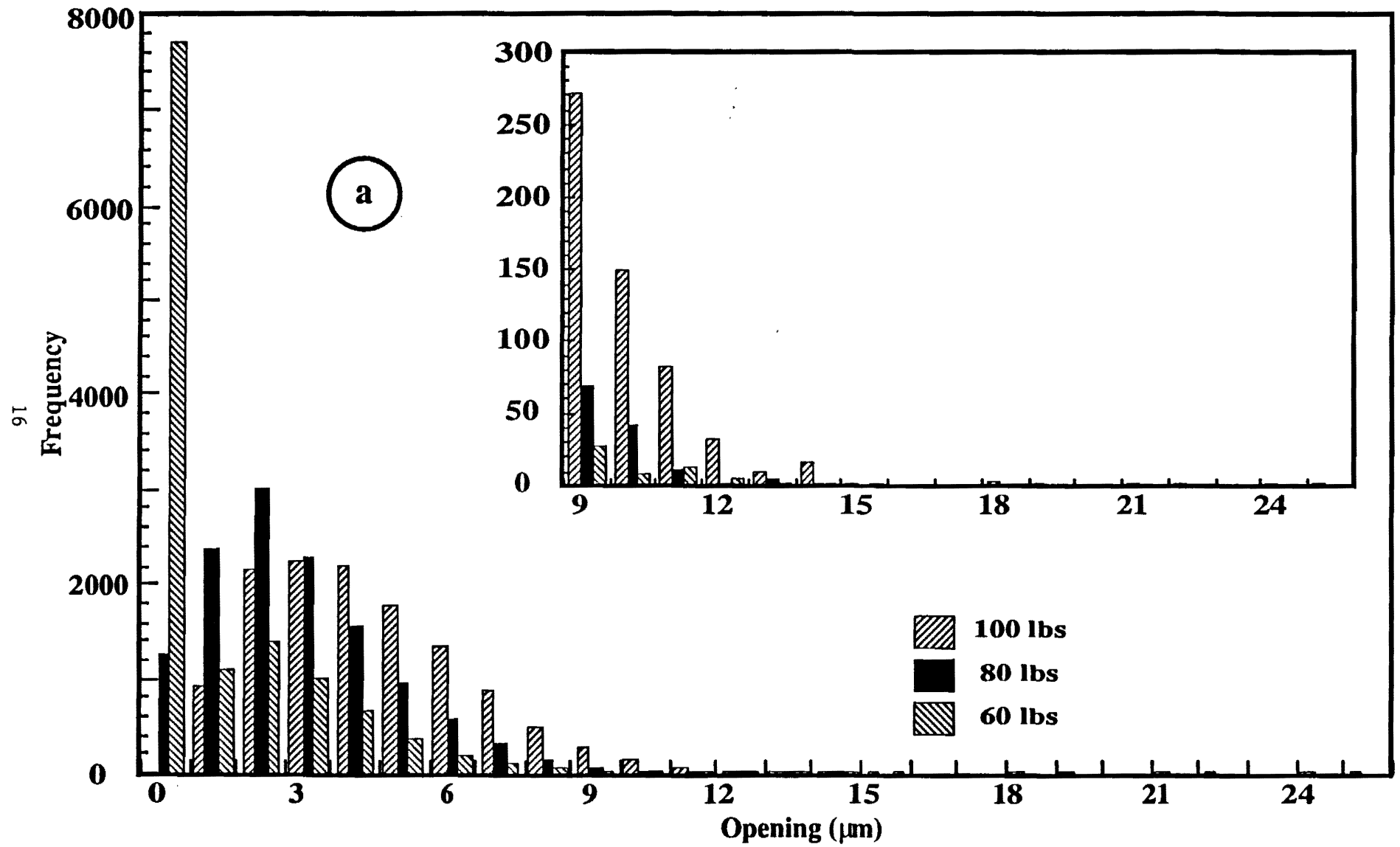
Figure 4   Histograms of crack opening measurements at : (a) 100, 80 and 60 lbs (45.4, 36.3 and 27.2 kg) and
(b) 90, 70 and 50 lbs (40.9, 31.8 and 22.7 kg).

Comparison of K for Multi-Asperities
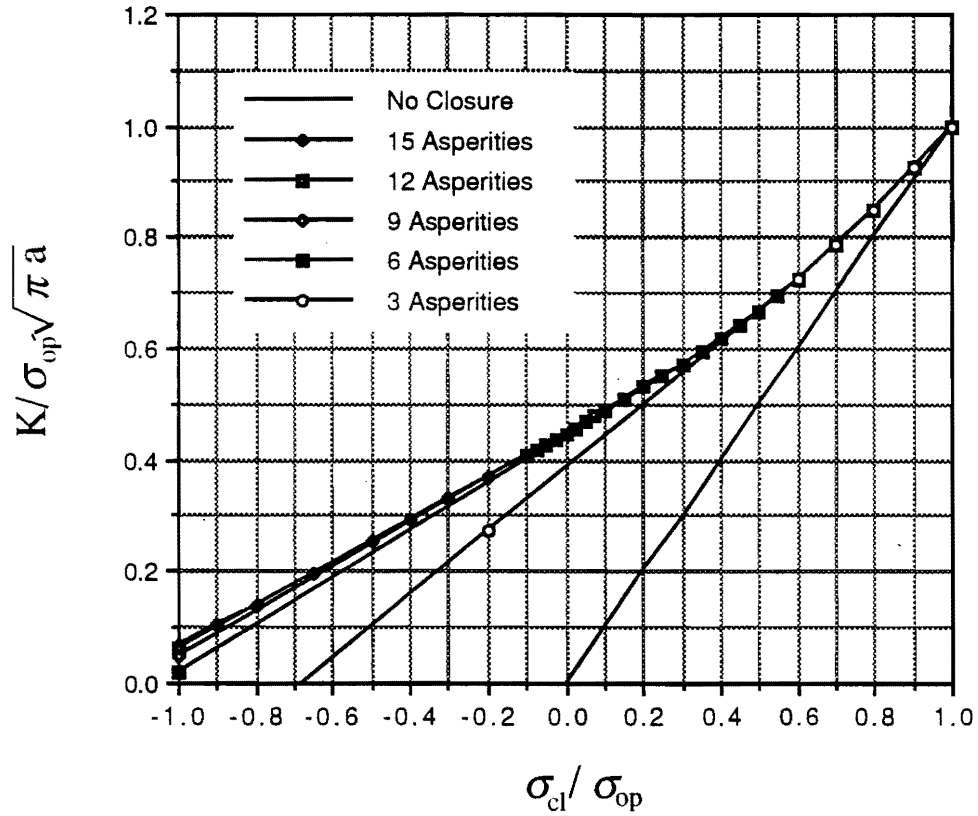
Fig. 5 Effects on closure stress intensity factor for a number of asperities distributed on fracture surface. Straight curves shown as a guide define items.

17

Westergaard Stress Fuction
(Irwin, 1957)

Singular Integral Equation
(Kaya-Erdogan, 1980)

$$\alpha = \alpha(\frac{a}{b}, \frac{c_1}{a}, \frac{c_2}{a})$$

Singular Integral Equation

Boundary Collocation Method

$$\alpha_1 = \alpha_1(\frac{a}{b})$$
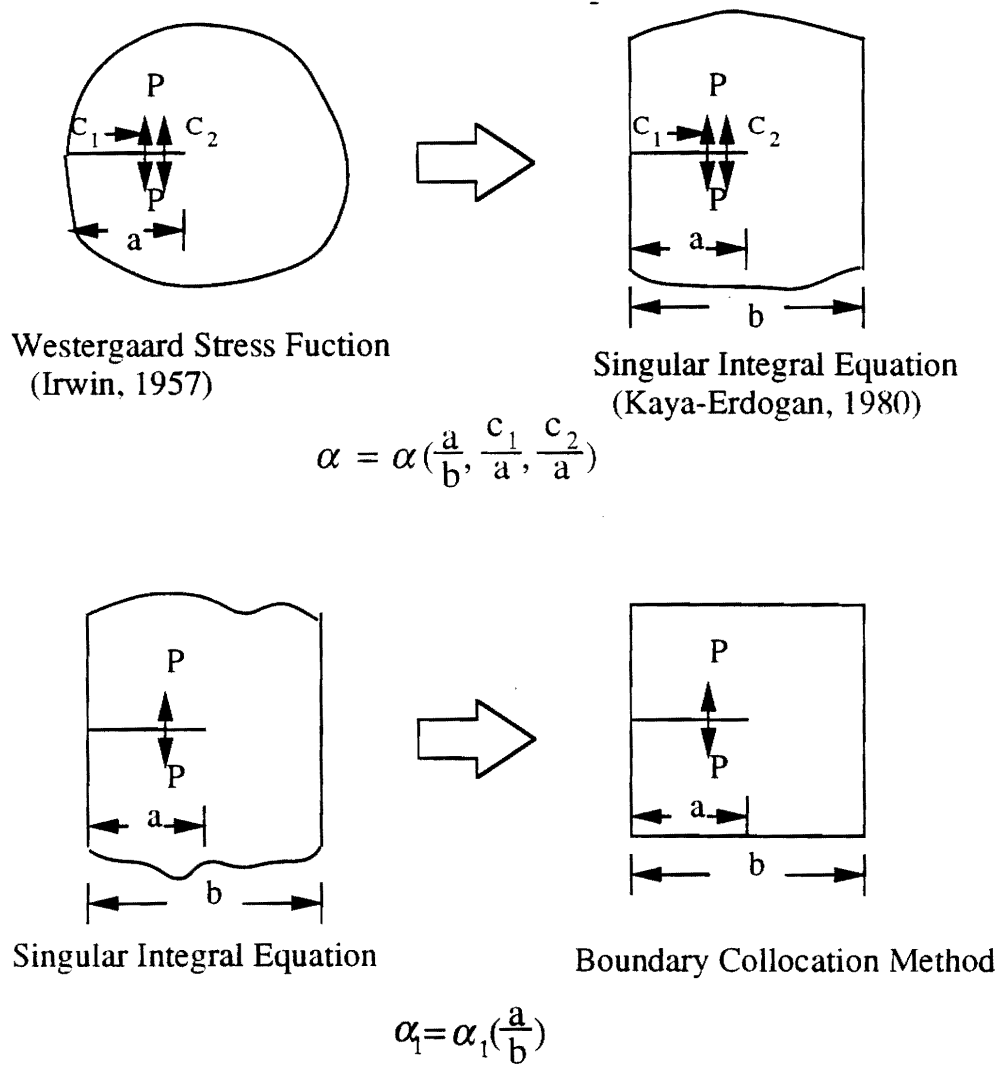
Fig. 6   Correction factors α and α_1 for CT specimen.

18
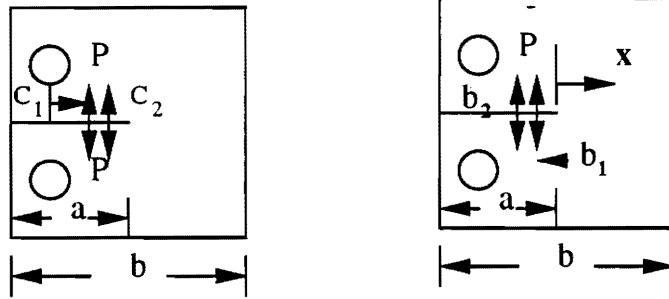
$$K_I = 2\sqrt{\frac{a}{\pi}} \frac{P}{B} \sqrt{2} \left(\sqrt{1 - \frac{c_1}{a}} - \sqrt{1 - \frac{c_2}{a}} \right) \alpha \alpha_1$$

$$COD = \frac{8a}{E'\pi} \frac{P}{B} \left[\sqrt{\frac{|x|}{a}} \left(\sqrt{\frac{b_2}{a}} - \sqrt{\frac{b_1}{a}} \right) \right.$$

$$\left. + \frac{1}{2} \left(\frac{b_2}{a} + \frac{x}{a} \right) \log \left| \frac{\sqrt{|x|} + \sqrt{b_2}}{\sqrt{|x|} - \sqrt{b_2}} \right| - \frac{1}{2} \left(\frac{b_1}{a} + \frac{x}{a} \right) \log \left| \frac{\sqrt{|x|} + \sqrt{b_1}}{\sqrt{|x|} - \sqrt{b_1}} \right| \right] \alpha \alpha_1$$

Fig. 7   Stress intensity factor and COD for CT specimen.

19

Contact Point   Crack Tip
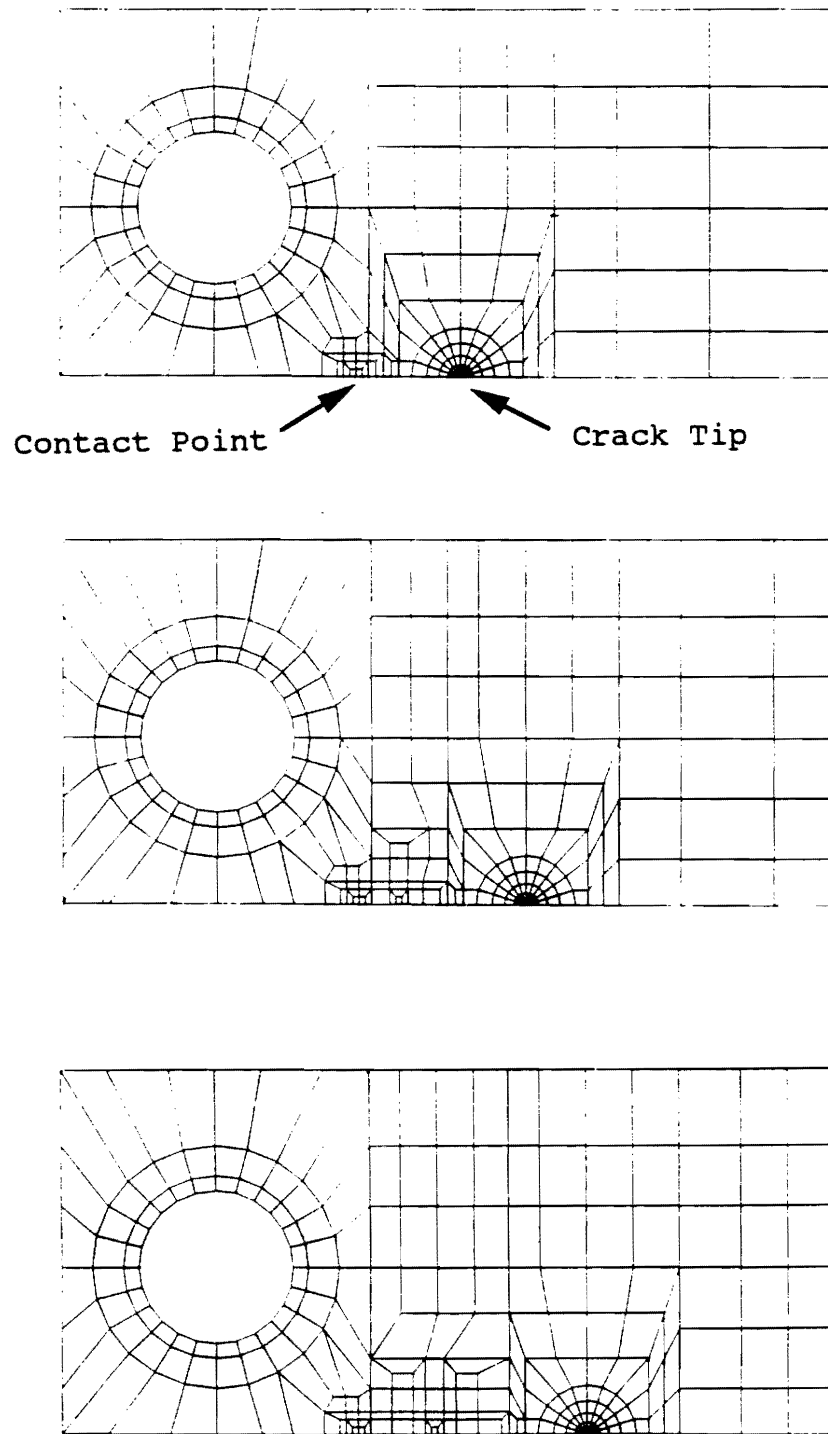
Fig. 8   Finite element meshes for calculating α_1.
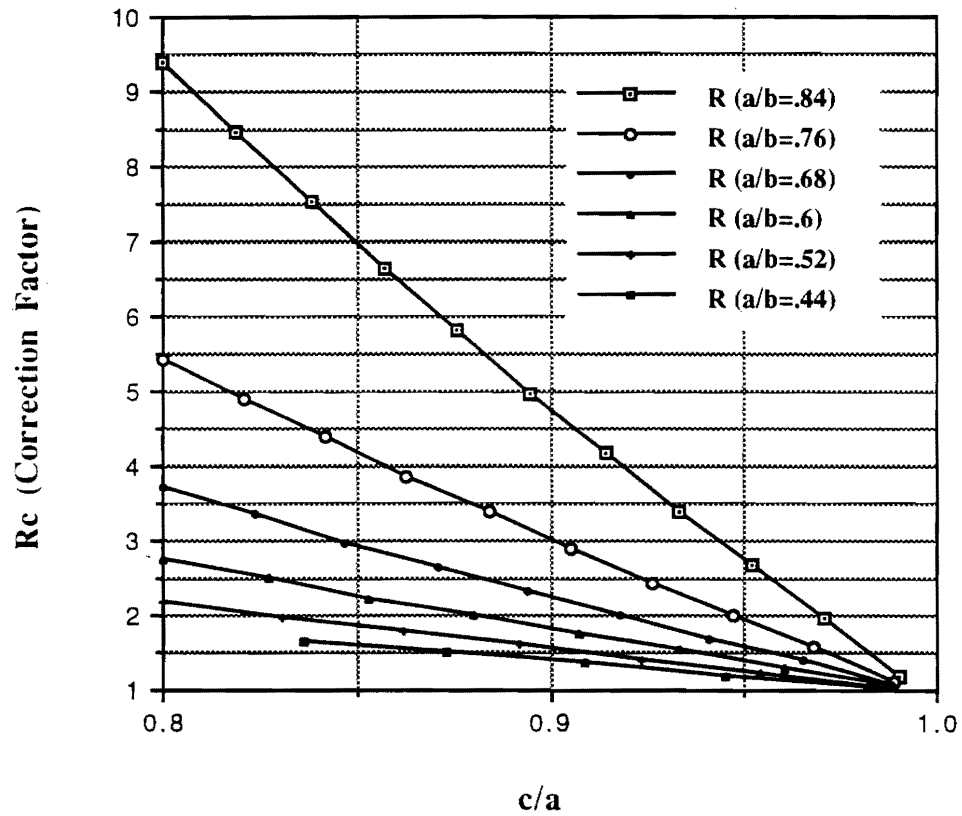
Fig. 9   Correction factor R vs contact point c/a for different
values of dimensionless crack length a/b.

21

Fatigue Crack Propagation (Al-Li 2090)
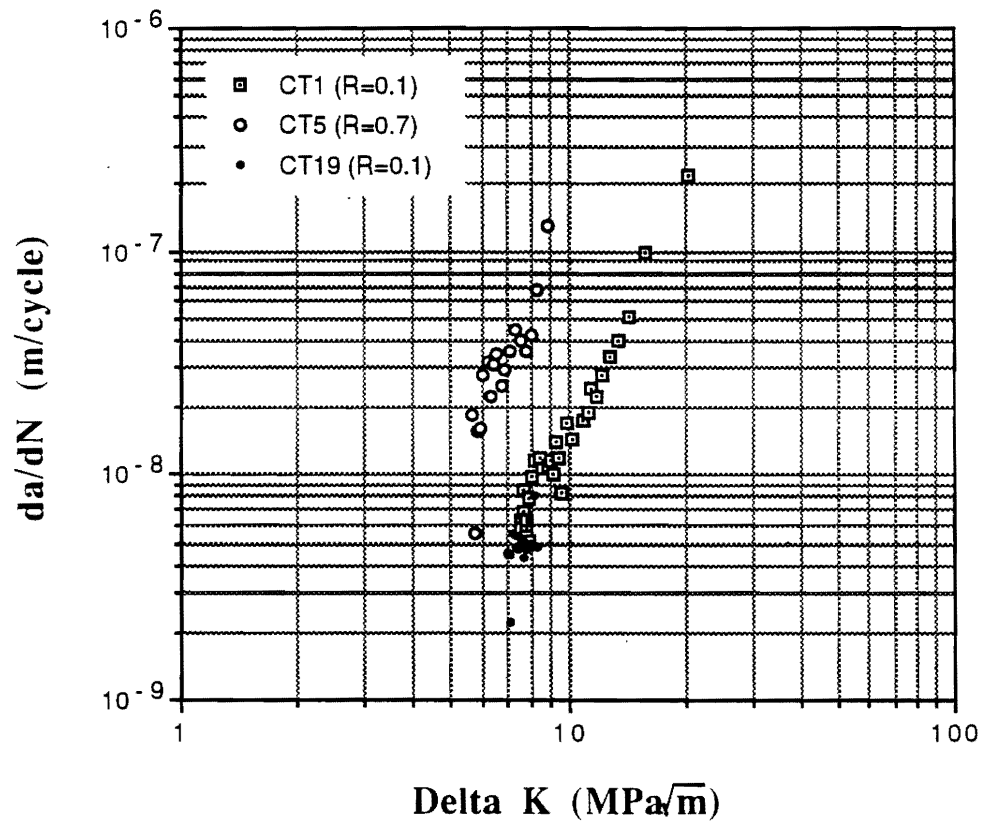
Fig. 10 Fatigue Crack Propagation Rate for Al-Li Alloy 2090.

FATIGUE CRACK PROPAGATION RATES
OF Al-Li ALLOY 2090
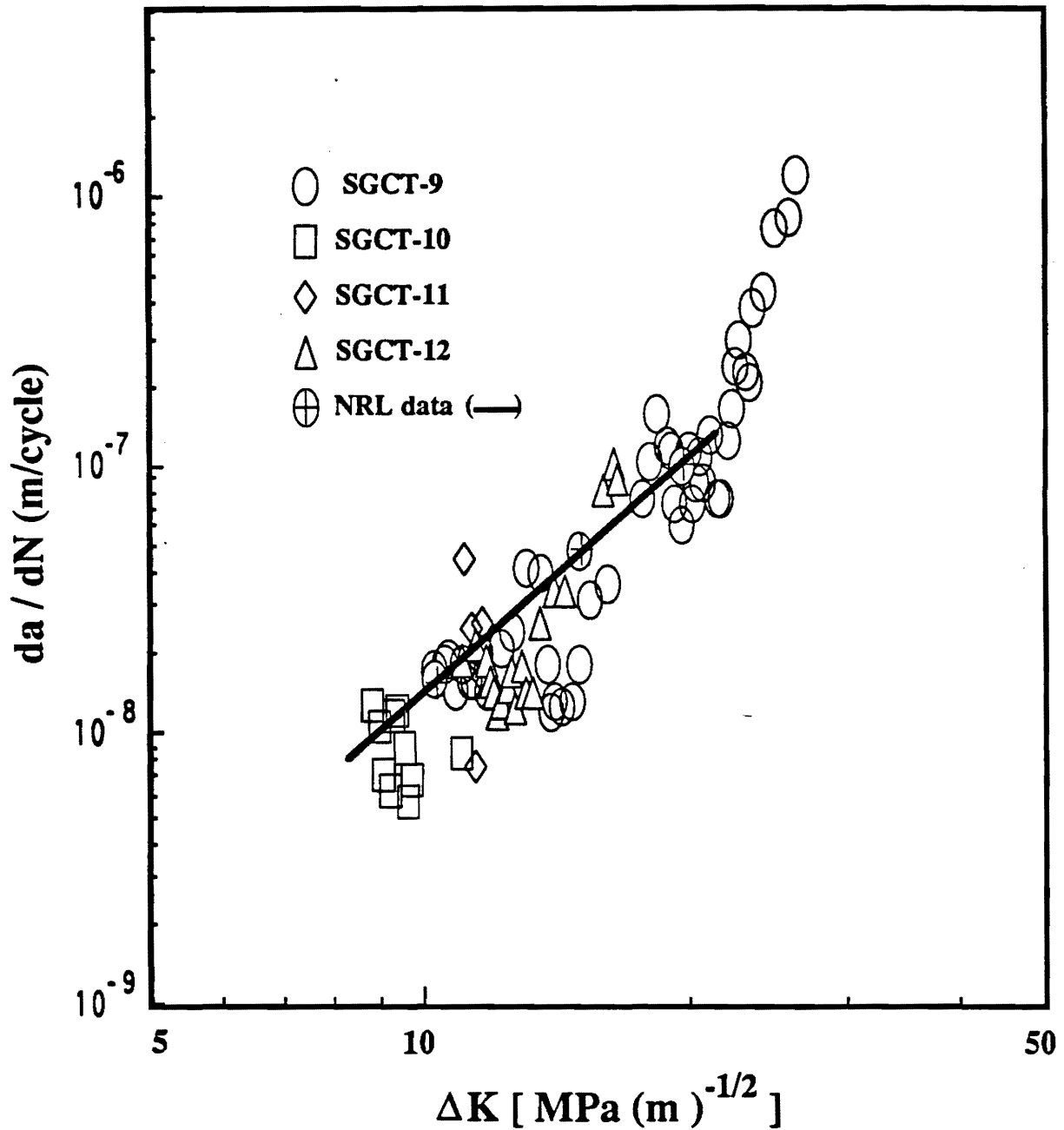
Figure 11 Crack propagation rates as a function of ΔK for SGCT samples 9-12 compared with data on a full size compact tension samples obtained on the same lot of material (L-T orientation) and under identical testing conditions at room temperature (haversine wave form, R: load ratio = 0.1 and frequency = 5 Hz) [8].

Ratio of Closure to Kmax (CT1,R=0.1)
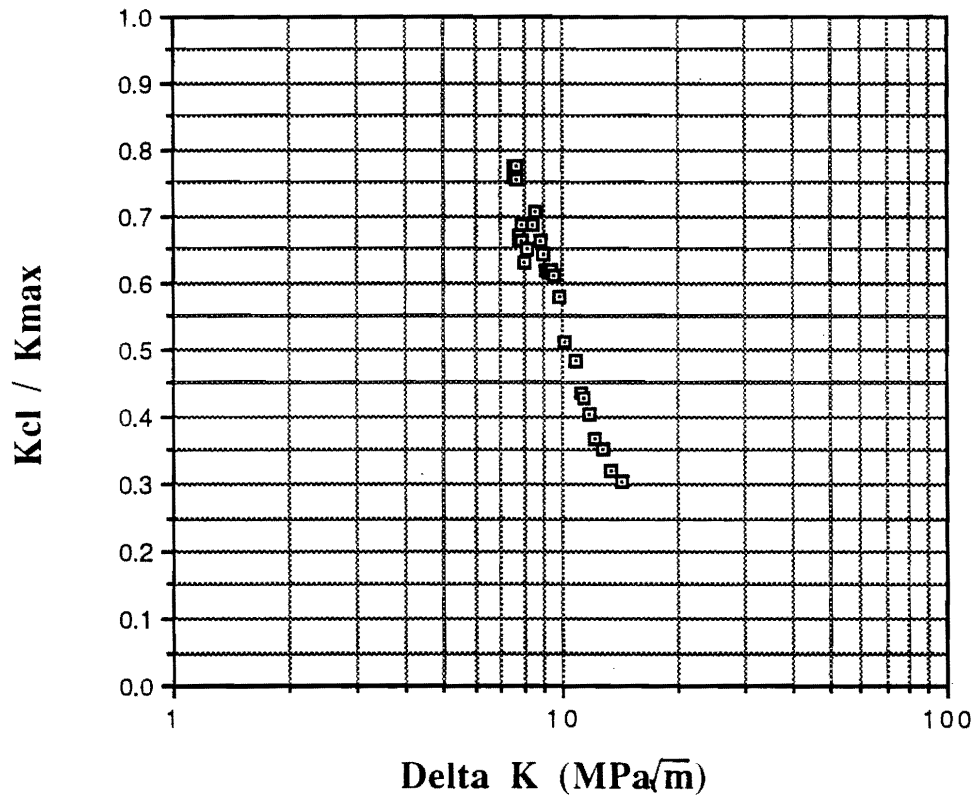
Fig. 12   Closure stress intensity factor vs. ΔK for sample CT1.

Comparison of Delta K and Keff (CT1,R=0.1)
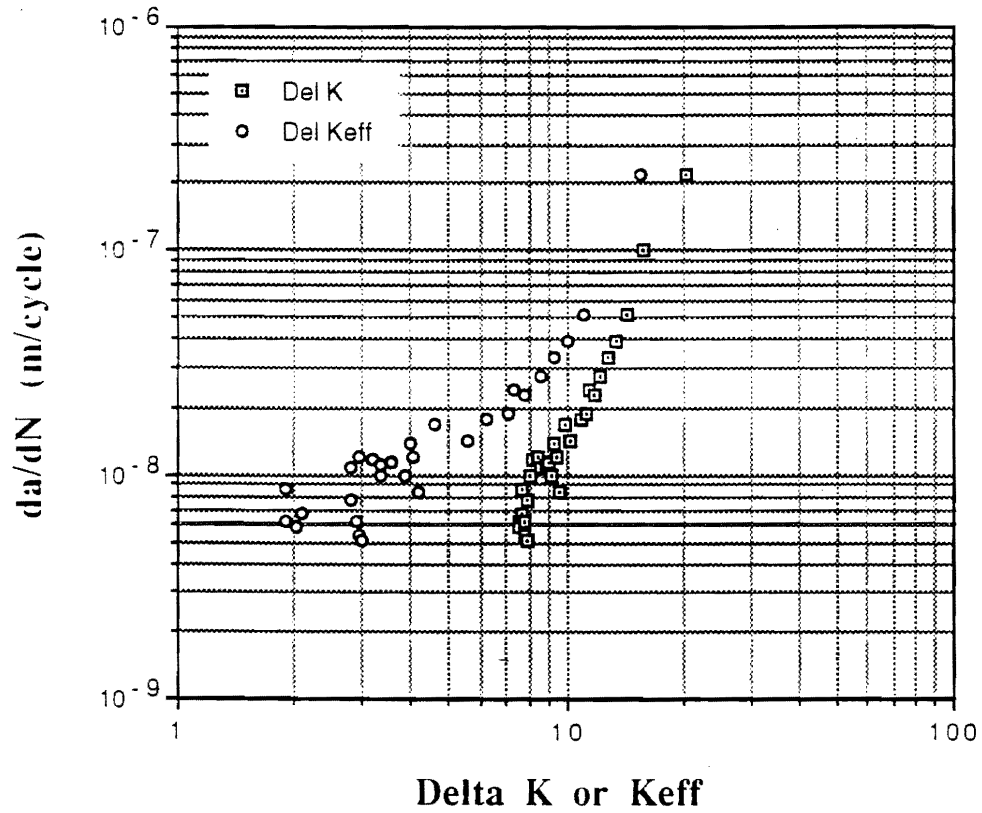
Fig. 13   Fatigue Crack Propagation Rate vs. ΔK_{eff}

da/dN vs. Crack Length for CT12
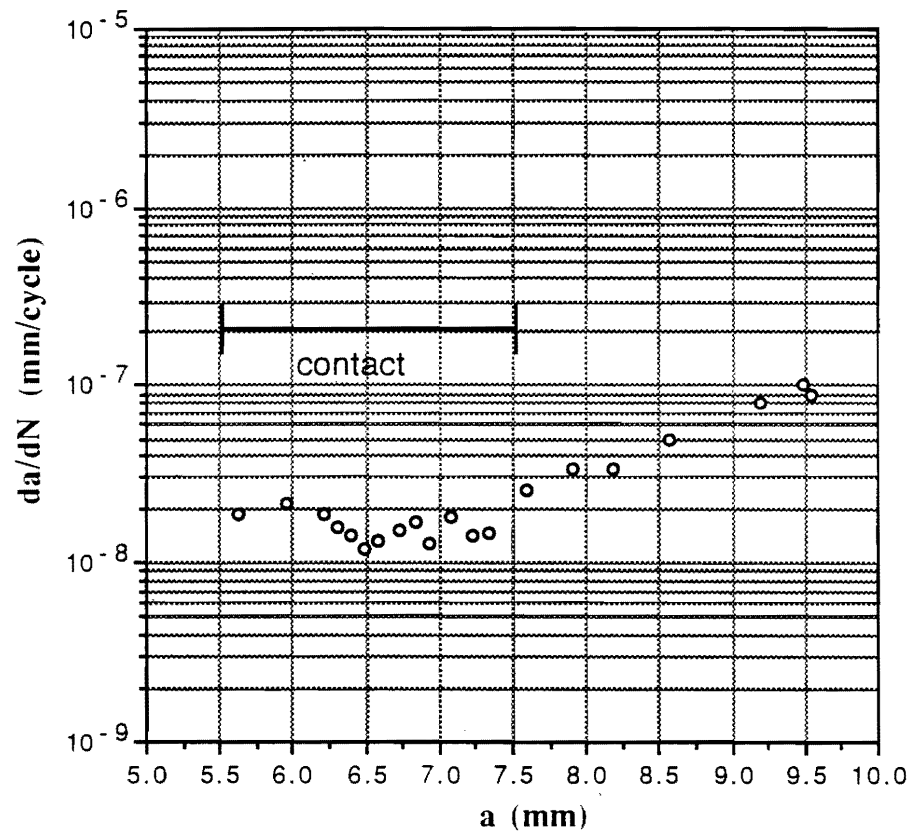
Fig. 14   Fatigue Crack Propagation Rate vs. Crack Length

$1200\mu\,\mathrm{m}$
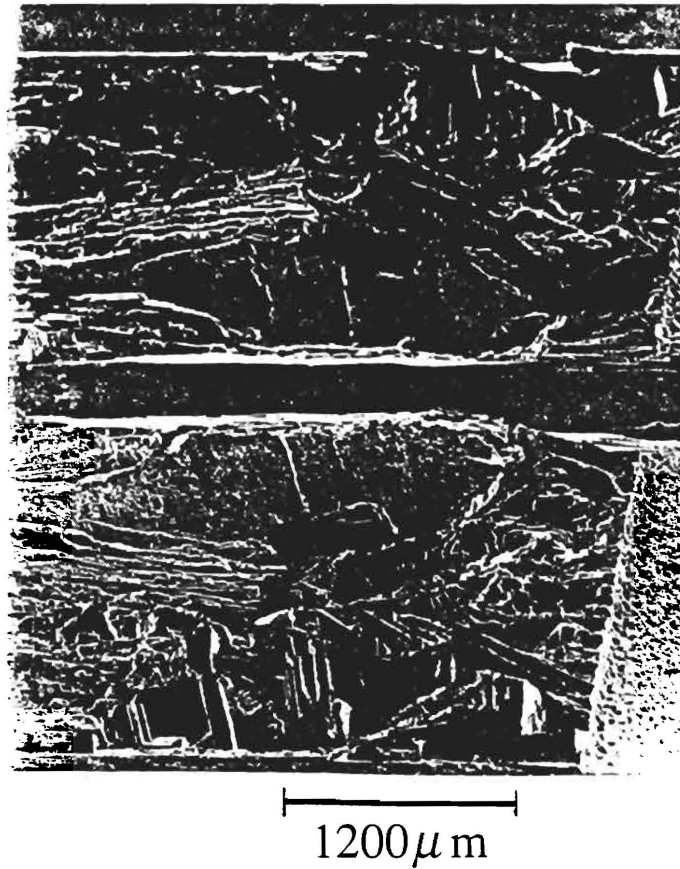
Fig. 15   Fracture surface of Al-li Alloy 2090 specimen.   Crack
propagation direction is from left to right.
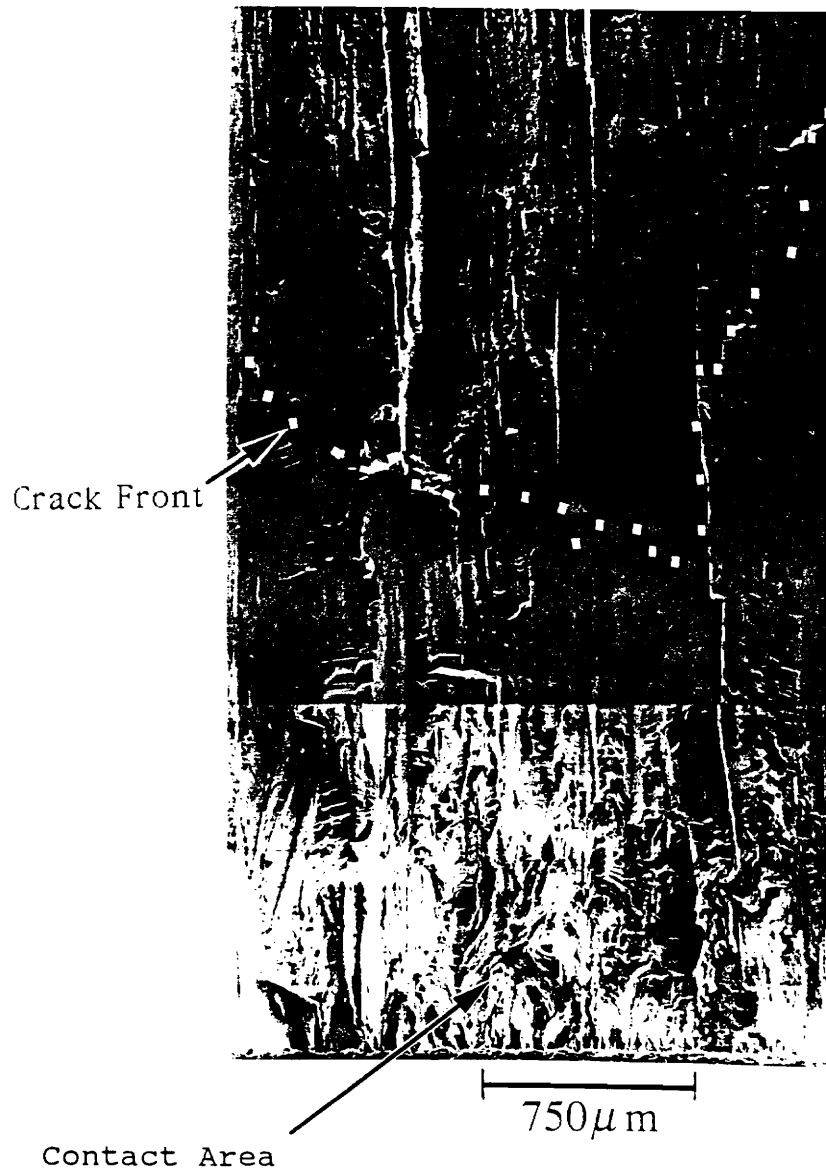
Fig. 16 Fracture surface of Al-li alloy specimen showing a non-uniform crack front (white sequence) and the contact area. Crack propagation direction is from bottom to top.

Final Report for

A Study of the Relationship Between Macroscopic Measures
and Physical Processes Occurring During Crack Closure

N0014-89-J-1708

Submitted to:

Office of Naval Research
Attn. Dr. George Yoder
ONR Code 1131
800 N. Quincy
Arlington, Virginia 22217-5000

by

Stuart R. Stock   Stephen D. Antolovich
Mechanical Properties Res. Lab   Dept. of Mechanical & Mat. Eng.
School of Materials Sci. & Eng.   Washington State University
Georgia Institute of Technology   Pullman, WA 99164-2920
Atlanta, Ga 30332-0245

Table of Contents

Abstract

This report is divided into Parts A and B which cover the numerical modeling with supporting fractography and the high resolution x-ray computed tomography of loaded samples, respectively. The figures for each part immediately follow the text of that part. The focus throughout is to relate macroscopic measures of crack closure to the physical processes occurring at and near the crack tip.

The most significant accomplishments of the program detailed in Part A include the following. Roughness-induced crack closure was characterized by fractographic analysis. The crack tip stress parameter, K, was justified as a forcing function at the crack tip in the roughness-induced crack closure problem. Analytical models were developed to predict the closure stress intensity factor as a function of crack length using a "phenomenological approach." The relations between fractographically measured parameters and the crack driving "force" was investigated.

In Part B, results of high resolution x-ray computed tomography of loaded notched tensile and compact tension samples are discussed. The use of a miniature load frame, developed as part of this project, allowed measurements of crack opening across the entire crack face to be made as a function of applied load. Discussion of these nondestructive measurements is included.

Part A. I. Introduction

In all computational work to date, crack closure was simulated through calculation of effective stress intensity factors. The situation addressed was the case of asperity contact with rigid or elastic asperities randomly distributed on a two-dimensional crack surface. Compact Tension geometry was assumed. For this work, micromechanical approaches were introduced as the basic means to obtain physically-based expressions calculating the forcing function at the crack tip. This method was employed because it provides a way of connecting to the results of the XTM experiments in measuring the effects of crack closure. In addition, stereological techniques were used to provide additional input required to characterize the three-dimensional nature of fracture surface and to represent the most salient measurable features on the actual fracture surface in two-dimensional form. Here, the most significant accomplishments were:

1. The characterization of the roughness-induced crack closure by the fractographic analysis.

2. Justification of the crack tip stress parameter, K, as a forcing function at the crack tip in the roughness-induced crack closure problem.

3.   Development of analytical models to predict
      the closure stress intensity factors as a
      function of the crack length using a
      "phenomenological approach".

4.   Investigation of the relations between
      fractographically measured parameters and the
      crack driving forces.

II. Fractographic Analysis

The motivation for this analysis is to answer the questions
"What is the nature of roughness-induced crack closure?" and
"What aspect of roughness height most significantly affects crack
closure measurements?" or equivalently "What is the relationship
between the roughness height and crack driving forces?".

A. Microscopic Observations

As seen in Figs. 1.1 and 1.2, roughness-induced crack
closure is evidenced by fracture surface contact. Fig. 1.1b
shows an enlarged area of the contact point indicated in Fig.
1.1a. It can be seen that very fine particles and oxides (from
EDX analysis) are exiting from the inside of the specimen. This
process stops when the crack length increases to some value where
there is a large degree of separation between the crack surfaces.
In Fig. 1.2, an abraded area near the specimen surface is also

shown. This was observed on the outside of specimen during the test.

In addition to the contact observations made externally, several different contact patterns which occurred inside of the specimen, are shown in Figs. 1.(3-5). In Fig. 1.3a it can be seen that opposite faces are wedged open by the roughness formed due to cracking on crystallographic slip planes. In Fig. 1.3b it is clear that the fracture surfaces can be shattered and distorted due to contact each other. Figures 1.4a and 1.4b show that either large or small particles torn from the basic fracture surface can block the contact of the fracture surfaces. Figures 1.5a and 1.5b show that separated grain boundaries can also abrade each other in the direction of loading. The nature and location of these various contact mechanisms along the fracture surface are summarized in Fig. 1.6. The "wedged open" contacts are normally found near the notch tip area since well-defined crystallographic deformation occurs mostly at the early stage of crack growth. Grain boundary separation occurs when large values of K_{max} are reached. Therefore, this contact mode tends to appear near the crack tip area for large crack lengths. The various documented contact patterns can be viewed in terms of idealizing the contact problem (i.e. appropriately and realistically idealizing the actual roughness on the fracture surface) to facilitate computation of the forcing function at the crack tip. When this is done, the most effective closure mechanisms arise from either the "wedged opened" or "debris

3

blocking" contact patterns. These can be modified to idealized shapes in contact on the fracture surface and used to develop expressions for the forcing function.

B. Quantitative Fractographic Analysis

From the preceeding section, it is observed that the <u>nature</u> of the roughness on the fracture surface plays a key role on the contact of asperities. However, the mechanism of the asperity contact is not defined through knowledge of only the roughness on the fracture surface. A quantitative fractographic analysis was performed to more fully understand the nature and significance of asperity contact. The initial step is to obtain the crack profile on the sections perpendicular to the crack propagation direction. The procedure involves several steps such as cutting the fracture surface from the specimen, mounting it in epoxy, vertical sectioning, polishing, and digitization of the profile. These various steps are shown in Figs. 1.7 and 1.8. A very important step is to define the reference line on the crack profile using least square methods, since this serves as a base line or plane necessary to represent the roughness on the plannar crack surface. Using the reference line the roughnesses on various sections in the thickness or crack propagation direction can be compared each other, as shown in Figs. 1.9 and 1.10. Also this idealizes the three-dimensional features on the complicated fracture surface to a two-dimensional representation in which the

4

roughness has an average height on the plannar crack surface.
The crack surface normally appeared to have mixed mode features.
This concept, which is summarized in Fig. 1.11, clearly
characterize the mixed mode fracture, i.e., modes I and II and
mode I and III. In this representation, asperity contact can be
considered to involve two components: (1) mechanical contact of
asperities due to the roughness on the fracture surface and (2)
mixed mode crack sliding displacements of the crack tip when the
load is applied. Fig. 1.12 shows the deviation of the plannar
crack (which involves Modes I and II) from the line perpendicular
to the loading direction for one of the Al-Li 2090 specimens.
The cracks for most specimens stayed in side groove and deviated
within $5°$, which is allowed in ASTM E-647 specifications. Mixing
of modes I and III is shown in Fig. 1.13 by angular deviation.
As the load range , ΔP, increases, the angular deviations, ϕ,
also increase. However, the deviations oscillate about the same
mean value as the crack length increases. From Figs. 1.12 and
1.13, it can be seen that the contributions of mixed mode
fracture resulting from the sliding displacements vary with
increasing crack length. The average roughness height increases
regularly in the early stages of crack growth, but varies after
reaching the mid-range of ΔK as shown in Fig. 1.14. This figure
shows a possible relationship between the average roughness
height and the nominal range of stress intensity factors for the
different ranges of applied load and R-ratio used in this study.

III. K as a Forcing Function In the Crack Closure Problem.

The <u>fundamental</u> question is whether the crack tip parameter, K, can be used as a forcing function at the crack tip in the crack closure problem. Fig. 2 shows the finite element results for the change of stress around the crack tip with and without closure. From this, it is clear that the change of stress near the crack tip for both the non-closure (slope A) and closure (slope B) varies linearly with the inversely square root of distance from the crack tip. Also, slope B is smaller than slope A, which indicates the forcing function is reduced due to the crack closure. Therefore, the stress intensity parameter, K, appears to be a valid parameter to represent the change of stress distribution when crack closure occurs.

IV. Analytical Modeling of Closure Stress Intensity Factors as a Function of Crack Length.

The goal of this work is to predict the variation of closure stress intensity factor as the crack length or the maximum of the range of stress intensity factor increases for constant applied load. A recent study by J.E. Allison, (1988) provides some schematic variations of closure for different closure mechanisms as shown in Fig. 3.1. As seen from the figure, two different curves are hypothesized for asperity contact: one is constant (for most titanium alloys) and the other is decreasing reversed-exponentially (for some ferrous alloys).

The following "phenomenological approach" is suggested in order to predict analytically the variation of closure stress intensity factors. This method uses the closure load, P_{cl}, as determined by extrapolating two compliance curves and finding the intersection as shown in Fig. 3.2a. Then a parameter, V_{cl}, corresponding to the closure load is introduced as a "representative" closure crack opening displacement. From the fractographic analysis, it was observed that the most asperity contact occurs in the wake zone behind the crack tip. Then the closure stress distribution in this area may be in the form of tailing off equation, which is shown in Fig. 3.2b. If the distributed contacts are converted to a single contact by an imaginary equivalent asperity, the "representative" closure crack opening displacement corresponds physically to the crack opening displacement which occurs at the location of the single asperity, C_{cl}.

Two different models are suggested to predict the variation of the closure load with crack growth, as shown in Fig. 3.3. In model A, when the crack grows, the new contact distance, C'_{cl}, would be assumed to be the distance linearly increased by an amount equivalent to the increase in crack length. In model B, the new contact distance is assumed to be independent of the increment in crack growth. Assuming that the mechanism of crack closure opening displacement at asperity contact remains unchanged, the new closure load must be reduced in order for the new contact to occur at C'_{cl}. This conceptual model predicts a

7

variation of the closure stress intensity factors as shown in Fig. 3.4. The only difference from the hypothesis made in the previous study is that model A predicts an exponentially decreasing value with crack extension. As shown in Figs. 3.5 and 3.6, the predictions of model A appear to be well correlated to experimental data obtained for Al-Li Alloy 2090. Here, the analytical result was obtained for $C_{cl}=C_1 a$, where a is a crack extension, and C_1 is experimentally observed to be less than 0.3.

V. Conclusions

The most significant contributions of this work lie in developing a more in-depth understanding of asperity contact mechanisms by means of direct observation and quantitative fractographic analysis and incorparation of this information into the development of quantitative models for crack closure. Also the finite element analysis clearly shows that the crack tip stress parameter, K, can be used as a valid parameter to represent the stress change around the crack tip due to the asperity contact. With some experimentally observed information, the analytical model predicts closure stress intensity factors which correlate well with experimental data.

a)
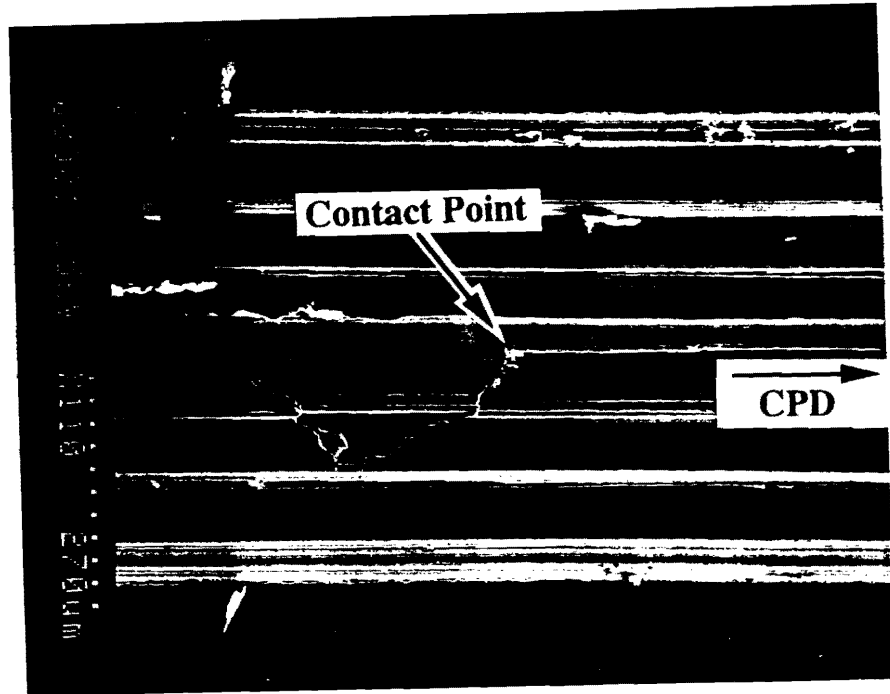
b)

Figure 1.1:   a) Fracture surface contact at the
                   kinked point. "CPD" means the crack
                   propagation direction.
               b) Enlarged area of a).
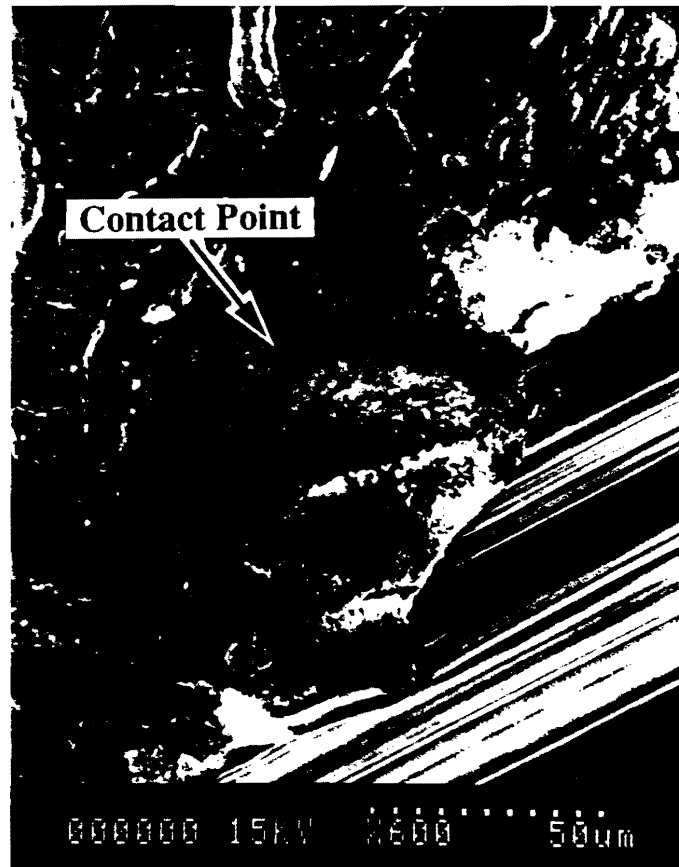
Contact Point

Figure 1.2: Abraded fracture surface on the inside of the
specimen at the contact point of a).

a)
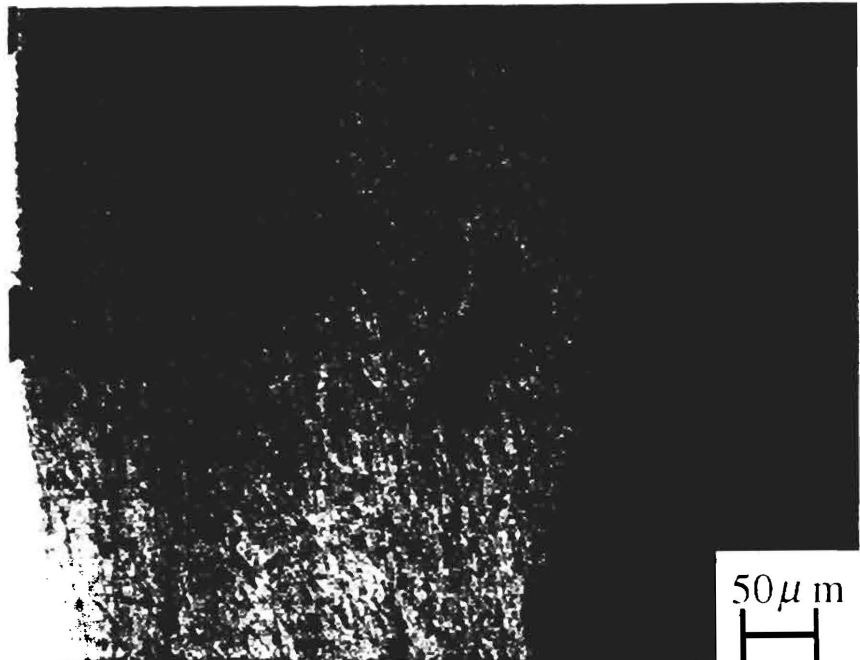
b)

Figure 1.3: a) Opposite faces are "wedged open".
            b) Fracture surfaces are shattered and
                distorted due to contact each other.

a)

20μ m

b)

20μ m
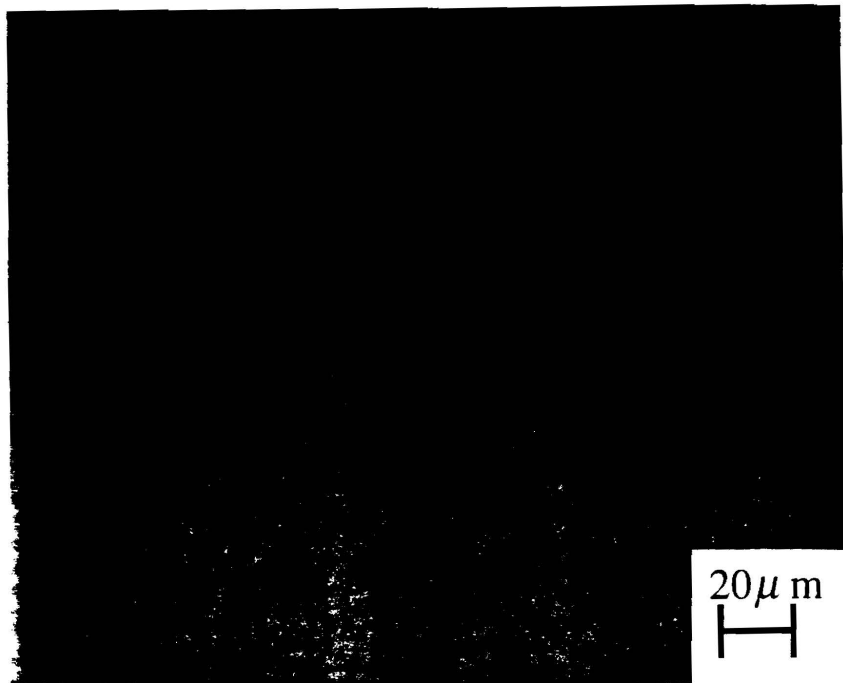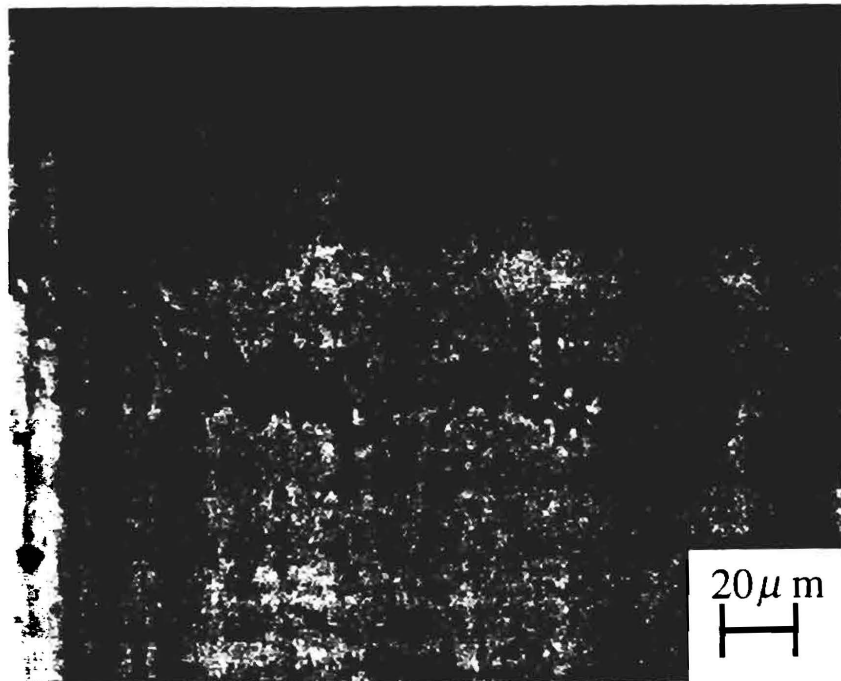
Figure 1.4: Either a) large or b) small particle torn from the fracture surface blocks to contact of surfaces.

12

a)

b)

Figure 1.5:   Separated grain boundaries a) abrade or
                b) contact in the direction of loading.

Notch Tip

Crack Tip

Wedged Open

Particle or Debris
Block

(Crystallographic Slip)

Delamination

(Higher Kmax)

(Large Plastic Zone)

Static Mode Mechanisms
Cleavage,Intergrannular
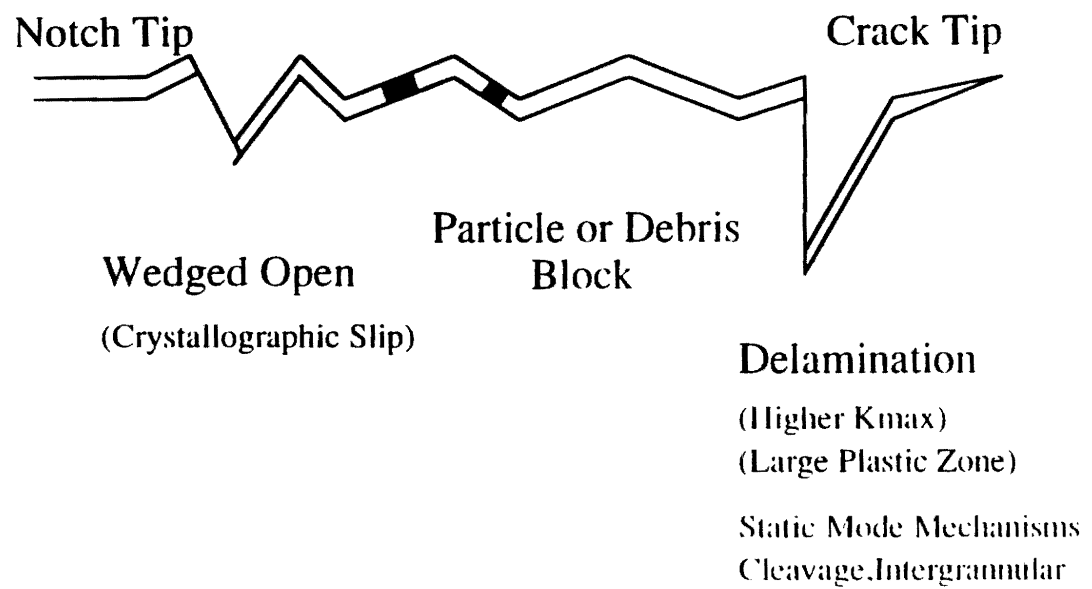
Figure 1.6:   Schematic view of various contact mechanisms
along the fracture surface.
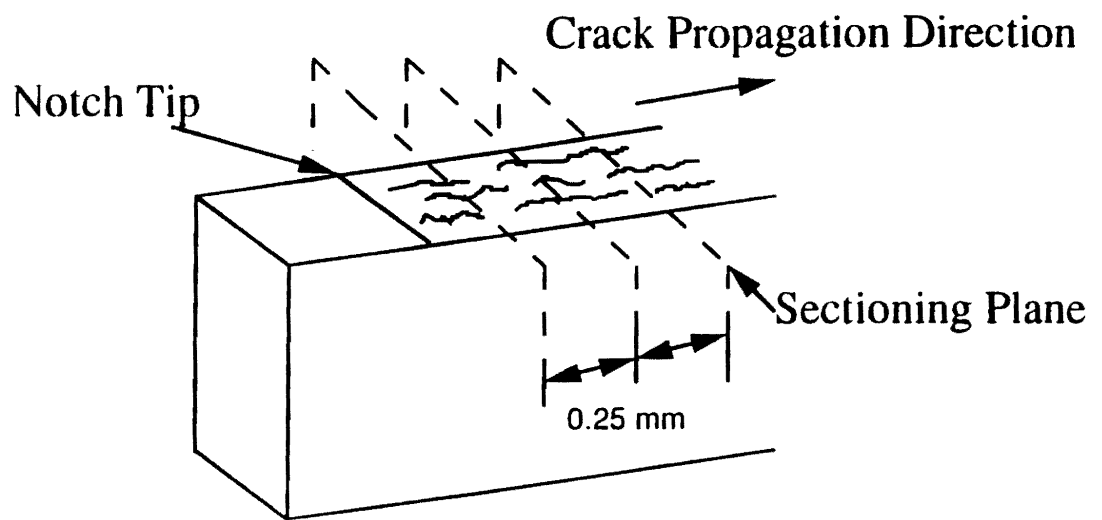
Figure 1.7: Sectioning scheme of fracture surface in the direction of crack propagation.
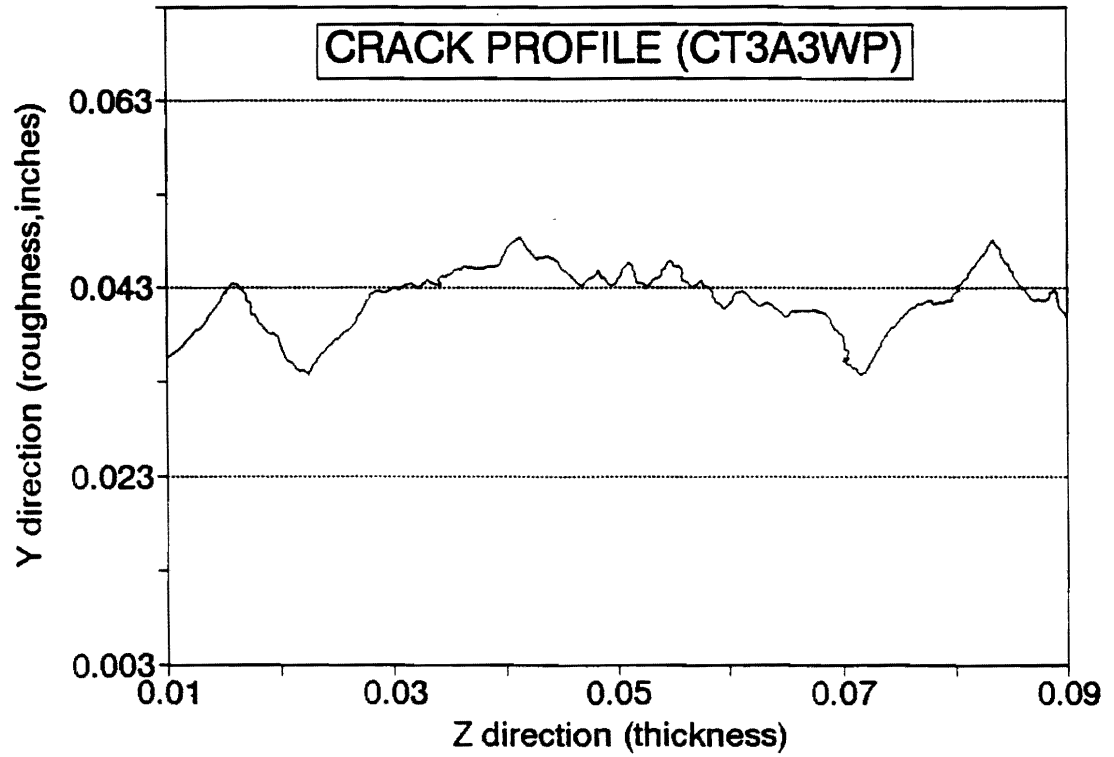
Figure 1.8:   Digitization of crack profile of which
               dimensions are actual.

16

Comparison of Roughness for Contact and Non-contact Sections
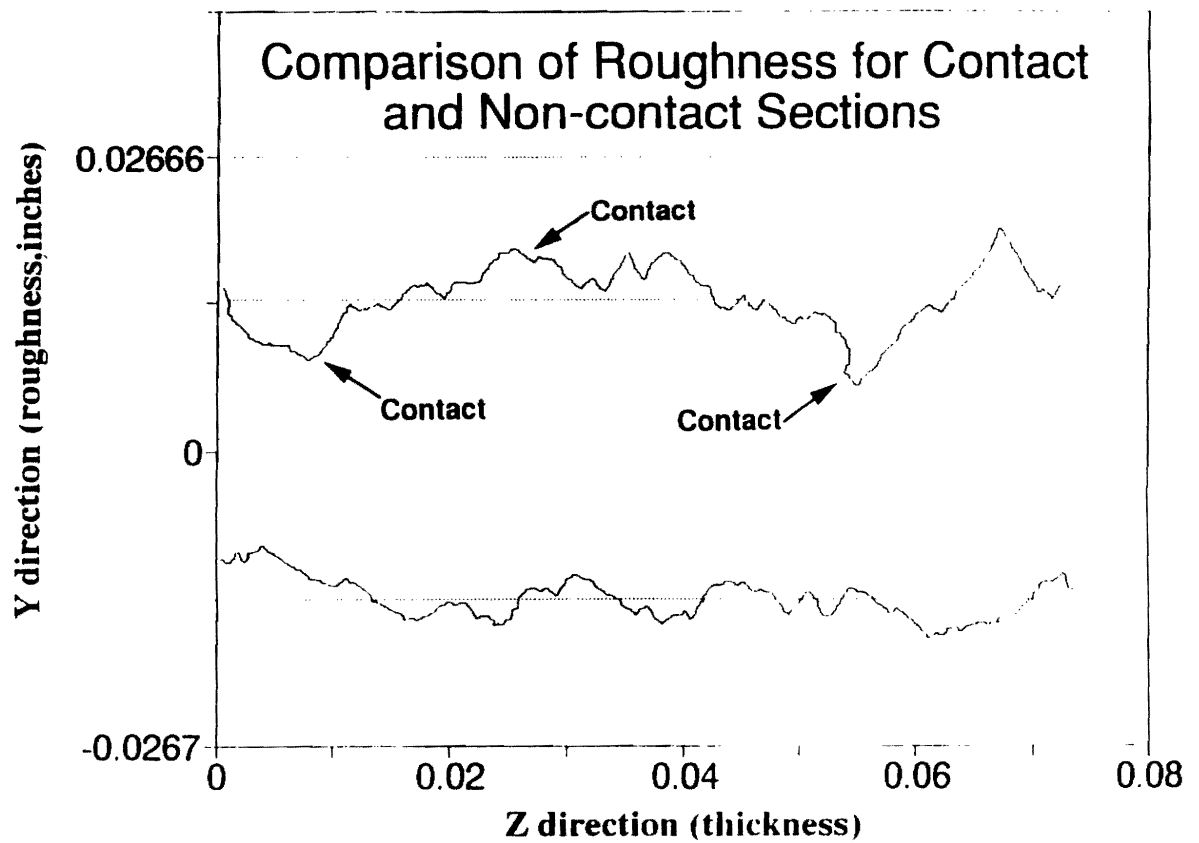
Figure 1.9:   Comparison of roughness on contact and non-contact sections in the thickness direction.
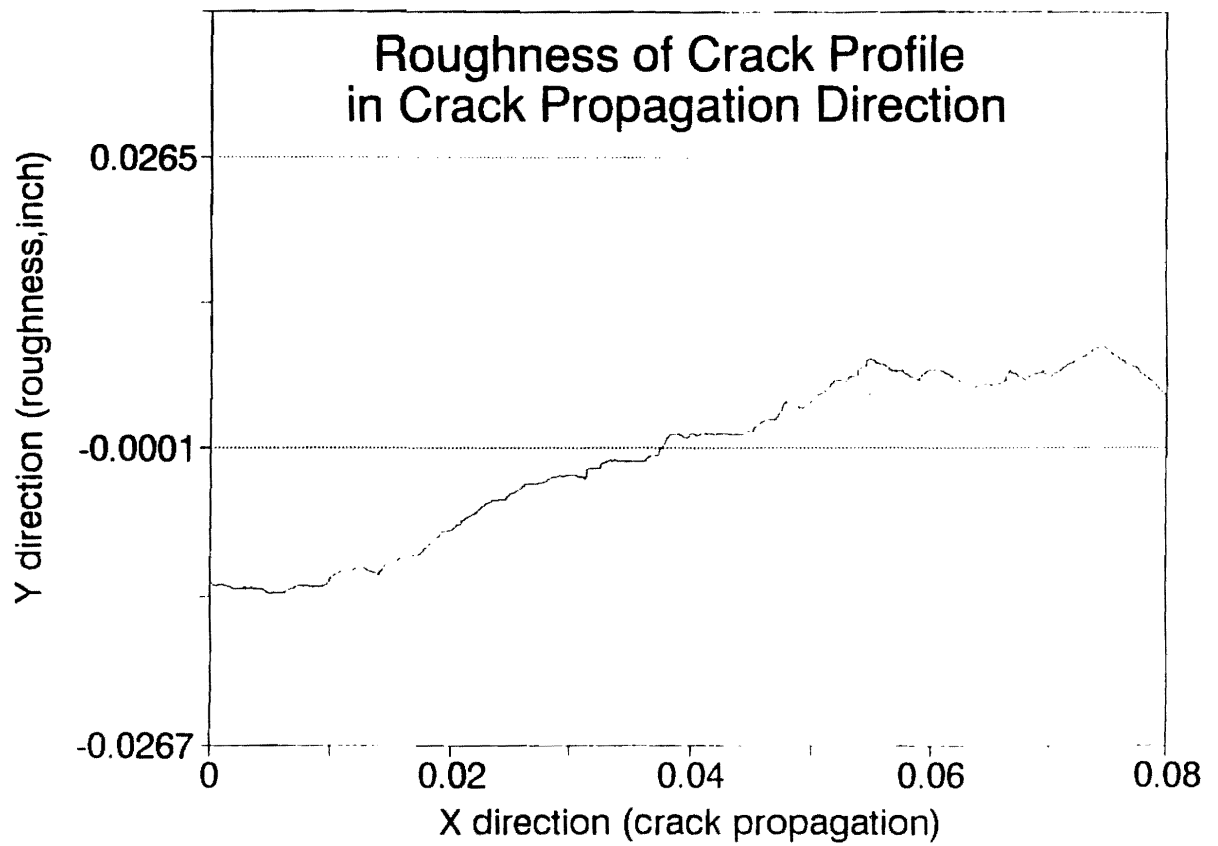
Figure 1.10: Roughness on the fracture surface in the crack propagation direction.

18
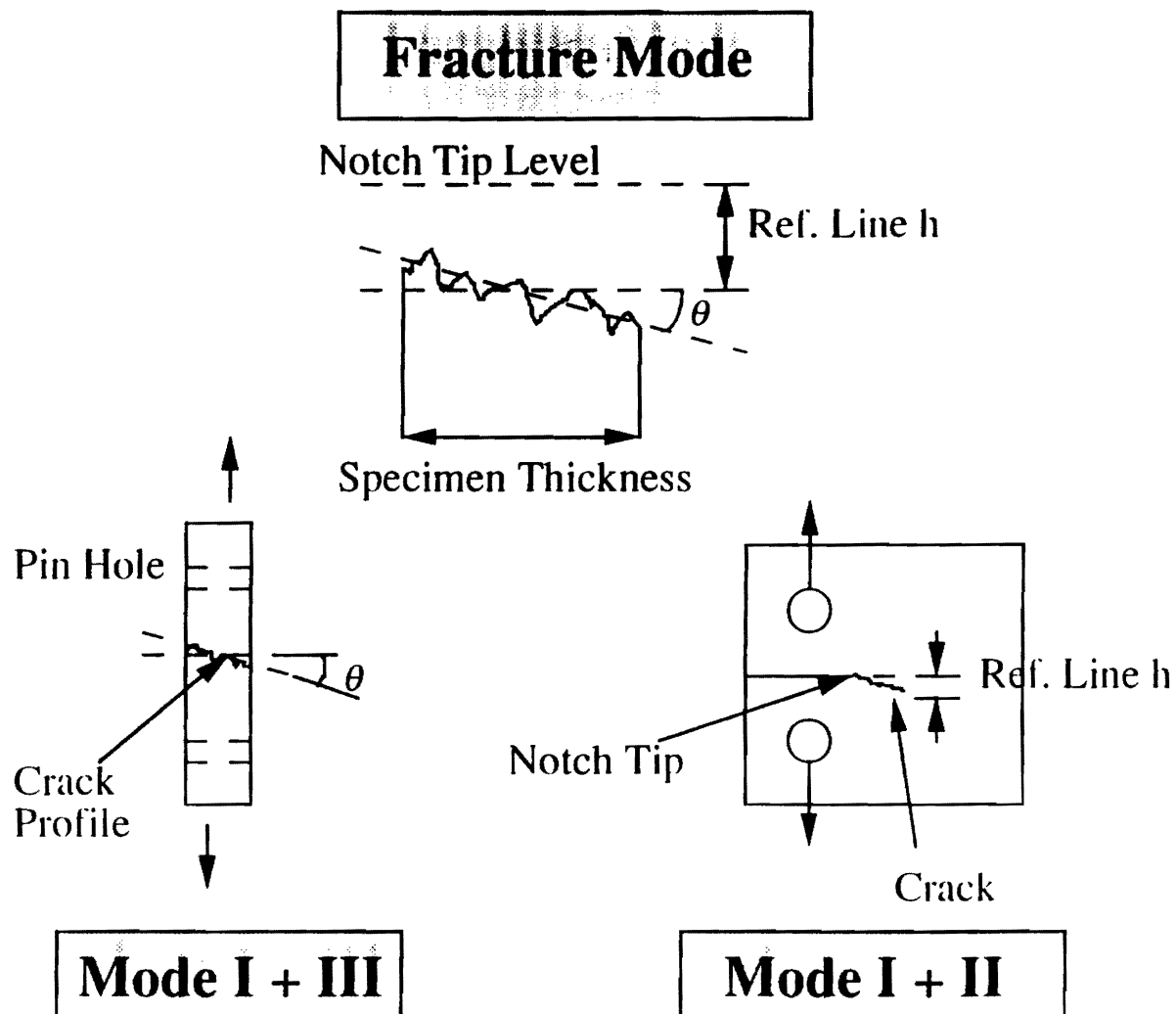
Figure 1.11:   Characterization of the mixed mode fracture
                 by fractographic analysis.
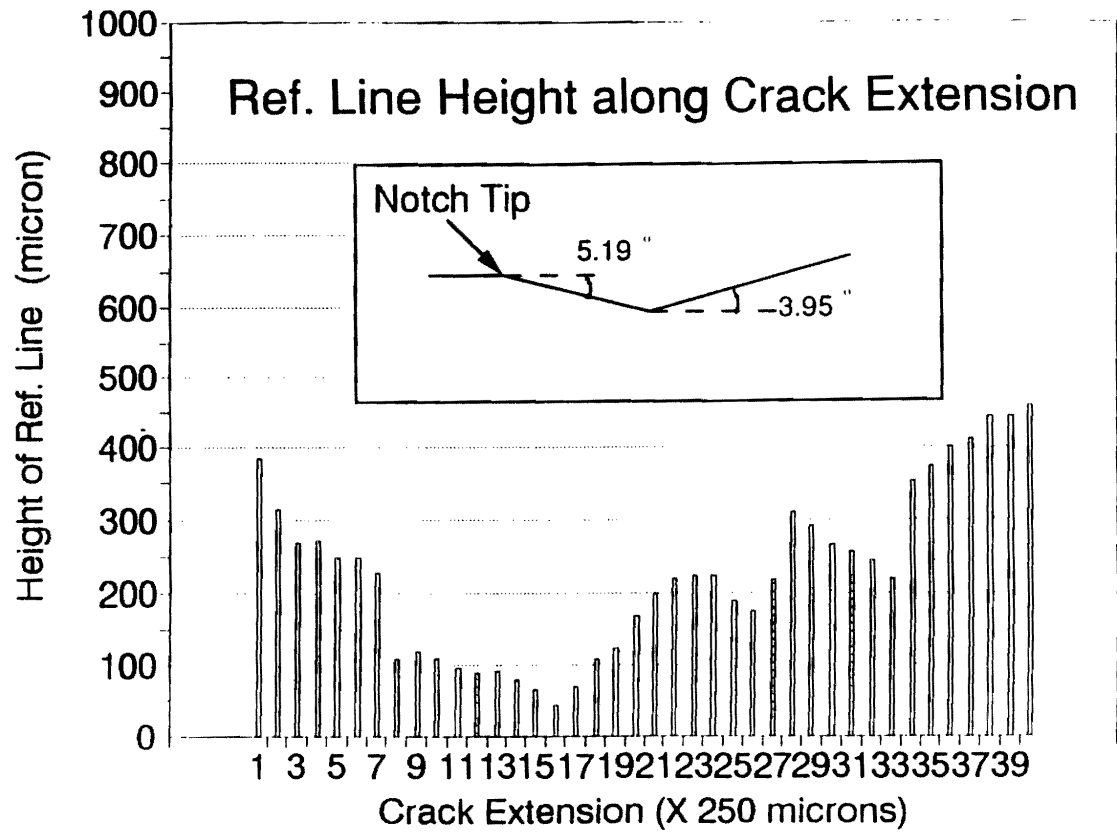
Figure 1.12:   Deviation of the planar crack (Mode I and II)
                along the crack extension.
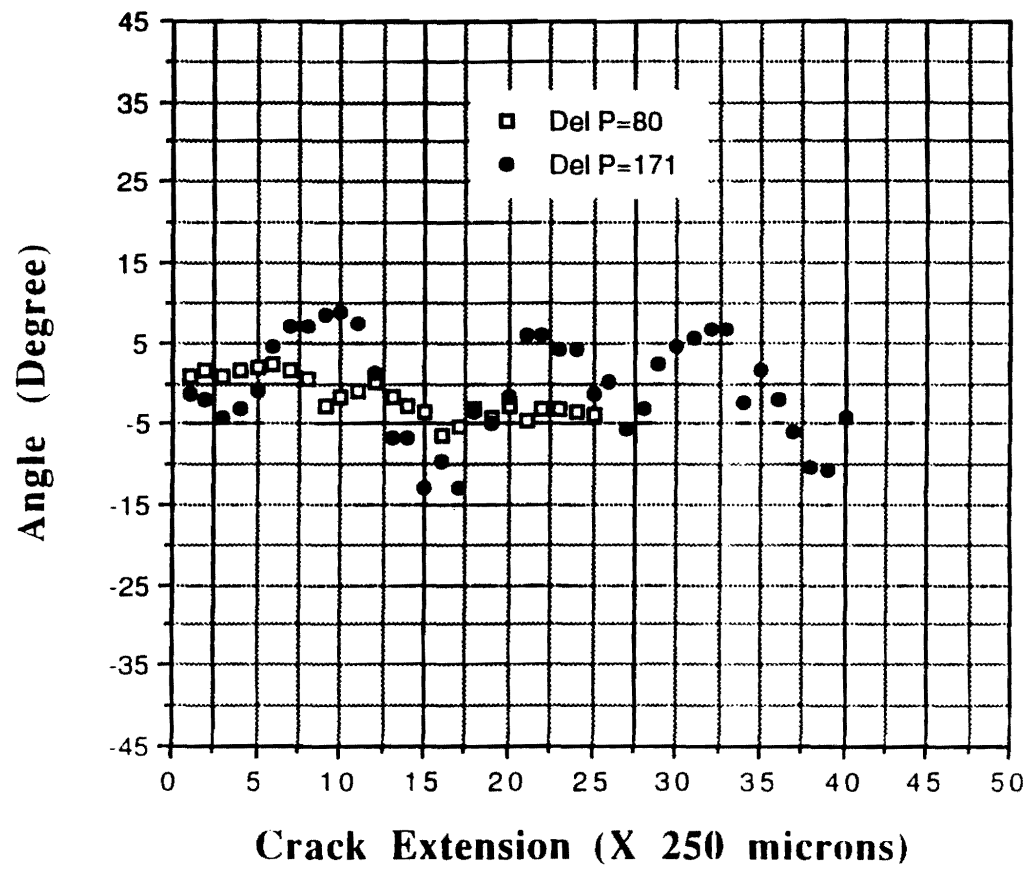
Figure 1.13: Representation of mixing of Mode I and III by angular deviation along the crack extension.

Ave. Height vs. Delta K for R and Delta P
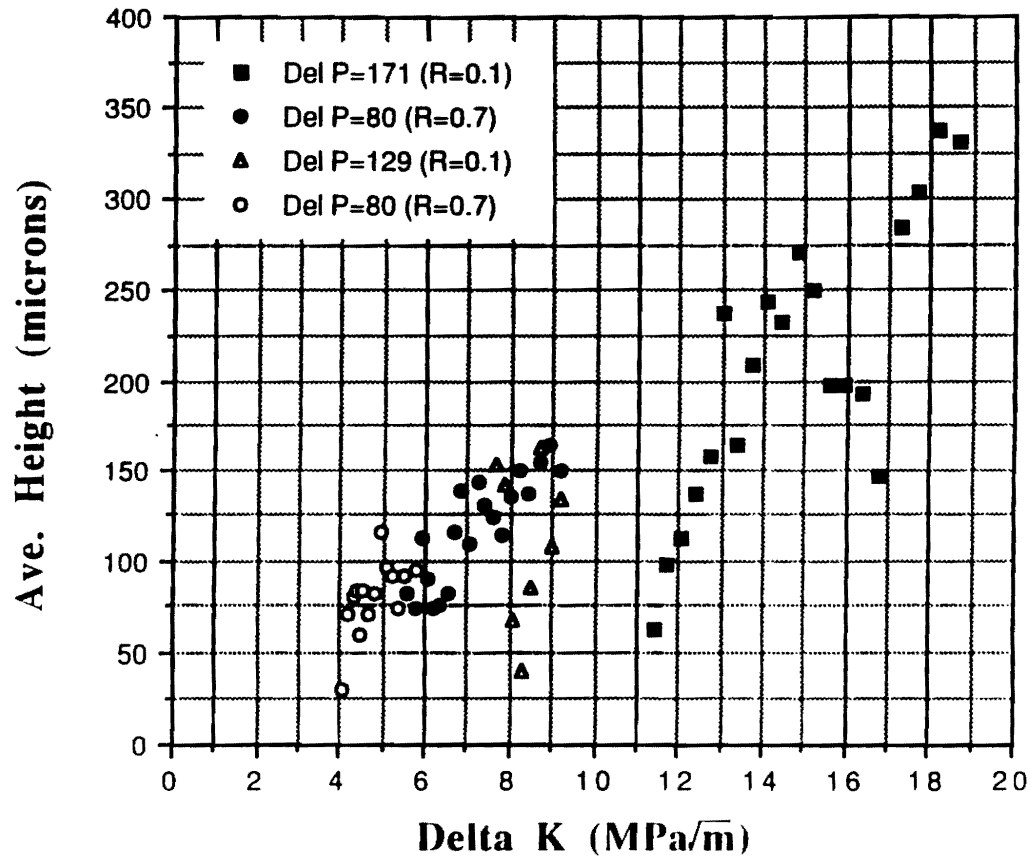
Figure 1.14: Average height of roughness versus the nominal range of stress intensity factors.

Variation of Delta Sigma Y along R (Closure and Non-closure,c/a=0.26)
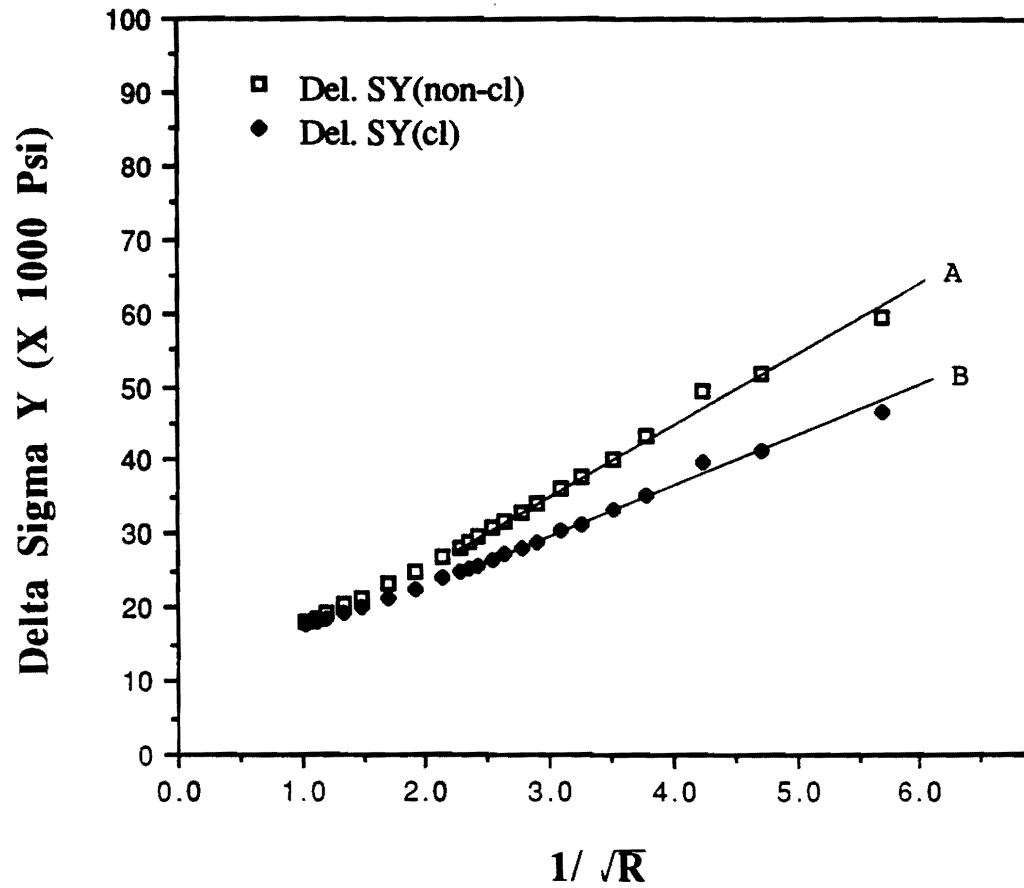
Figure 2: The change of stress near the crack tip with and without closure versus the inversely square root of distance from the crack tip.
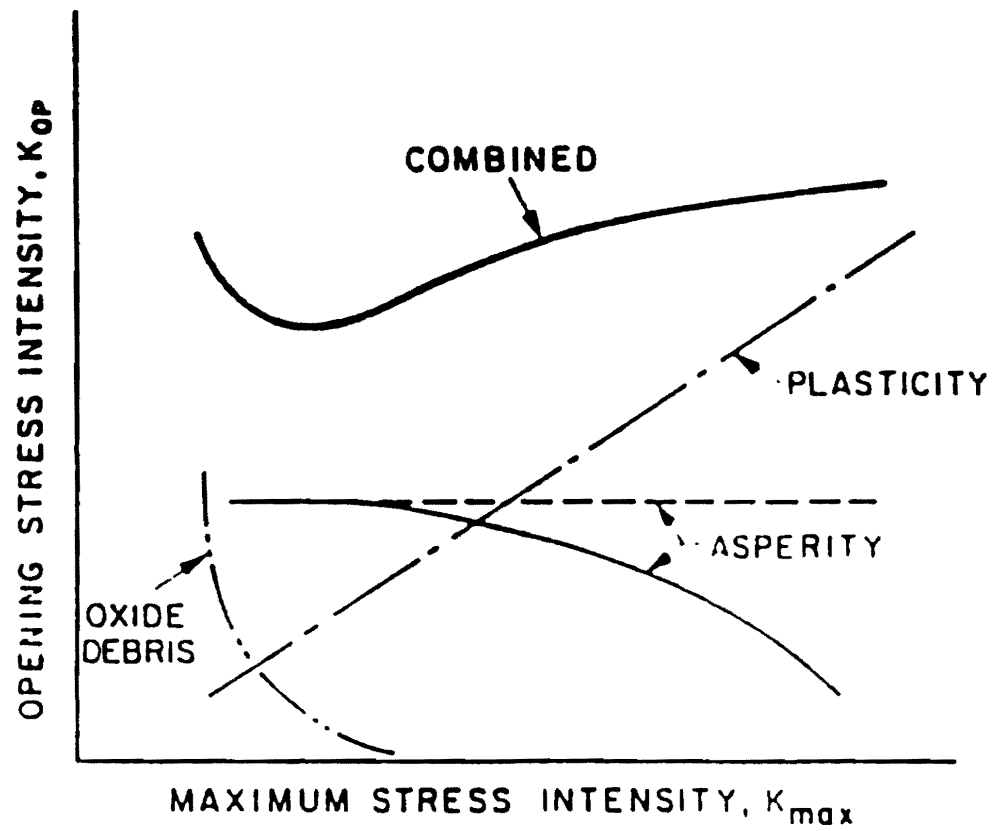
Figure 3.1:   Schematic variations of closure for different
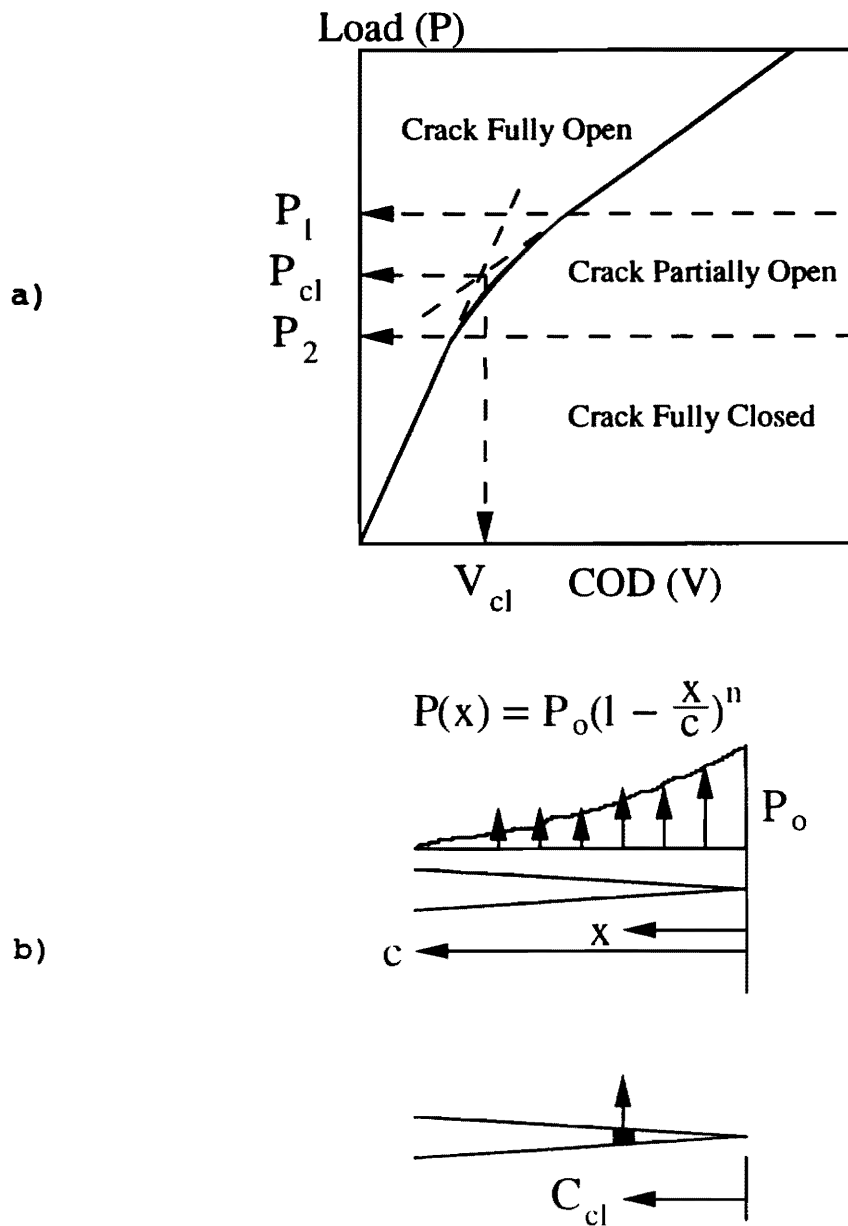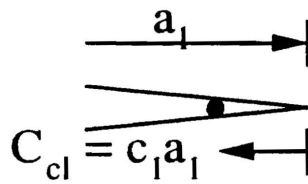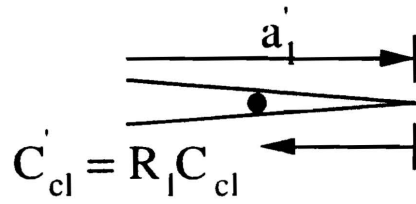   closure mechanisms. (J.E. Allison, 1988)

a)

Load (P)

Crack Fully Open

P_1

P_{cl}

Crack Partially Open

P_2

Crack Fully Closed

V_{cl} COD (V)

b)

$$P(x) = P_o(1 - \frac{x}{c})^n$$

P_o

c x

C_{cl}

Figure 3.2: a) Determination of closure load, P_{cl}, and "representative" closure crack opening displacement, V_{cl}, by extrapolating two compliance curves.
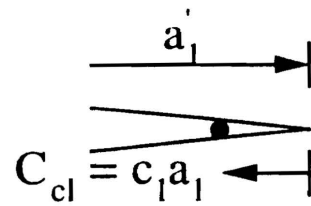 b) Closure stress distribution in the wake zone behind crack tip.
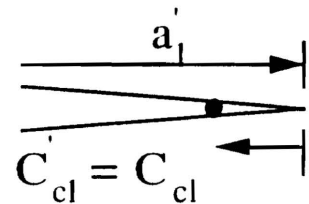
25

Model A

$$a_1$$

$$C_{cl} = c_1 a_1$$

Model B

$$a_1'$$

$$C_{cl} = c_1 a_1$$

$$\boxed{1}$$

$$a_1'$$

$$C_{cl}' = R_1 C_{cl}$$

$$a_1'$$

$$C_{cl}' = C_{cl}$$

$$\boxed{2}$$

$$R_1 = \frac{a_1'}{a_1} = \frac{a_1 + \Delta a}{a_1}$$

$$R = \frac{V_{cl}^2}{V_{cl}^1} \qquad P_{cl}^2 = \frac{V_{cl}(a)}{R} P_{cl}^1$$

Figure 3.3: Schematic view of models predicting the variations of the closure load with crack growth.

26

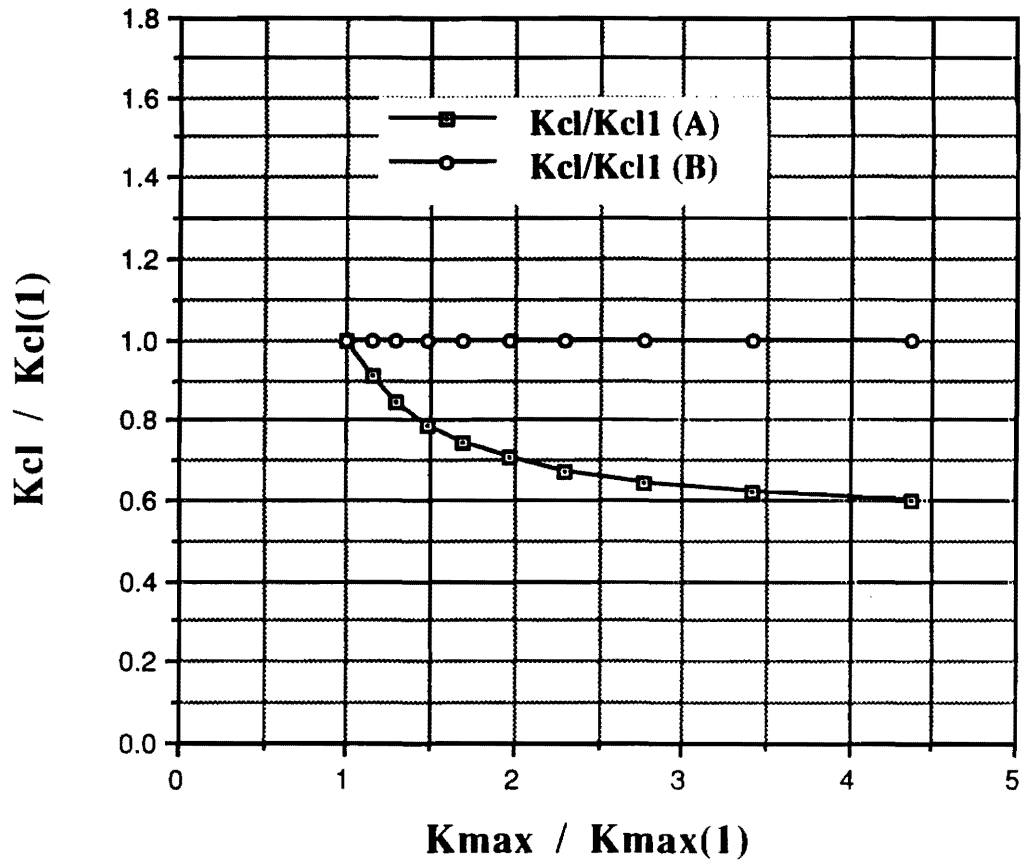# Comparison of Kcl/Kcl(1) for Model A and B

Figure 3.4:   Variation of normalized closure stress
intensity factors along the crack growth.
$K_{cl}(1)$ and $K_{max}(1)$ are the first measured K_{cl}
and K_{max}, respectively.
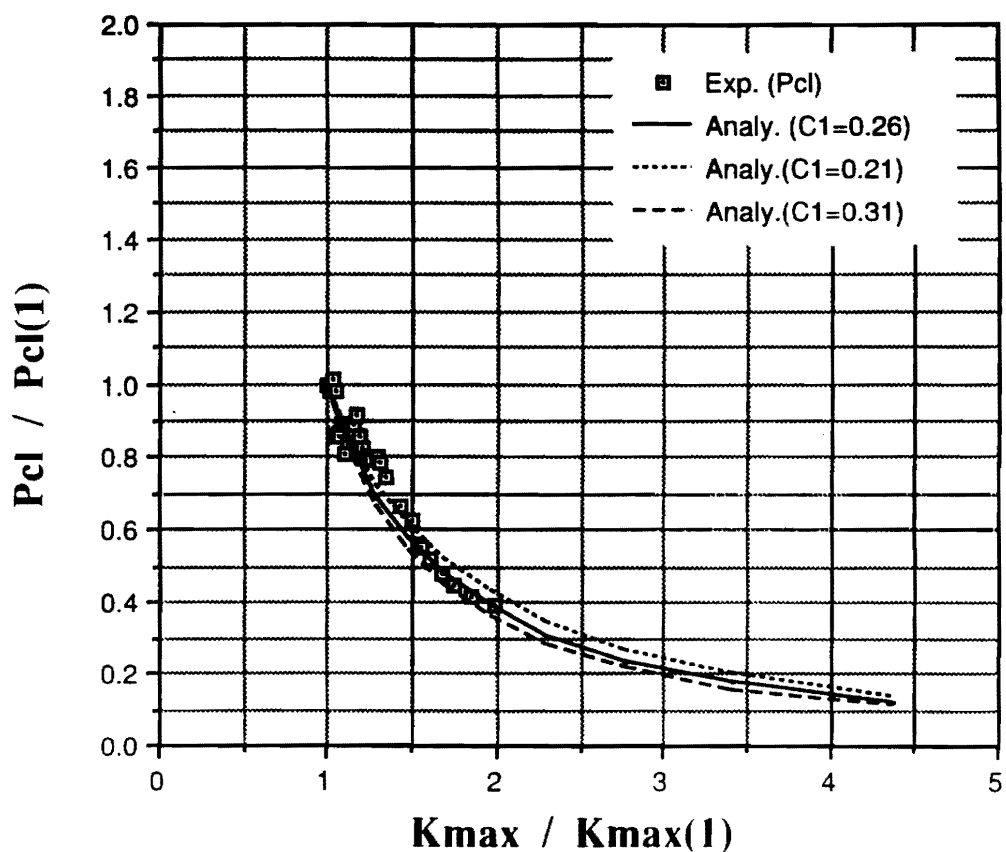
Comparison of Analy. Pcl with Exp. Data

Figure 3.5: Comparison of analytical closure load in model A with experimental data.
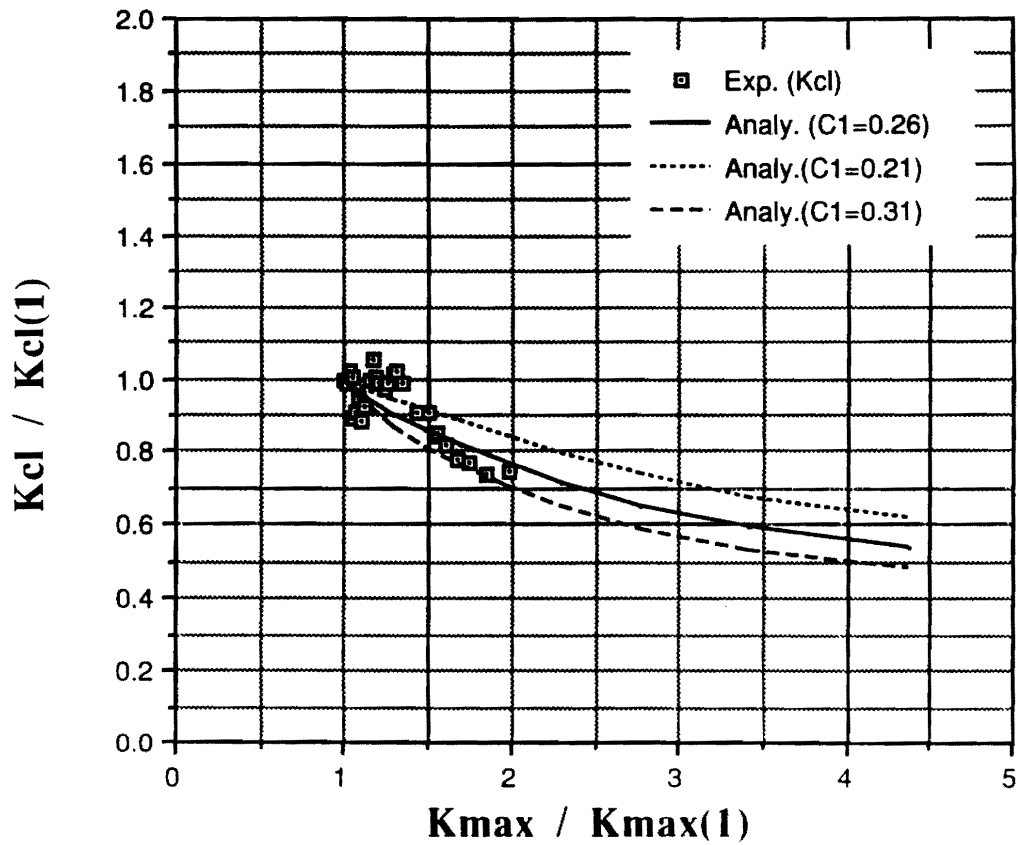
Comparison of Analy. Kcl with Exp. Data

Figure 3.6: Comparison of analytical closure stress intensity factors for various C_1 values with experimental data.

Part B. I. Introduction

The goal of observing crack face interactions in the interior of intact samples was accomplished using very high resolution x-ray computed tomography. Two notched tensile and one compact tension samples were imaged under load using a miniature load frame designed for use with computed tomography under this program. New methods were developed for measuring the amount of opening as a function of position for different applied loads. Two schemes for presenting the crack opening data as a function of position were devised in order to allow one to emphasize the position of the crack tip or to clearly observe the geometry of the surfaces coming into contact at different loads.

II. Direct Observation of Physical Crack Closure

The experiments in which the notched tensile samples (NT-3 and NT-4) were imaged have been discussed in earlier reports, and, for brevity, this will not be repeated here. Two additional imaging experiments were performed on a compact tension sample (CT-2). The first set of measurements were made with the Air Force Materials Laboratory's Tomography system (in collaboration with Air Force and ARACOR personnel, the Air Force's on site contractors). The second was with the high resolution digital radiography apparatus at Lockheed Missiles in Palo Alto, CA. Both were successful in showing changes in crack opening as a function of position and applied load. Only the results from Lockheed are discussed below: the volume element (voxel) size with the ARACOR system was

30

considerably larger than the isotropic 20 μm pixels obtained in the reconstructed Lockheed data.

Fatigue crack growth rates in sample CT-2 and the other samples tested were essentially identical with those reported in the literature for full-sized compact tension samples. After pre-cracking of CT-2, its crack length was 5.6 mm, and at the end of the test, after 651,080 cycles, the crack tip was about 15.2 mm from the load line (i.e., with W = 25.4 mm, the remaining uncracked ligament was about 10.2 mm). The corresponding stress intensity ranges were 15 and 19 MPa$\sqrt{}$m, respectively. The reader should note that P_{max} was initially 106 kg and it was decreased periodically to prevent unstable crack growth.

The Lockheed x-ray system was used in the following configuration: a 2048 x 2048 x 12 bit fiber-coupled camera system was used with a 10 μm focal spot of a Kevex microfocus source operated at 160 kV and 0.06 mA and with a geometrical magnification of 1.8. Images were acquired at 359 angles (the rotation axis was parallel to the stress axis), each radiograph was recorded with 10 sec exposure and the volume containing the crack was reconstructed with isotropic 20 μm voxels using the Feldkamp cone beam reconstruction algorithm. Data was collected at five applied loads: 42, 35, 28, 21 and 8 kg (approximately 92, 77, 62, 46 and 18 lbs). The maximum load was that the sample experienced during the final increment of crack growth.

The load-displacement curve for sample CT-2 was recorded using a laser extensometer after the x-ray imaging. The curve is shown

31

in Figure 1 with the loads at which tomography was performed labeled by arrows and the letters a-e. The closure load, determined by linear extrapolation of the upper and lower ranges of the curve, is seen to be about 16 kg (35 lbs).

From the reconstructed data, the three-dimensional volume of material containing the crack can be numerically sectioned along any arbitrary plane. In the case of sample CT-2, visualization is best (and comparison of the crack within the same volume of material at different loads is most precise) if one numerically sections along the planes containing the stress axis and the sample face (Figure 2): in other words, the cuts span the sample thickness from one face to the other, and the side-grooves appear in the left and right of each cut separated by 1.75 mm. Figure 2 shows every tenth cut, i.e., the 20 μm thick cuts of material are spaced by 200 μm, at the highest load. The numbers in the lower left of each cut give the cut's distance in mm from the notch tip. Darker pixels correspond to voxels with lower absorption, the tips of the two side-grooves (1.75 mm apart) are visible at the left and right center of each image and the stress axis is vertical.

The series of cuts reveals that volumes of asperity-dominated crack geometry alternate with relatively planar sections of the crack. Considerable crack branching is visible throughout. The multiple asperities in the material nearest the notch give way to a single large asperity (seen near the left side-groove in cuts 0.3 through 1.1) on one side of a relatively flat crack. The gentle waviness of the crack continues between 1.3 and 3.1 mm, with the

crack inclined at a slight angle to the surface in cuts between 1.3 to 1.9 mm, a transition region where the crack bows concave up and the crack running directly across the sample between cuts 2.3 and 3.1 mm from the notch.

Multiple asperities dominate the crack geometry from 3.3 to 6.1 mm. After this the crack becomes relatively flat until 8.1 mm where the asperities appear to become important once again. The contrast from the crack begins to disappear beyond 8.3 mm for cuts at 8 kg load, but at 42 kg load the crack is visible across the entire cross section until about 8.6 mm. Some discontinuous-appearing sections of the crack are seen until about 9.6 mm, which is about the maximum extent of the crack seen in carefully aligned radiographs, but the contrast of the crack differs little from the noise in the image surrounding it. The compliance measurements indicate that the crack extended about 9.7 mm from the notch, which is in good agreement with the tomographic results. The sample is still intact, so that no further comparisons can be made between the actual crack surface and the tomography results.

Crack opening as a function of position was measured numerically for the maximum and minimum loads, and the procedure consists of several steps. First the average value of the linear attenuation coefficient μ_{avg} of the voxels of uncracked material was determined away from the crack, and any voxels with $\mu < 0.9\mu_{avg}$ were identified as potentially being partially or totally occupied by a crack. The approximate position of the crack was marked manually, and the value of each voxel above and below the approximate center

of the crack was checked until a value of $\mu > 0.9\ \mu_{avg}$ was encountered. The partial volumes of crack in the voxels between the two limits were then summed to give the total crack opening.

Figure 3 shows two pairs of cuts at the maximum and minimum loads (42 and 8 kg, respectively), and this clearly shows the amount and location of the physical crack closure. The location of the top and bottom pairs of cuts are 2.96 mm and 5.12 mm, respectively, from the end of the notch, and these are used to illustrate measurements for different crack morphologies. The total crack opening at each position is shown in the plot below each pair of cuts; the uppermost curve gives the opening at the higher load. Across the two thin volumes of material, there is considerable variation in crack opening and in the amount the opening changes (which gives the amount by which the two crack faces have moved together). In these two cuts the flatter areas of the crack tend to be more open, and subtle differences with position in a single cut are seen in the amount of crack closure. At other locations which are not shown here, however, large differences in crack closure are seen in adjacent areas of the crack. Openings from crack branches away from the main crack are not included here. When crack branching is seen, the crack openings of the branches are recorded separately for further analysis.

Two different methods have been employed to show how crack opening varies as a function of position over the entire crack. In the first, the measured crack opening is projected onto a plane.

34

This show quite directly how the crack tip closes as the applied load decreases. Figure 4 shows this type of representation for notched tensile sample NT-4: increasing amounts of opening are indicated by the progression of colors black, red, blue, green and white.

It is also possible to combine the three-dimensional topography of the crack with the opening measured at each position. In order to understand this scheme, one should first consider a three-dimensional representation of crack position within the interior of the sample (Figure 5 shows a three-dimensional mesh plot of the crack's surfaces). The notch is at the left, and the plot extends about one-half of the distance between the notch tip and backface. The crack extends somewhat farther than is shown in Figure 5, but quantification of opening beyond the positions shown cannot be done reliably over continuous stretches of the crack because of the small amount of opening produces changes of contrast comparable to the noise in the data.

One should note that the contour lines show the relative height of different portions of the crack surface in representations such as Figure 5. One can quite simply superimpose a color-table map of crack opening (such as in Figure 4 for a notched tensile sample) onto the three-dimensional image of the crack "plane." The result is Figure 6, where the colors represent the amount of opening at each position on the three-dimensional crack face. The reader should note that each pixel being assigned a particular color (black, red, blue, green or white, in order of

increasing opening) is accurately located in space relative to the white contour lines showing sample geometry. For brevity, only the amount of crack opening at the maximum load is shown in Figure 6, although similar plots have been prepared for the minimum load and for the difference in opening between maximum and minimum loads. The arrow in Figure 6 points to a very prominent asperity face which, even at maximum loading, is nearly closed. The resulting mixed I-III mode contact upon unloading may be typical of contact producing maximum closure indications.
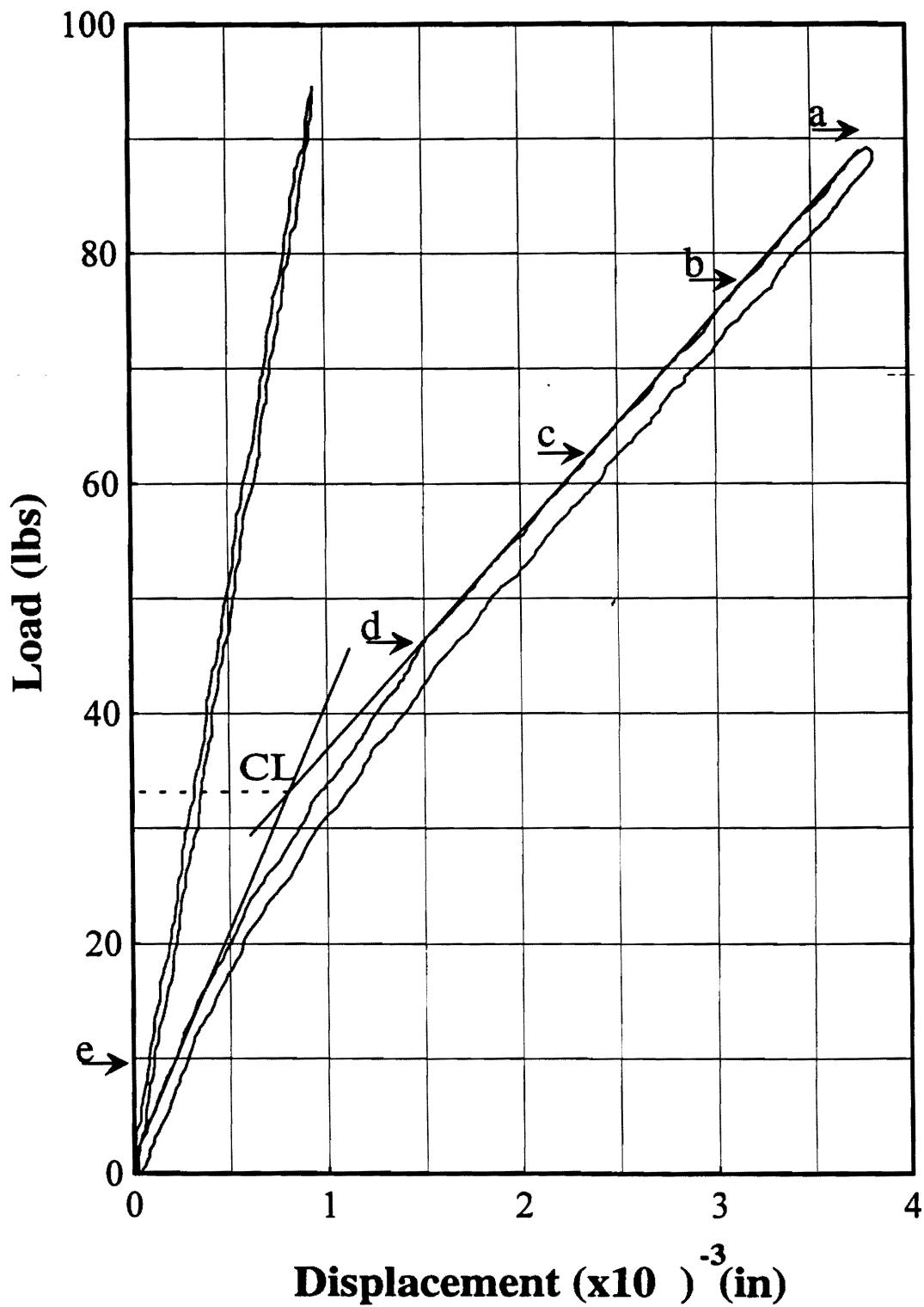
Figure 1. Load-displacement curve for sample CT-2 for the same crack length as for the computed tomography imaging. The letters a-e indicate the loads at which x-ray imaging was carried out, and "CL" indicates the closure load determined by linear extrapolation of the upper and lower portions of the curve.
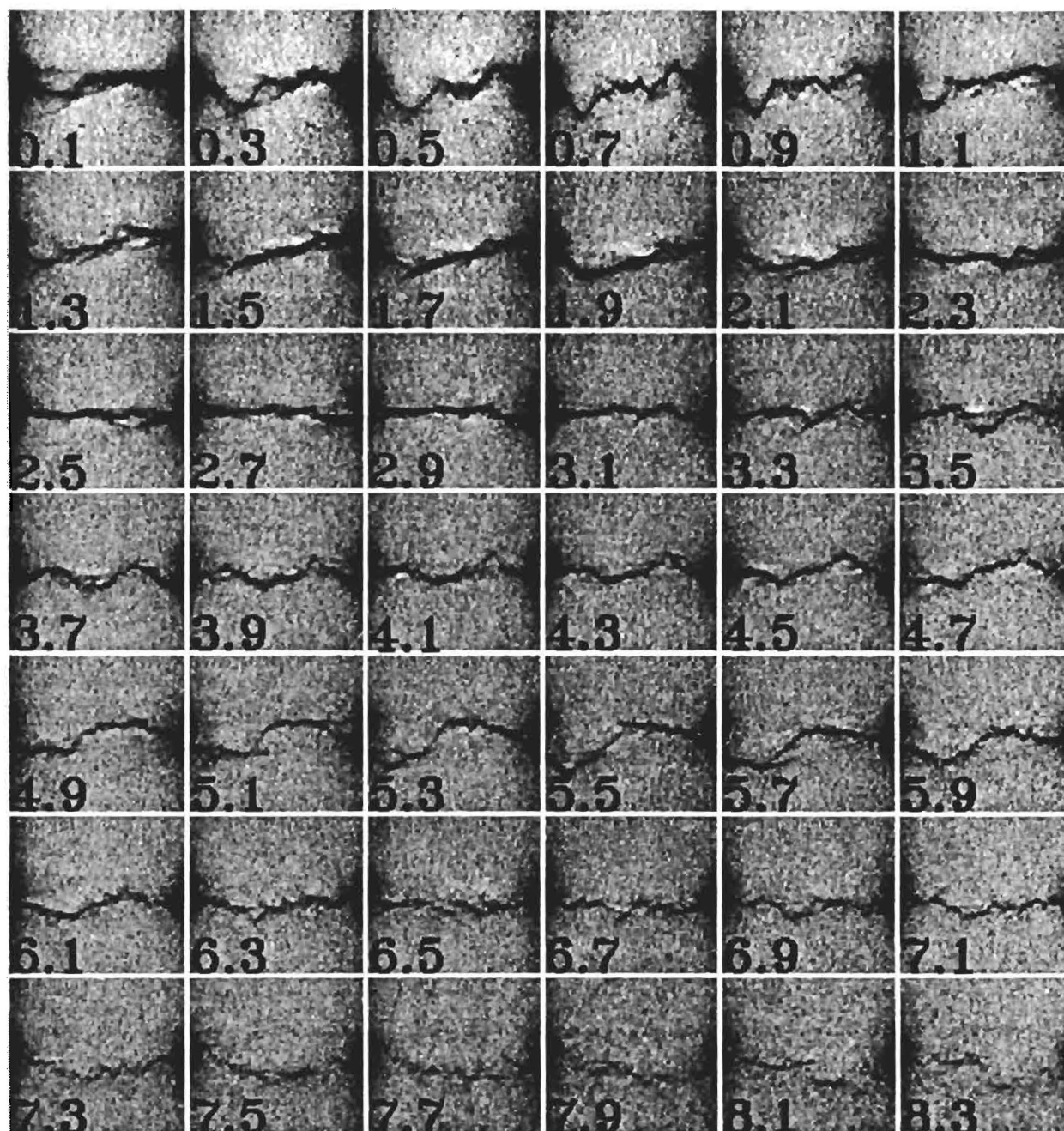
Figure 2. Series of reconstructed sections parallel to the notch tip and showing the crack morphology in sample CT-2. Lower absorption pixels are darker, and the numbers indicate the distance between the cut and the tip of the notch (in mm). The two side-grooves appear on the left and rights sides of each cut, and their separation is 1.75 mm.
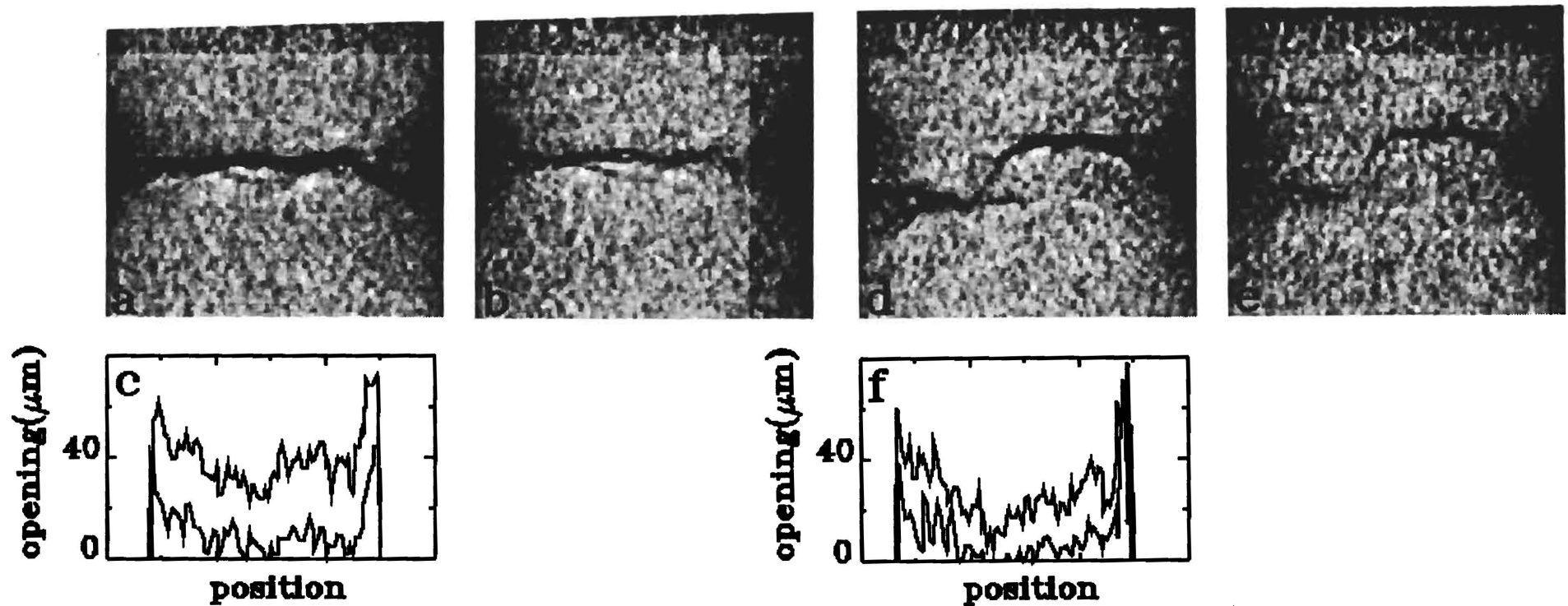
Figure 3.   Cuts and measured crack openings.   In the images the darker pixels show lower x-ray attenuation, the stress axis is vertical and the ends of the side-grooves, visible at the left and right center of each image, are 1.75 mm apart.   a. and b. are cuts 2.96 mm from the end of the notch under 42 kg and 8 kg load, respectively.   d. and e. are cuts 5.12 mm from the notch under 42 kg and 8 kg load, respectively.   c. and f. show crack opening across each cut 2.96 mm and 5.12 mm from the notch, respectively; the upper curve in each corresponds to the higher load.

(in μm)

< 0.4   3   6   9   12   > 15
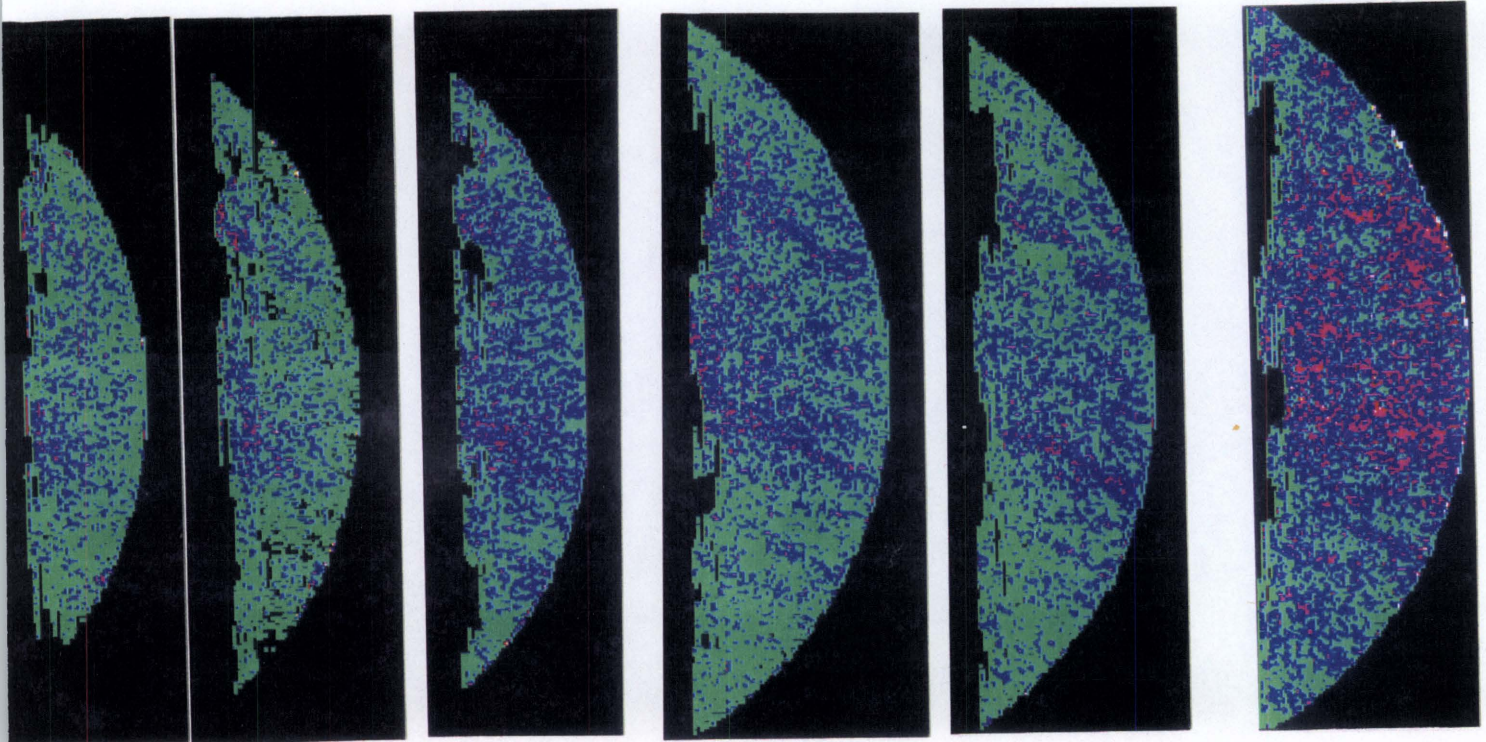
LOAD (in lbs)
50   60   70   80   90   100
LOAD (in kg)
22.7   27.2   31.8   36.3   40.9   45.4

Figure 4   Crack openings measured parallel to the load axis. The color bar
                 indicates the ranges of opening shown for 60, 70, 80, 90 and 100 lbs
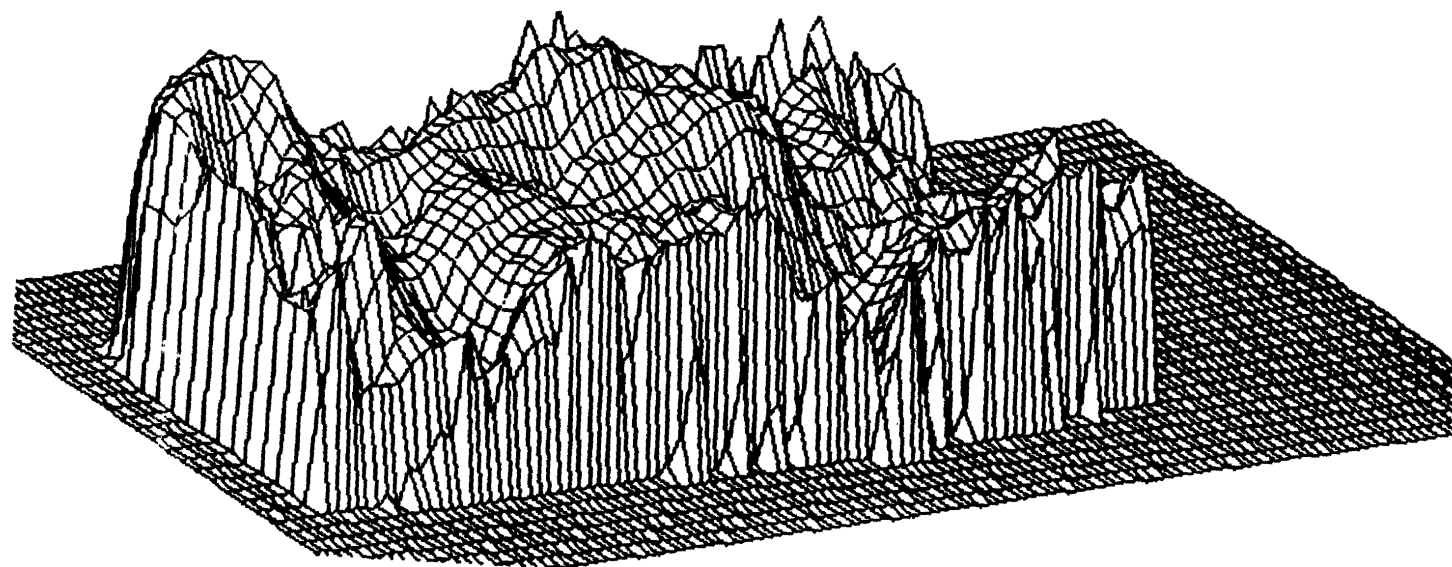   (22.7, 27.2, 31.8, 36.3, 40.9 and 45.4 kg) loads.

Figure 5. Contour map of crack face position within sample CT-2. The notch is at the left, and the tip of the crack is slightly beyond the right edge of the sample
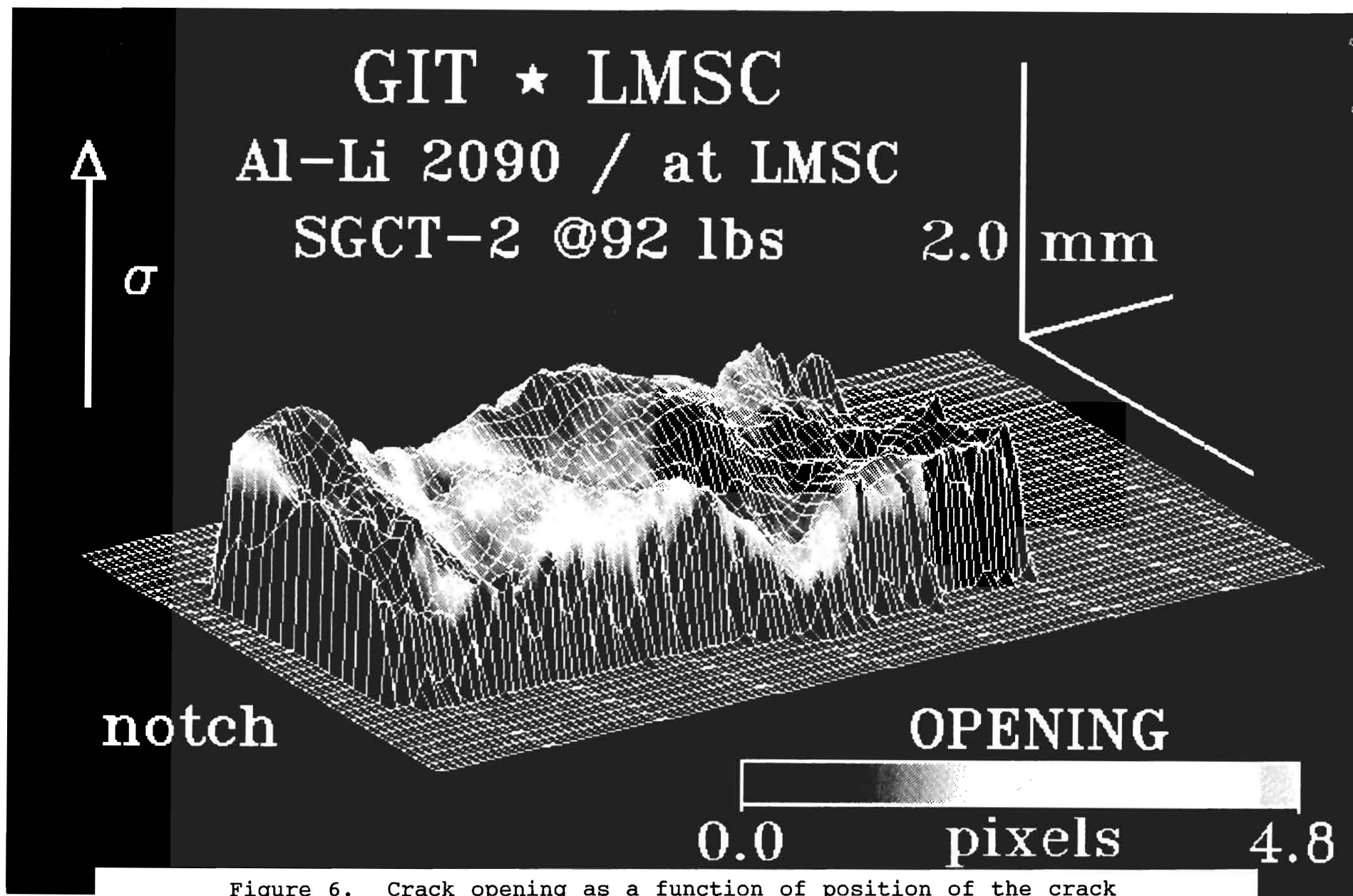
Figure 6. Crack opening as a function of position of the crack faces for the maximum load on sample CT-2. The contour lines delineate position, and the color progression black, red, blue, green and white denotes increasing opening.